METAMORPHISM AND HYDROTHERMAL ALTERATION OF EARLY PROTEROZOIC DIABASES IN THE REPUBLIC MINE, NORTHERN MICHIGAN

A THESIS
SUBMITTED TO THE FACULTY OF THE GRADUATE SCHOOL OF
THE UNIVERSITY OF MINNESOTA

BY

XINPING YIN

In Partial Fulfillment of the Requirements for
the Degree of
Master of Sciences

September 1994

DEDICATION

To My Parents,

Who have sacrificed so much

and

Have asked for so little,

Thank you .....

TABLE OF CONTENTS

LIST OF FIGURES

LIST OF TABLES

ACKNOWLEDGMENTS

I wish to take this opportunity to express my appreciation to several individuals who have contributed to this thesis.

First and foremost on the list of thanks is my advisor Dr. James A. Grant of the University of Minnesota, Duluth not only for his initiating this project and for critical comments to make the thesis complete, but also for his encouragement and patience in my graduate program during the past years.

I gratefully acknowledge Dr. John C. Green and Dr. Paul D. Siders of the University of Minnesota, Duluth for their constructive criticism of the thesis and serving on the thesis committee. Dr. Penny Morton of the University of Minnesota, Duluth is thanked for her helpful suggestion in data processing. Geologists Thomas D. Waggoner, William Kangas and Tsu-ming Han in the Cleveland Cliffs Iron Company of Ishpeming, Michigan graciously allowed access to work on the Republic Mine and provided the Geologic Map of the Republic Mine. I would like to thank my fellow gradate students Dimitrios Xirouchakis, Jamie Walker and Rich Patelke for their invaluable help.

Special thanks are given to Senior scientists Qixi Yin and Fu Bin of The Department of Analytical Chemistry, Beijing General Research Institute of Mining and Metallurgy, Beijing, China who carried out the chemical analysis for all rock samples; to Dr. Jeremy S. Delaney of the Department of Geological Sciences, Rutgers University for instructing me on how to use the microprobe; and to Drs. Maria L. Crawford and William A. Crawford of Department of Geology, Bryn Mawr College for their invaluable comments and generous help.

The Department of Geology, University of Minnesota, Duluth is deeply acknowledged for providing financial assistance for field work during the summer of 1990 and the facilities to complete the thesis.

Finally, I am deeply indebted to my wife Yin Yin who improved the English version of the thesis and let me take root in front of the computer and microscope for a couple of years and kept me alive in the meantime.

ABSTRACT

Early Proterozoic diabases in the Republic Mine, Northern Michigan have undergone pre-metamorphic hydrothermal alterations, followed by regional and retrograde metamorphism. High calcic plagioclase, pyroxene and olivine were completely decomposed in all the diabases during pre-metamorphic hydrothermal alteration which is characterized by increasing acidity and oxygen fugacity, the distinct loss of silicon, calcium and sodium, and gain of water, other major elements and most trace elements. Chemical composition of the diabases near the contact between the metadiabases and banded iron formation in the keel of the syncline was then changed from mafic to peraluminous during later hydrothermal alteration which may be related to fluid-driven regional metamorphism. This later hydrothermal alteration is characterized by distinct loss of total rock mass, water and iron group elements and gain of most felsic chemical components. Regional metamorphism is characterized by low-pressure amphibolite facies with peak pressure ~ 2.25 kb and temperature ~ 609 °C and with constant low oxygen fugacity ($\log f_{O2}$ = -21.2 ~ -20.0). The mineral assemblage Am+Pl+Q±Bt±Spn±Carb of mafic metadiabases was formed near the culmination of the regional metamorphism. The mineral assemblage Grt+Ms+Bt±And±Kfs of peraluminous metadiabases, however, was formed during retrograde phase of regional metamorphism which is characterized by decreasing temperature recorded by zoned garnets and their coexisting micas. The layer faults along the contact between the metadiabases and banded iron formation and axial faults cutting the keel of the syncline were well developed during F2 deformation of the Penokean Orogeny. They served as channels for fluid flow and controlled the amount of hydrothermal fluids and heat carried by them so as to determine the intensity and the distribution of pre-metamorphic hydrothermal alteration and retrograde metamorphism.

CHAPTER 1: INTRODUCTION

1.1. RESEARCH GOALS AND METHODS

In the Marquette Range, the early work focused on the economic geology of the banded iron-formation (BIF) (e.g., Anderson, 1968; Boyum, 1964, 1975). During the past two decades, more attention has been paid to the Penokean deformation and metamorphism of Early Proterozoic rocks, including metadiabases and Negaunee banded iron formation (e.g., Cannon, 1973, 1975; Klasner, 1978; and Haase, 1982). The hydrothermal alteration and its relationship to metamorphism in the area, however, have never been studied in detail (Cannon, 1990, personal communication), and neither has the geochemistry of the metadiabases. This work focuses on the mineralogy, petrology and geochemistry of the metadiabase and its altered products in an attempt to unravel the temporary, spatial and genetic relationship of metamorphism and hydrothermal alteration of the metadiabase in the Republic Mine, the southwestern part of the Republic Quadrangle, Marquette County, Northern Michigan (Fig. 1 and 2).

Field work was done by pace and compass, using the Republic Mine Open Pit Map (1:1200, Cleveland Cliffs Iron Company, 1981), the Bedrock

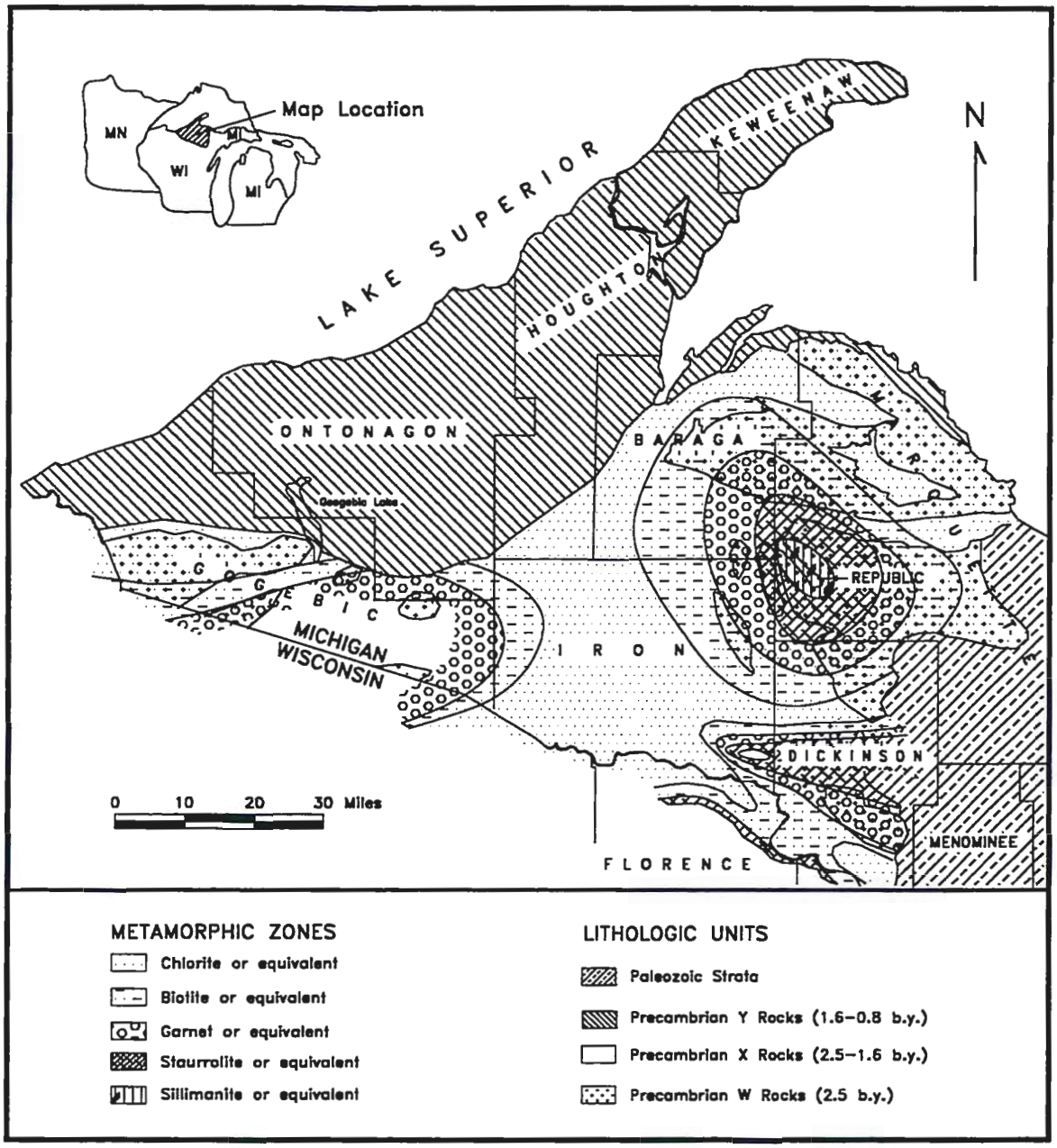

Fig. 1: Geologic Map of Northern Michigan
(After James, 1956, Cannon and Klasner, 1972)

Note: Precambrian W=Archean, X=Early Proterozoic and Y=Middle Proterozoic, respectively.

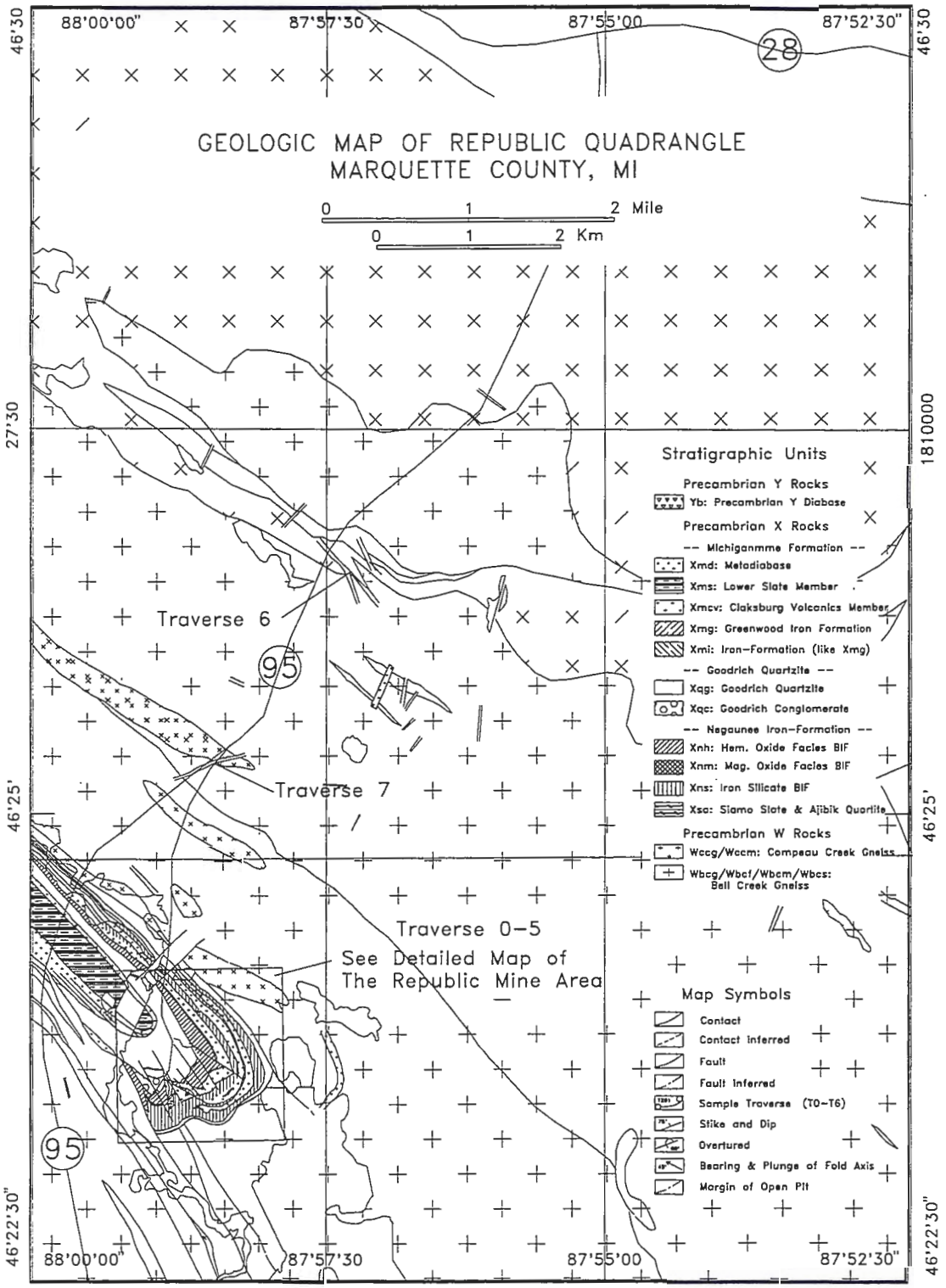

Fig. 2: Geologic Map of Republic Quadrangle
(after Cannon, 1975)

Geologic Map of the Republic Quadrangle, Marquette County, Michigan (1:24000, Cannon, 1975) and the Detailed Geologic Map of the Republic Mine Area (1:6000, Cannon, 1975). Approximately 250 specimens, including Archean granitic gneiss, Early Proterozoic Negaunee Iron Formation, Goodrich Quartzite and metadiabase, and Keweenawan diabase, were collected from eight traverses crossing the stratigraphic units (Fig. 2 and 4). All the specimens were sectioned for microscopic observation. Minerals were identified using both transmitted and reflected light microscopy and confirmed by microprobe analysis. Chemical analyses were carried out for major and minor elements (except Fe^{+2} and Fe^{+3} which were analyzed by wet-chemical analysis), using the Siemens SRS-300 X-ray Fluorescence Spectrometer at the Department of Analytical Chemistry, Beijing General Research Institute of Mining and Metallurgy, Beijing, P. R. of China. Some samples were microprobed using the JEOL JXA-8600 Superprobe at the Department of Geological Sciences, Rutgers University, New Jersey.

1.2. STRATIGRAPHY

The major stratigraphic units of the Marquette district consist of Archean gneissic rocks, Early Proterozoic stratified rocks and diabase, and Middle Proterozoic diabase (Fig. 1 and 3). Age determinations (Goldich and

ERA	GROUP (Formation)	MEMBER	DESCRIPTION
Y (Pt_2)	Keweenawan	Diabase	Nonmetamorphosed diabase dikes
X (Pt_1)		Pegmatite	Coarse-grained, microcline-quartz-muscovite rocks, Relatively rare but most abundant near Republic.
		Metadiabases	Amphibolitic rock, much with relict diabasic texture. Mostly as sills in Pt_1 rocks and dikes in Ar rocks. Much is probably associated with rocks of the Clarksburg Volcanics Member
	Baraga (Michigamme)	Upper slate	Metapelite and metagraywacke with cal-silicate concretions.
		Bijiki Iron-Formation	Mostly cherty silicate iron-formation. Some grunerite schist.
		Lower slate member	Metapelite and metagraywacke with some pyritic carbonaceous slate.
		Clarksburg Volcanics Member	Mafic pyroclastic rocks with intercalated meta-argillite and iron-formation.
		Greenwood Iron-Formation	Cherty silicate Iron-formation.
		Goodrich Quartzite	Massive to banded protoquartzite with conglomerate near base.
	UNCONFORMITY		
	Menominee	Negaunee Iron-Formation	Mostly cherty silicate iron-formation with oxide iron-formation near top.
		Siamo Slate	Laminated metapelite.
		Ajibik Quartzite	Banded to massive, light colored quartzite
	UNCONFORMITY		
W (Ar)		Gneiss of northern and southern complexes	Complex of granitic and mafic gneiss, pegmatite and greenstone.

Fig. 3: Stratigraphic Column of Western Marquette Range
(After Cannon and Klasner, 1972)

Note: Ar=Archean, Pt_1=Early Proterozoic, Pt_2=Middle Proterozoic, respectively.

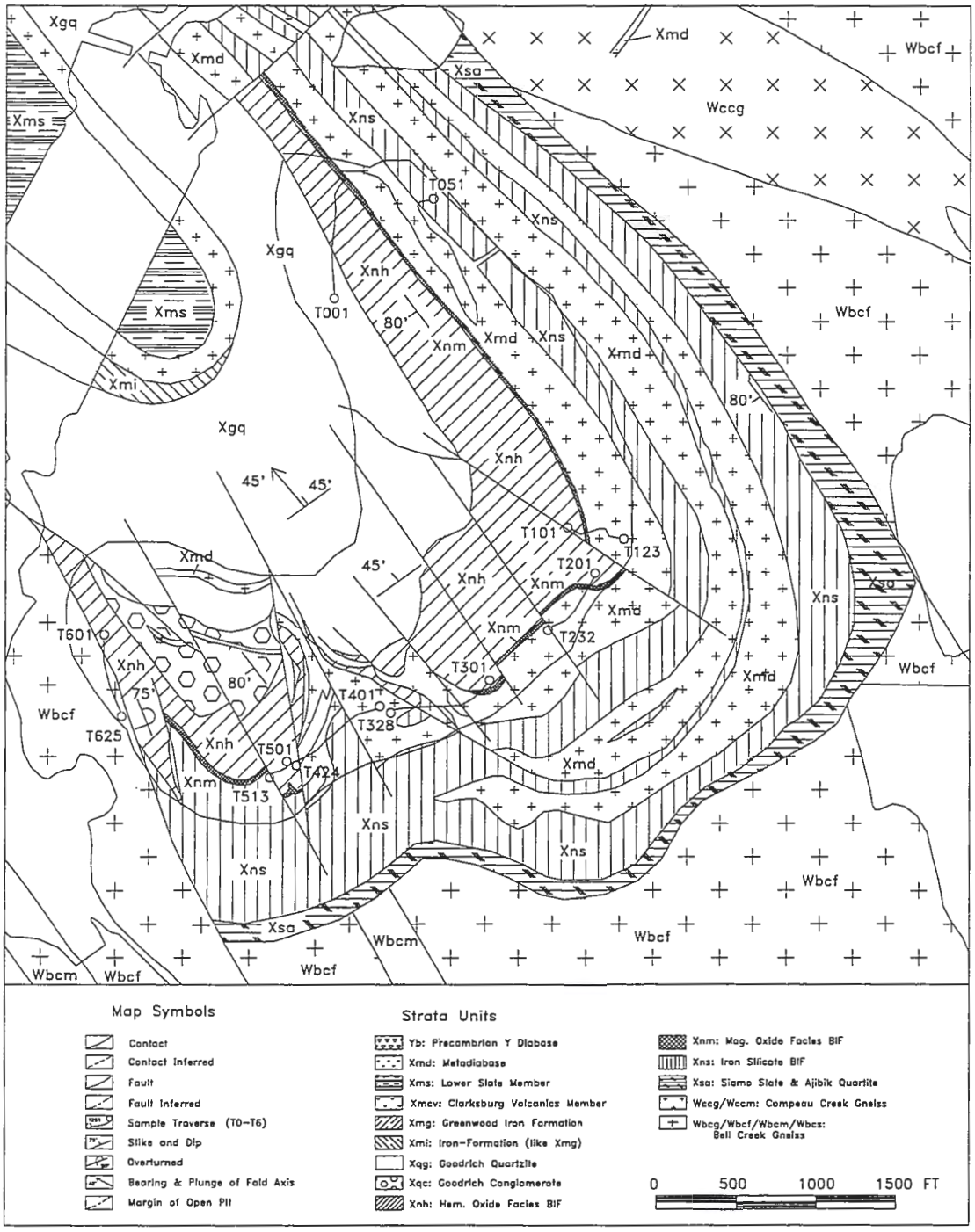

Fig. 4: Geologic Map of the Republic Area
(after Cannon, 1975)

others, 1961; Aldrich and others, 1965; Goldich, 1973; Woolsey, 1971; Van Schmus and Woolsey, 1975) and detailed mapping (Cannon, 1973 and 1975) suggest that the Archean rocks are older than 2.5 b.y., the Early Proterozoic rocks formed during 2.3-1.8 b.y., and the Middle Proterozoic rocks formed about 1.1 b.y. (Van Schmus and Hinze, 1985). The Early Proterozoic metadiabase in the area, occurring mostly as dikes in Archean rocks and as sills in Early Proterozoic rocks, may be related to the Clarksburg Volcanic Member of the Michigamme Formation (Cannon, 1973 and 1975; Klasner and Cannon, 1974; Cannon and Klasner, 1972). Based on James (1955), Boyum (1964 and 1975), Cannon (1971, 1973 and 1975), Cannon and Gair (1970), Cannon and Klasner (1972) and Klasner (1978), Archean rocks consist of granitic rocks, including migmatitic gneisses, pegmatite and mafic dikes. The Menominee Group of the Marquette Range Supergroup was deposited unconformably on deeply eroded and probably peneplaned Archean basement (Cannon and Klasner, 1972 and the references therein). The uplift and erosion following the deposition of the Menominee Group led to deep dissection of the sediments and complete removal in some areas, which resulted in the Baraga Group directly lying on the Archean basement. The clean quartz sands at the base of the Baraga Group, the overlying graywacke-shale sequence, the mafic volcanic rocks and the iron-formations of the Michigamme Formation indicate a highly active tectonic environment when these rocks formed (Cannon and Klasner, 1972). The

contact between Marquette Range Supergroup and Archean basement is now a fault in most of the western Marquette Range (Cannon and Klasner, 1972).

The Republic Mine exposes a nearly complete cross section of the Republic syncline and part of the Marquette Range Supergroup (Fig. 2 and 4). According to Cannon (1973) and Klasner (1978), Archean gneissic rocks constitute the basement in the Republic area and are overlain by rocks of the Marquette Range Supergroup. During the second phase of the Penokean Orogeny, uplift of the basement block resulted in the fault contact between the Supergroup stratigraphic units and the basement at the eastern limb of the syncline, and the truncation of the supergroup units by the fault at the southwestern part of the syncline (Fig. 4).

1.3. STRUCTURES AND PENOKEAN OROGENY

Previous geological mapping and structural analysis, the gross geometry of Penokean structures and the age determinations (Goldich and others, 1961; Aldrich and others, 1965; Goldich, 1973; Woolsey, 1971; Van Schmus and Woolsey, 1975, Cannon, 1971, 1973 and 1975; Klasner and Cannon, 1972; Cannon and Gair 1970; and Klasner, 1978) indicate:

(1) the regional Penokean structures are the results of uplift of Archean rock, with the Early Proterozoic rocks occupying intervening structural basins. These structures range in geometry from broad synclinal basins to tightly folded synclines;

(2) the Early Proterozoic rocks have undergone substantial internal deformation and horizontal shortening which did not occur in the Archean basement rocks;

(3) the folds in the Early Proterozoic rocks trend east-west and southeast-northwest, while the folds in the Archean rocks have divergent trends; and

(4) the folds in the Archean rocks are cut by swarms of pre-Penokean metadiabase dikes, which are not folded but were regionally metamorphosed during the Penokean Orogeny. This suggests that, unlike the adjacent Early Proterozoic sedimentary rocks, the Archean rocks were not internally deformed during Penokean folding.

These facts together place constraints on possible deformation styles and suggest a sequence of Penokean deformation in the area (Cannon, 1971, 1973 and 1975; and Klasner, 1978) as follows:

(1) the regional structures are products of vertical tectonism rather than of regional horizontal compression;

(2) the Archean rocks moved as rigid fault blocks. The deformation of Early Proterozoic sedimentary rocks resulted in at least one decollement surface at or near the base of the Early Proterozoic sedimentary section, and produced the (F1) folds with west and west-northwest trending fold axes; and,

(3) the rigid block uplift of the Archean rocks passively draped the earlier folded Early Proterozoic rocks into basins. This produced a second set of folds (F2) that are especially tight in some narrower synclines, such as the Republic trough.

The trends of these two ages of divergent folds are at high angles and are easily separated in some areas. In the present area, however, the trends of these folds are within about 20 degrees or less. The earlier folding may be obliterated by the intense later phase of folding.

The Republic syncline, a northwest-trending (F2) fold, is located in the center of the Marquette regional metamorphic node (Fig. 1, James, 1955). Early Proterozoic metasedimentary rocks constitute the core of the Republic syncline, and are flanked by Archean rocks. The unconformity between Archean and Early Proterozoic rocks was a surface of major slippage when basement

blocks were uplifted during the Penokean Orogeny, as shown by fault contacts in many places. The Republic syncline is truncated against the Archean gneiss at the west end of the open pit, on a high angle reverse fault dipping about 85^{o} SW. (Fig. 4). F2 folding of the sedimentary rocks is very intense, and F1 structures have not been recognized because either F1 structures were completely overprinted by F2 deformation or there were no original F1 structures.

The U-shaped southeast end of the syncline and minor folds reflect the upright northwest-trending axial plane of the syncline plunging northwest (Fig. 4). The tectonic fabrics are defined by northwest-striking and nearly vertical axial plane cleavages, and northwest-plunging minor folds have the same plunge direction as the fold axis of the Republic syncline (Fig. 4). These fabrics together with numerous steep faults nearly parallel the axial plane of the syncline, and a great amount of interlayer sliding suggests that all the structures in the open pit may be related to the F2 folding (Cannon, 1971, 1973 and 1975; and Klasner, 1978). The stratigraphic units in the limb are almost vertical and their dip decreases gradually to about 45^{0} at the keel of the syncline (Fig. 4). The structures are relatively simple on the limb but extremely complicated in the fault-breached keel where differential slip was common between and within stratigraphic units. These structures are one of the most important controls of hydrothermal activity in the syncline, as discussed below.

1.4. METAMORPHISM AND HYDROTHERMAL ACTIVITY

Regional metamorphism, beginning during the deformation of the Penokean Orogeny but culminating after deformation, is a low-pressure type characterized by andalusite- and sillimanite-bearing mineral assemblages (James, 1955; and Cannon, 1973). Five metamorphic zones were mapped by James (1955), separated by the Biotite, Garnet, Staurolite and Sillimanite isograds. Much fluid was released by dewatering during compaction and diagenesis of the Early Proterozoic rocks, and from the dehydration reactions in these rocks during the progressive regional metamorphism. These hydrothermal fluids may play a key role in the hydrothermal alteration of the rocks in the study area.

CHAPTER 2: PETROGRAPHY

In the Republic Mine, there are three sills of Early Proterozoic metadiabase in the Negaunee Iron Formation and several other small metadiabase bodies in the Goodrich Quartzite and Archean granitic gneiss (Fig. 4). The Negaunee Iron Formation is unconformably overlain by the Goodrich Quartzite. The contact between the Negaunee Iron Formation and the metadiabase is clear in the limb and becomes more and more complicated toward the keel of the Republic syncline. The width of the transitional zones between metadiabases and the Negaunee Iron Formation increases from a few centimeters to a few meters from the limb to the keel of the syncline.

2.1. METADIABASE AND ITS ALTERED PRODUCTS

Unaltered Early Proterozoic metadiabases can only be found outside of the Republic Mine where they are gradational into altered metadiabases similar to the amphibolite in the Republic Mine. They are black, coarse-grained with typical diabasic texture and consist of euhedral plagioclase and subhedral olivine and pyroxene. All the metadiabases in the Republic Mine have undergone extensive metamorphism and different degrees of hydrothermal alteration. Generally speaking, the major rock types from the center of the

metadiabases to the contact between the metadiabase and the banded iron formation are: (1) the least-altered metadiabases: massive hornblende-plagioclase amphibolite; (2) actinolite schist; (3) cummingtonite schist; (4) quartz-muscovite-biotite-garnet-andalusite schist; (5) quartz-biotite-garnet-muscovite schist; and (6) garnet-chlorite schist with varying amount of biotite and iron-magnesium amphiboles (Table 1).. There are a few relict peraluminous rocks within the chlorite schist near the contact in the keel of the syncline, with a mineral assemblage potassium feldspar, andalusite, garnet, biotite and quartz. From the limb to the keel of the syncline, massive amphibolite gradually disappears and the rocks rich in aluminum and silica become dominant, culminating in the andalusite and muscovite schist. The whole series of rock types can be observed in the keel of the syncline. On the limb of the syncline, there is no andalusite schist or muscovite schist and no relict peraluminous rocks within chlorite schist.

1. AMPHIBOLITE

Hornblende-plagioclase amphibolite occurs mainly at the center of the metadiabase sills in the limb of the syncline, except for very few small relict bodies scattered in the keel. All the amphibolite in the open pit has undergone hydrothermal alteration, and the unaltered amphibolite can only be observed outside of the Republic Mine (Fig. 2). It is black to dark green, massive, coarse-

Table 1: Esitmated Mode of Metadiabases

Rock Type	Amphibolite	Act Schist	Cum Schist	And Schist	Ms Schist	Chl Schist
n	10	12	15	10	12	15
Mineral	Avg (Range)	Avg (Range)	Avg (Range)	Avg (Range)	Avg (Range)	Avg (Range)
Spn	5 (3-7)	0 (0-1)	----------	----------	----------	----------
Hbl	40 (30-50)	----------	----------	----------	----------	----------
Act	1 (0-2)	40 (30-50)	----------	----------	----------	0 (0-1)
Cum/Gru	----------	----------	25 (10-60)	----------	----------	15 (0-30)
Bt	3 (1-5)	10 (5-15)	15 (10-25)	20 (15-40)	10 (5-15)	5 (0-5)
Grt	----------	----------	----------	10 (5-15)	6 (5-10)	10 (0-80)
Chl	0.5 (0-2)	2 (1-5)	3 (1-7)	0 (0-1)	1 (0-2)	37 (10-70)
Ep	0.5 (0-2)	0 (0-1)	0 (0-1)	----------	----------	0 (0-1)
MIR*	5 (2-7)	10 (5-15)	15 (10-20)	10 (5-15)	5 (2-10)	20 (15-25)
Hm	----------	----------	----------	----------	----------	1 (0-2)
RPL	30 (20-40)	15 (10-20)	6 (3-7)	0 (0-1)	0 (0-1)	0 (0-5)
CPL	2 (1-5)	5 (2-6)	9 (6-10)	0 (0-1)	0 (0-1)	0 (0-1)
Ms	----------	----------	1 (0-2)	12 (10-15)	45 (25-65)	1 (0-3)
Ser	2 (1-5)	4 (3-8)	8 (6-10)	1 (0-3)	----------	----------
Qtz	10 (5-12)	13 (10-15)	17 (15-20)	22 (15-35)	32 (20-40)	10 (5-10)
And	----------	----------	----------	25 (10-50)	0 (0-1)	0 (0-1)
Carb	1 (0-3)	----------	----------	----------	----------	----------
Ap	----------	1 (1-5)	1 (2-5)	0 (0-1)	1 (0-3)	1 (0-3)
APL	50 (40-60)	70 (60-80)	90 (80-100)	95 (90-100)	100	100

Note: *MIR=Mt/Ilm/Rt; RPL, CPL and APL=Relict, Crystallized, Altered plagioclase, respectively. Other notations see Appendix A.

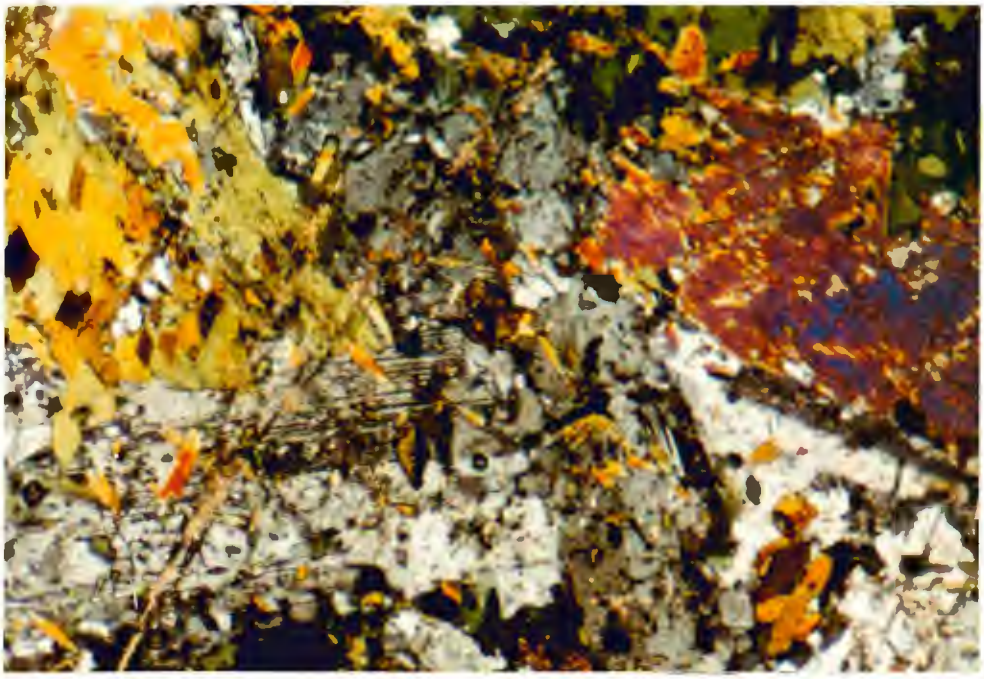

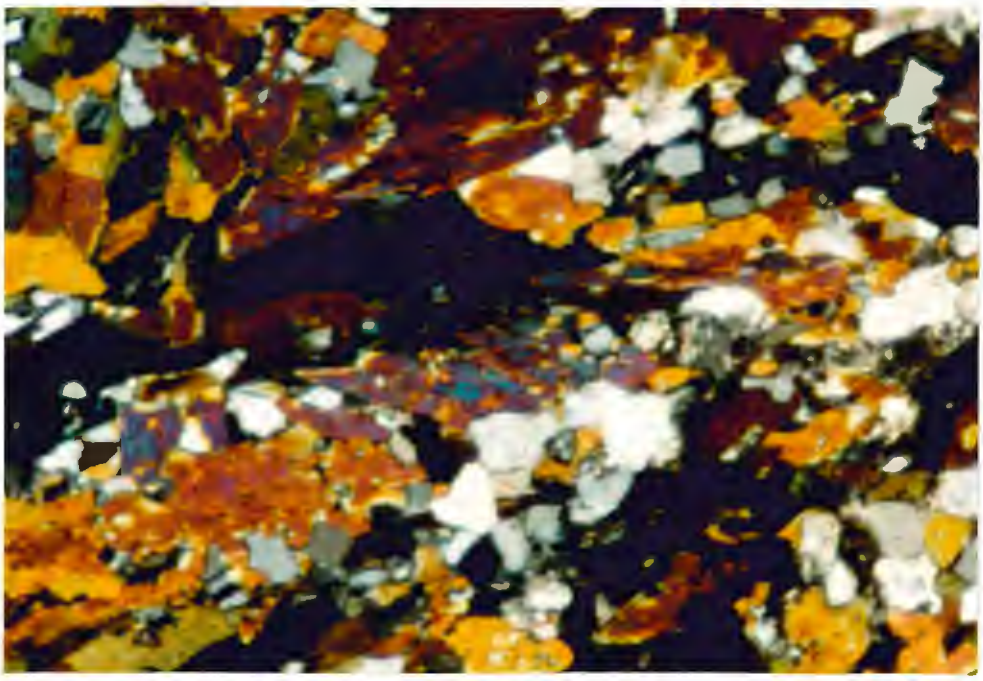

Fig. 5 (upper): **Amphibolite** (Sample-MI91039, View=4mm)
Fig. 6 (lower): **Actinolite Schist** (Sample-MI91223, View=4mm)

grained, granoblastic with relict diabasic texture (Fig. 5). Hornblende is dark-green, subhedral, coarse-grained with inclusions of plagioclase (An~30), quartz, magnetite and sphene occurring along its cleavages and fractures. Some hornblende has been altered to form epidote, biotite, chlorite and a little actinolite. Plagioclase is subhedral, coarse-grained with distinctive polysynthetic albite twinning and minor Carlsbad twinning (Fig. 5). Most of the relict plagioclase is about An 55. About 50 percent of relict plagioclase has undergone slight sericitization along its cleavages, fractures and edges, where the plagioclase composition is about An 50. Most recrystallized plagioclase with An 45 occurs as grains between the relict plagioclase and hornblende to form mosaic texture. The other major minerals are biotite and quartz. Accessory minerals are sphene, magnetite, ilmenite, rutile, apatite and epidote (Table 1). Sphene generally has undergone some degree of alteration to form epidote with an ilmenite core. Carbonate, pyrrhotite and pyrite are also found in the amphibolite.

2. ACTINOLITE SCHIST

There is no sharp distinction between the amphibolite and actinolite schist because of the gradual decrease of hornblende and relict plagioclase with the gradual increase of actinolite, biotite, magnetite, quartz and recrystallized plagioclase. These gradual changes in both mineral assemblages

and textures, the gradual decrease of An content of relict plagioclase and the pseudomorphous replacement of hornblende by actinolite suggest the formation of actinolite schist from amphibolite. The complete replacement of hornblende is chosen as the limit between amphibolite and actinolite schist. Actinolite schist is black to green, coarse-grained, with granoblastic texture (Fig. 6). Actinolite is pale green, subhedral, coarse-grained, with inclusions of plagioclase (An~30) and quartz. However, it is not possible to distinguish actinolite from hornblende in the field. The darker color, larger extinction angle (Z^C about 18~25 degree) of hornblende under microscope can be used to distinguish it from actinolite which is always pale green and with smaller extinction angle (Z^C about 12~15 degree). Some biotite replaces the edge of actinolite or occurs along its cleavages. Most relict plagioclase is subhedral, coarse-grained plagioclase (An~50) with polysynthetic twinning. But the plagioclase grains in actinolite schist are not as clean as those in amphibolite because of more extensive alteration. About 70 percent of relict plagioclase has undergone extensive sericitization along cleavages, fractures and edges, where its An content is reduced to about 45. The recrystallized plagioclase has An content abut 40. There is 10 percent biotite and 13 percent quartz. Accessory minerals are magnetite, ilmenite, rutile, apatite and epidote (Table 1).

3. CUMMINGTONITE SCHIST

Actinolite schist grades into cummingtonite schist as cummingtonite appears and becomes dominant, with a distinct decrease in actinolite. The boundary between them is defined by the complete disappearance of all calcium amphiboles. Cummingtonite schist is dark green, coarse-grained, with a texture dominated by amphibole prisms (Fig. 7). Pseudomorphic texture defined by the cummingtonite replacing actinolite is common. Cummingtonite is colorless or pale green to pale yellow in thin sections, euhedral, coarse-grained with a few plagioclase (An~30) and quartz inclusions. The distinctive twinning on {100}, positive optical sign and higher indices of cummingtonite distinguish it from actinolite. About 90 percent of the relict plagioclase with about An 40 has undergone extensive sericitization. The recrystallized plagioclase with about An 35 has undergone more extensive sericitization than those in the actinolite schist. The plagioclases included in cummingtonite grains have about An 30. Other minerals are 15 percent biotite and 17 percent quartz. Major accessory minerals are magnetite, ilmenite, apatite and epidote (Table 1). From the limb to the keel of the syncline, and especially from the center toward the contact between the metadiabase and the banded iron formation, the amount of cummingtonite increases with increasing biotite. In these two directions, all kinds of plagioclase decrease until the mineral is no longer present.

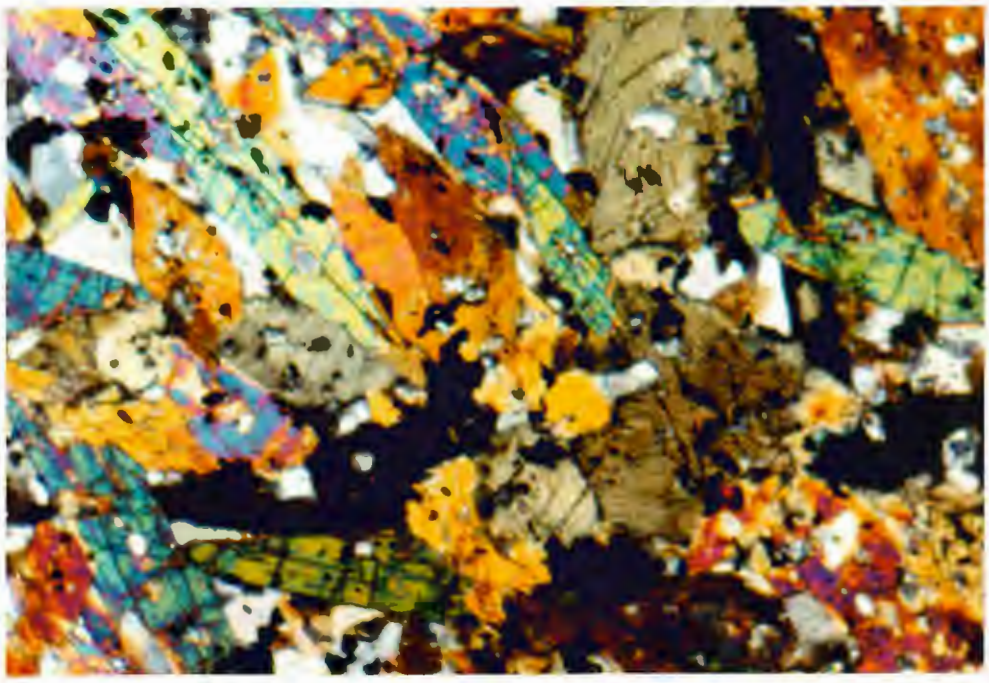

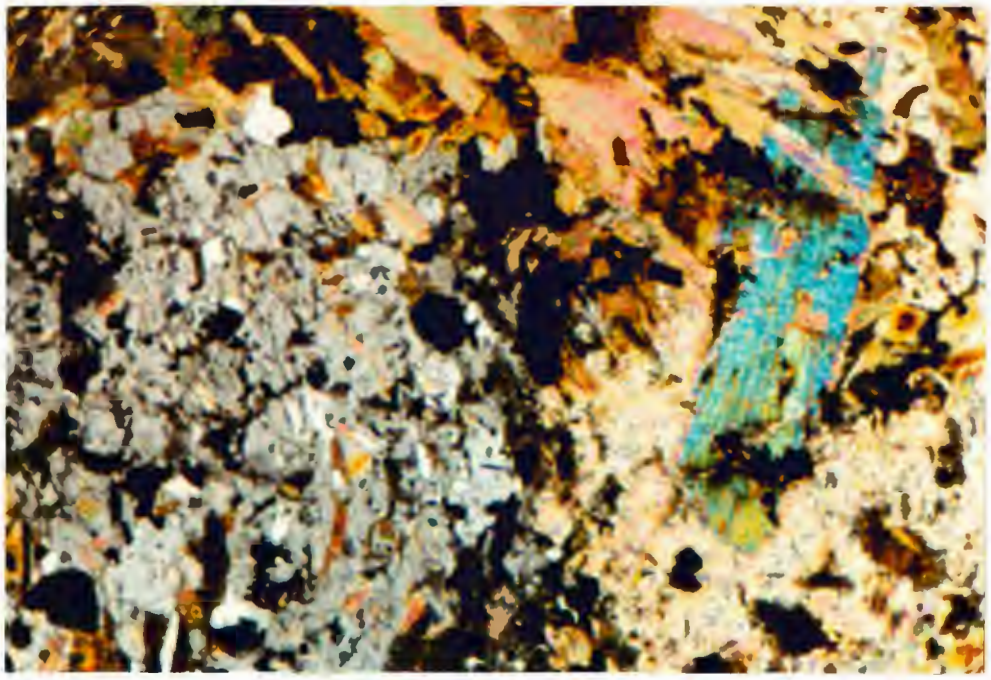

Fig. 7 (upper): **Cummingtonite Schist** (Sample-MI91120, View=4mm)
Fig. 8 (lower): **Andalusite Schist** (Sample-MI91208, View=4mm)

4. ANDALUSITE SCHIST

Andalusite schist is only found in the keel of the syncline. There is a gradual transition from cummingtonite schist to andalusite schist as the result of gradual change of mineral assemblages and textures. Garnet and andalusite occur after the complete decomposition of all kinds of amphiboles and plagioclases, with gradual increase of biotite and quartz. Quartz-muscovite-biotite-garnet-andalusite schist is black or dark-gray, coarse-grained, with granular lepidoblastic texture (Fig. 8). Andalusite (25-35 percent) is colorless or pale pink under microscope, subhedral to anhedral, with a diameter about 0.2 to 2 mm. The prismatic {110} cleavages nearly at right angles are distinctive, where sericite and biotite formed along these cleavages as the result of later hydrothermal alteration. Garnet (about 10 percent) has a diameter from 0.5 to 5 mm. The garnet is zoned, with a relatively clean outer rim and unclean core. Garnet and magnetite are surrounded by the foliation of muscovite and biotite and with pressure shadows of quartz and mica, suggesting their pre-tectonic origin (Spry, 1969; and Yardley and others, 1990). The other dominant minerals are 20 percent quartz, up to 20 percent biotite, about 12 percent muscovite and 10 percent magnetite (Table 1). Major accessory minerals are ilmenite, rutile, apatite and epidote.

5. MUSCOVITE SCHIST

Muscovite schist is only found in the keel of the syncline. With the gradual decrease of andalusite and biotite, more and more muscovite and quartz formed. There is no abrupt change in mineral assemblages and textures between andalusite and muscovite schist. Muscovite schist is defined by the disappearance of andalusite although a few andalusites may be found within fault zones near the contact. The muscovite schist occurs mostly near the contact between the metadiabase and the banded iron formation. The schistosity has a strong axial planar orientation. Quartz-biotite-garnet-muscovite schist is dark-gray or gray, medium- to coarse-grained, with granular lepidoblastic texture (Fig. 9). Garnet and magnetite are surrounded by the foliation of muscovite and biotite and with pressure shadows of quartz and mica, suggesting their pre-tectonic origin (Spry, 1969; and Yardley and others, 1990) which is more distinct than that in andalusite schist (Fig. 9). In most cases, there is about 45 percent muscovite, 10 percent biotite and 30 percent quartz. Garnet is about 6 percent, with a diameter from 2 to 10 mm. The zoning of garnet is not very clear under the microscope. The garnet geochemistry, however, shows its distinct zoning pattern consisting of a core, middle zone and rim, as discussed in the next chapter. The same accessory minerals are found here as in the andalusite schists (Table 1).

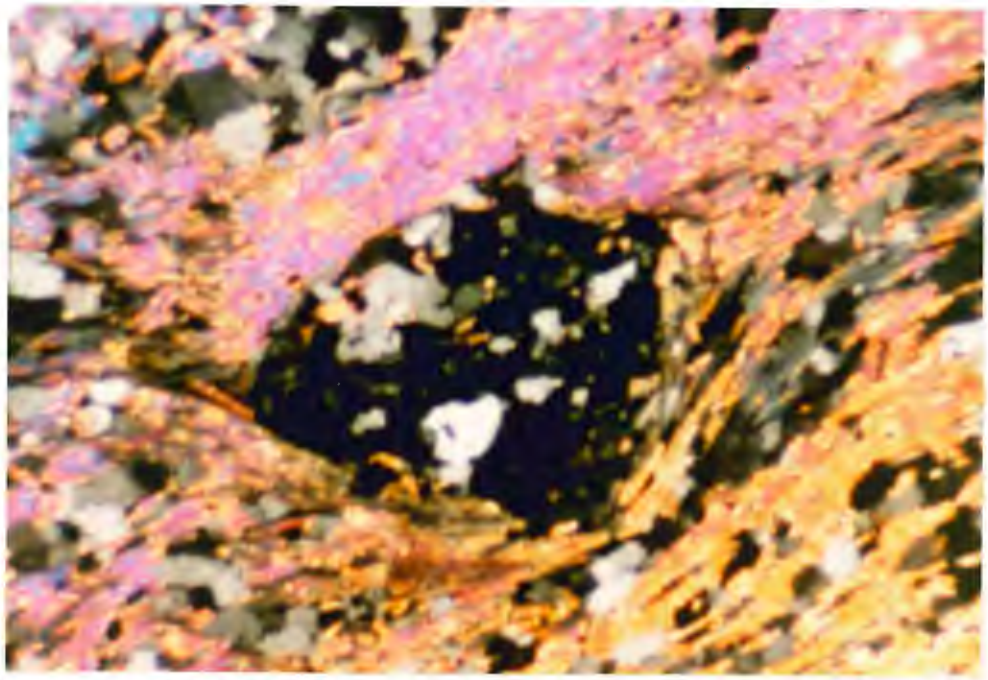

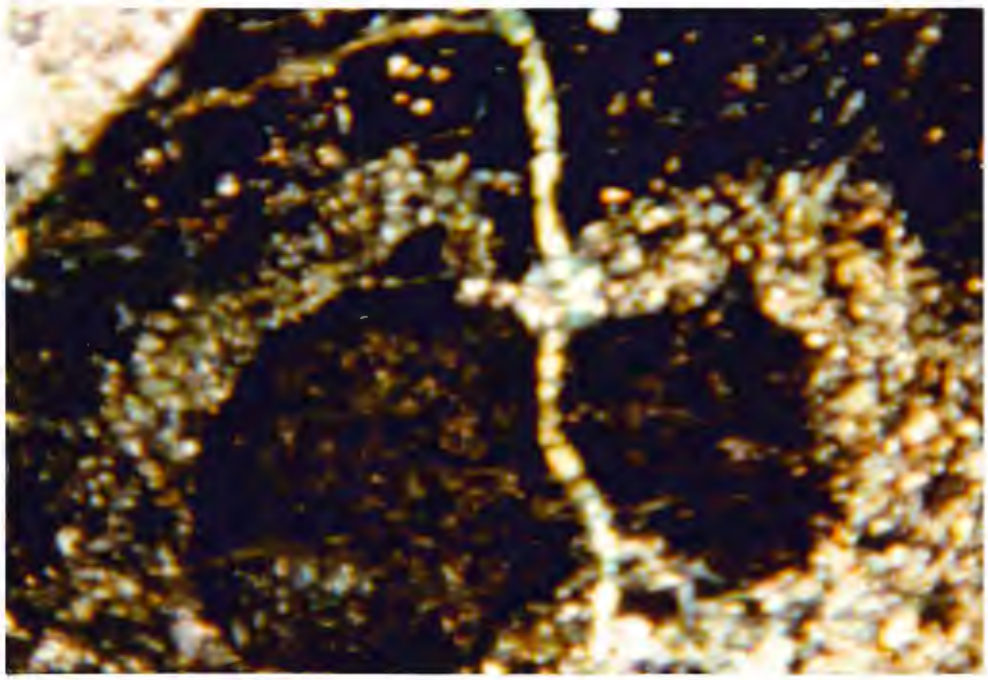

Fig. 9 (upper): **Muscovite Schist** (Sample-MI91417, View=4mm
Fig. 10 (lower): **Zoned Garnet** (Sample=MI91422, View=4 mm)

6. CHLORITE SCHIST AND RELICT PERALUMINOUS ROCKS

With distinct decrease of muscovite, quartz and biotite, chlorite, iron-magnesium amphiboles and iron-titanium oxides gradually dominate the rock. The mineral assemblages of rocks on the contact between the altered metadiabase and the banded iron formation are rather complicated. Generally speaking, the rocks are chlorite-dominated schist with varying amounts of quartz, biotite, garnet, iron-magnesium amphiboles and iron-titanium oxides. The dominant iron-magnesium silicate is chlorite in the limb where the relict plagioclases in the schist are distinctive and may be as high as 30 percent in the mode. In the keel of the syncline, there is no relict plagioclase but various amphiboles, garnet and chlorites. In the keel of the syncline, andalusite and potassium feldspar associated with biotite, quartz and garnet occur as relict peraluminous rock bodies, on the scale of few centimeters, within the chlorite schist near or within the contact between metadiabases and the banded iron formation. The chlorite schist is dark-green, fine to coarse grained, with granular lepidoblastic texture. Chlorite and biotite show strong axial planar orientation. Amphiboles may occur as veins along or crossing the rock units at the contact or within the banded iron formation. From the limb to the keel of the syncline, the amphibole species in the contact zones between the altered metadiabase and the iron formation gradually change from cummingtonite to grunerite. Two

generations of chlorite are found in chlorite schist. One is a typical equilibrium mineral with good tabular crystal form and low first grade interference color, and another shows anomalous brown, bluish or purplish interference colors. The amount of garnet varies from nil on the limb to 80 percent in the keel of the syncline, with the diameter from 0.5 to as large as 15 mm. Its distinctive zoning (core, altered middle zone with biotite and quartz, and rim) can be seen under the microscope and all of the zones are cut by later hydrothermal biotite-chlorite-quartz veins (Fig. 10). Major accessory minerals are magnetite, ilmenite, rutile, apatite and epidote, along with hematite which is only found in chlorite schist in the keel of the syncline.

7. DISCUSSION AND SUMMARY

The structures and fabrics of metadiabases are simple and clear in the limb but very complicated in the keel of the syncline. Schistosity in all the metadiabases is parallel to the axial plane of the Republic syncline except a little is parallel to radial cleavages related to the syncline. Massive textures can only be found in hornblende-plagioclase amphibolite in the limb of the syncline. All the other rocks show increasing schistosity from the limb to the keel of the syncline and from the center of the metadiabases to the contact between the metadiabases and banded iron formation. In these two directions, the grain size and idiomorphism for the same mineral species increase. In the Republic Mine,

the best-preserved relict diabasic texture, with subhedral plagioclase and hornblende, is found in amphibolite in the limb of the syncline. This texture is preserved to lesser extents in actinolite and cummingtonite schist. The fabric changes gradually from relict diabasic texture in amphibolite to granoblastic in actinolite schist and cummingtonite schists, lepidoblastic granular in andalusite schist and granular lepidoblastic texture in muscovite schist and chlorite schist. All types of the metadiabases contain the typical magmatic ulvospinel-magnetite exsolution texture, with rounded or various irregular grain shapes (Klein and Hurlbut, 1985); which indicates all the altered metadiabases may have formed from the same protolith, the Early Proterozoic diabase. Pseudomorphic texture and mineral replacement are common in all metadiabases. Relict plagioclase, garnet and andalusite become irregular in their shapes and are surrounded or separated by the new-formed minerals such as sericite or muscovite, biotite and chlorite. The isolated grains of these remaining minerals have optical continuity, showing that they are relict from one pre-existing grain. The garnet and magnetite in andalusite schist, muscovite schist and chlorite schist show characteristic pre-tectonic origin.

2.2. OTHER RELATED ROCKS

1. NEGAUNEE IRON-FORMATION

The Negaunee Iron Formation can be divided into three types of iron formation (Cannon, 1975): (1) iron silicate iron formation (Xns), (2) magnetite-rich oxide facies iron formation (Xnm), and (3) hematite-rich iron formation (Xnh) (Fig. 4). The amount of martite and specular hematite and the grain size of all minerals gradually and significantly increase in the banded iron formation from the limb to the keel of the Republic syncline.

(1) Iron silicate iron formation: banded grunerite-magnetite iron-formation, consisting of layers of coarse-grained grunerite with large to nil magnetite content, interlayered with gray chert, or locally chert free. Grunerite is rarely oriented and fine-grained garnet is commonly disseminated throughout grunerite layers. Clinopyroxene, epidote, biotite and actinolite are common accessory minerals.

(2) Magnetite-rich iron formation: wavy-bedded chert-magnetite iron formation consisting of gray chert and nearly pure layers of magnetite with only trace amounts of iron silicates.

(3) Hematite-rich iron formation: wavy-bedded jaspilite with red and maroon jasper interlayered with specular hematite in 2 cm thick layers. Major accessory minerals are biotite, muscovite, chlorite, hornblende, garnet and fayalite. Variable amounts of magnetite are disseminated in hematite layers and commonly converted to martite.

2. GOODRICH QUARTZITE

The quartzite is a fining-upward clastic sequence with a discontinuous unit of oligomictic iron-formation pebble conglomerate at the base, grading up into thickly bedded vitreous to feldspathic quartzite and into more argillaceous rock which commonly contains abundant biotite, garnet or chloritoid (Cannon and Klasner, 1972). From limb to keel of the syncline, the Goodrich Quartzite changes from relatively clean quartzite to polymictic conglomerate containing quartz, muscovite, hematite, magnetite and some feldspar with varying amounts of iron-formation clasts. The deposition of the clasts of iron-formation and the later hydrothermal activities concentrated a variable amount of iron and locally formed iron ore in the Republic Mine.

2.3. VEINS AND VEIN MINERALS

There are many veins in all kinds of metadiabase, Negaunee Iron Formation and Goodrich Quartzite, which suggests extensive hydrothermal activity in the area. Quartz veins and chlorite veins are found in both the limb and the keel but carbonate veins and sulfide veins are only found in the limb of the syncline. The width of quartz veins and carbonate veins varies from a few mm to tens of cm. There are some grunerite veins, specularite veins, chlorite veins and garnet veins at or near the contact between the metadiabases and the banded iron formation. Veins are much more abundant in the keel than in the limb of the syncline. The orientation of these veins is mainly parallel to orientation of the fault system related to the formation of the syncline.

CHAPTER 3: GEOCHEMISTRY

Analytical data greater than $(\bar{x}+3\sigma)$ or smaller than $(\bar{x}-3\sigma)$ ($\bar{x}$ is average and σ is standard deviation) are excluded from the total sample population before other data processing to avoid random sampling and analytical errors. Distribution patterns for all elements are examined prior to discussing the geochemical data and applying any statistical method. Multi-population analysis is used to define the possible episodes of various geological processes. Mineral chemistry gives insight into the mineralogical changes in the metadiabases during different geological processes. Isocon analysis (Grant, 1986) gives quantitative estimates of changes in both mass and composition for whole rocks and for different elements compared to protolith(s). Isocon analysis results may also provide information about the character and possible episodes of various geologic processes. Based on the evidence from field geology, mineralogy, mineral chemistry and rock chemical composition, the protoliths of various metadiabases will be evaluated.

3.1. ELEMENT DISTRIBUTION AND MULTI-POPULATION ANALYSIS

The theory and the procedure for testing element distribution patterns are briefly introduced in Appendix C. Different element distribution

patterns reflect the physical and chemical conditions of geological processes. Generally speaking, for a single geologic process, an element shows either AND (Arithmetic Normal Distribution) when it is evenly distributed in various minerals or LND (Logarithmic Normal Distribution) when it is concentrated in a certain mineral (e.g., Huang, 1979). The distribution patterns for all elements in the various metadiabases in the research area exhibit neither AND (except silicon and total iron) nor LND (Appendix C2 and C3), suggesting multi-episode geological processes resulting in complicated chemical changes of the altered metadiabases in the study area.

The number of sample sub-populations or subspaces for elements may be related to the number of episodes of various geological processes through which rocks evolved. Each subspace in the total sample space may stand for a group of data from rocks affected by a particular geological process. The multi-population analysis method can be used to distinguish each sub-population from the total population and from each other. The theory and the procedure for multi-population analysis are summarized in Appendix D. Although cumulative probability diagrams are used to analyze the sub-populations in the thesis, the multi-peak curves in the histograms have the same results (Fig. 11). Figure 12 shows that almost all the major and trace elements of all 36 samples in this study have three subspaces in the cumulative probability diagrams or multi-peak curves in the histograms, suggesting at least

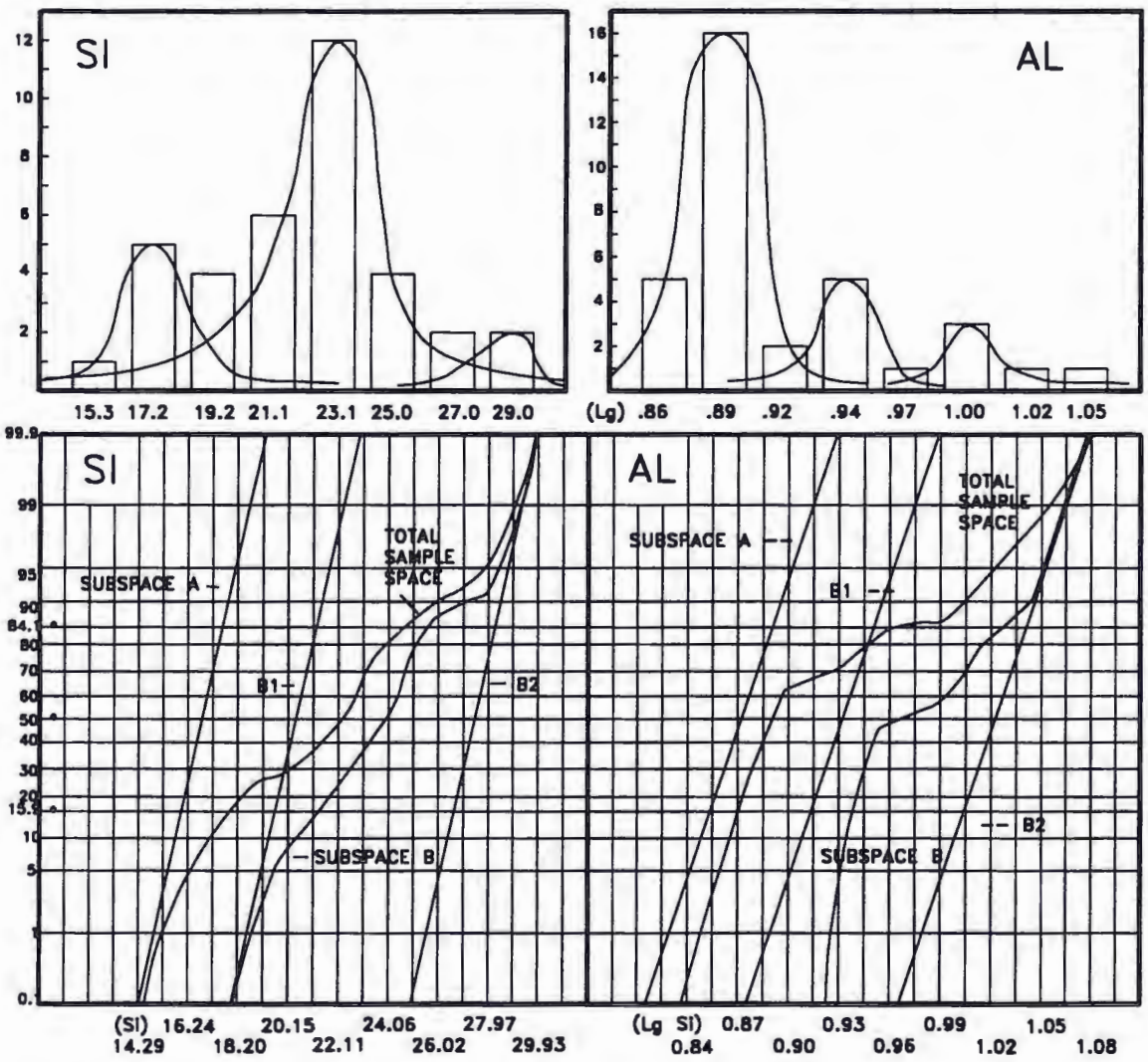

Fig. 11: Multi-population Analysis

Note: (1) Chemical compositions of all 36 samples (Appendix B) are used for multi-population analysis. (2) x-axis is element concentration (wt.%) and y-axis is cumulative probability. (3) Si inflection points are 44.44 and 88.89; Subspace A=44.44, B1=44.45, B2=11.11. Al Inflection points are 67.65 and 85.29; Subspace A=67.65, B1=12.46, B2=9.89.

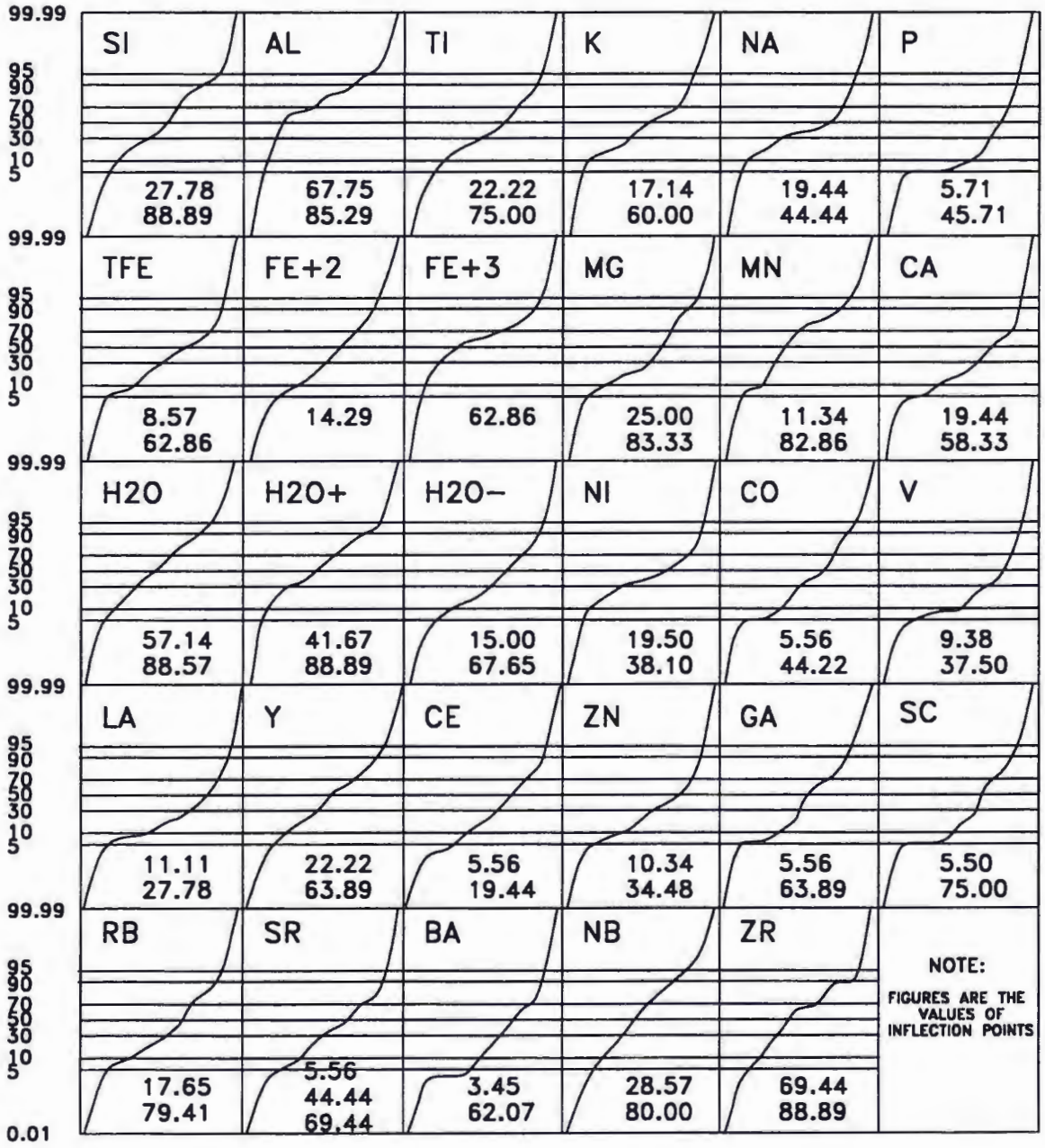

Fig. 12: Multi-population Analysis Results

Note: (1) Chemical compositions of all 36 samples (Appendix B) are used for multi-population analysis. (2) Number=value of the inflection points. (3) Y-axis=cumulative probability; X-axis=element concentration which is not plotted because only the number of possible subspaces and the weight for each subspace are of interest.

three different geological events to form the altered metadiabases observed today. The percentages of the subspaces for an element in its total sample space indicate its different geochemical behavior during different geological processes, especially if the subspace standing for original chemical composition can be determined. Multi-population analysis alone, however, cannot discriminate the original subspace from others.

3.2. CHEMICAL COMPOSITION OF METADIABASES

Table 2 and Figure 13 summarize the chemical compositions of different metadiabases. The original chemical analyses are listed in Appendix B. Some selected element ratios in Table 3 will be discussed in the following sections. The least-altered metadiabase or amphibolite still has typical diabase chemical composition in both major and trace elements (Table 2), compared to the average chemical composition of diabases (Turekian and Wedepohl, 1961; Wedepohl and others, 1969-1978). Hydrothermal alteration, however, has dramatically changed the chemical composition of the metadiabases from mafic to peraluminous.

For those metadiabases in the limb of the syncline, Si, Ca, Na, Sr, Cr, V, Sc, Th and total felsic components gradually decrease with increasing Al, Ti, K, P, both Fe^{+2} and Fe^{+3}, H_2O^+, H_2O^-, total mafic components and almost all

Table 2: Chemical Compositions of Metadiabases

Rock Type	Am	Act	Cum	And	Ms	Chl	Avg
n	4	8	7	7	5	4	35
SIO2	49.28	47.01	45.36	47.45	49.84	34.40	46.28
TIO2	1.95	2.98	3.55	3.58	3.29	3.31	3.16
AL2O3	14.70	13.98	15.01	19.63	16.98	16.40	15.97
FE2O3	3.53	5.69	5.83	6.06	5.72	11.04	6.09
FEO	8.22	10.06	12.46	9.68	8.34	14.06	10.49
MGO	6.42	5.69	6.10	3.69	3.19	7.18	5.28
MNO	0.19	0.31	0.27	0.30	0.32	1.11	0.37
CAO	9.44	7.76	2.99	1.37	2.86	2.23	4.14
NA2O	2.92	2.33	1.90	1.07	0.88	0.66	1.75
K2O	1.24	1.51	2.61	3.52	4.61	3.09	2.72
P2O5	0.19	0.25	0.33	0.34	0.44	0.27	0.31
H2O+	1.54	1.71	2.86	2.86	2.89	5.04	2.72
Total	99.58	99.26	99.26	99.55	99.37	98.77	99.29
BA	274	367	420	376	588	934	448
CE	31	41	51	109	84	58	63
CO	50	60	73	58	51	99	65
GA	21	22	20	23	21	18	21
LA	20	34	53	77	54	61	51
NB	24	29	29	44	39	26	33
NI	32	41	64	68	13	171	58
RB	16	24	26	42	44	31	30
SC	31	32	26	23	24	29	27
SR	474	241	118	63	101	50	165
V	311	349	217	96	181	165	228
Y	16	15	16	26	24	12	19
ZN	6	88	131	102	43	103	86
ZR	98	144	163	303	239	167	193

NOTE: Unit: oxide-wt%, element-ppm; other notations see Appendix A.

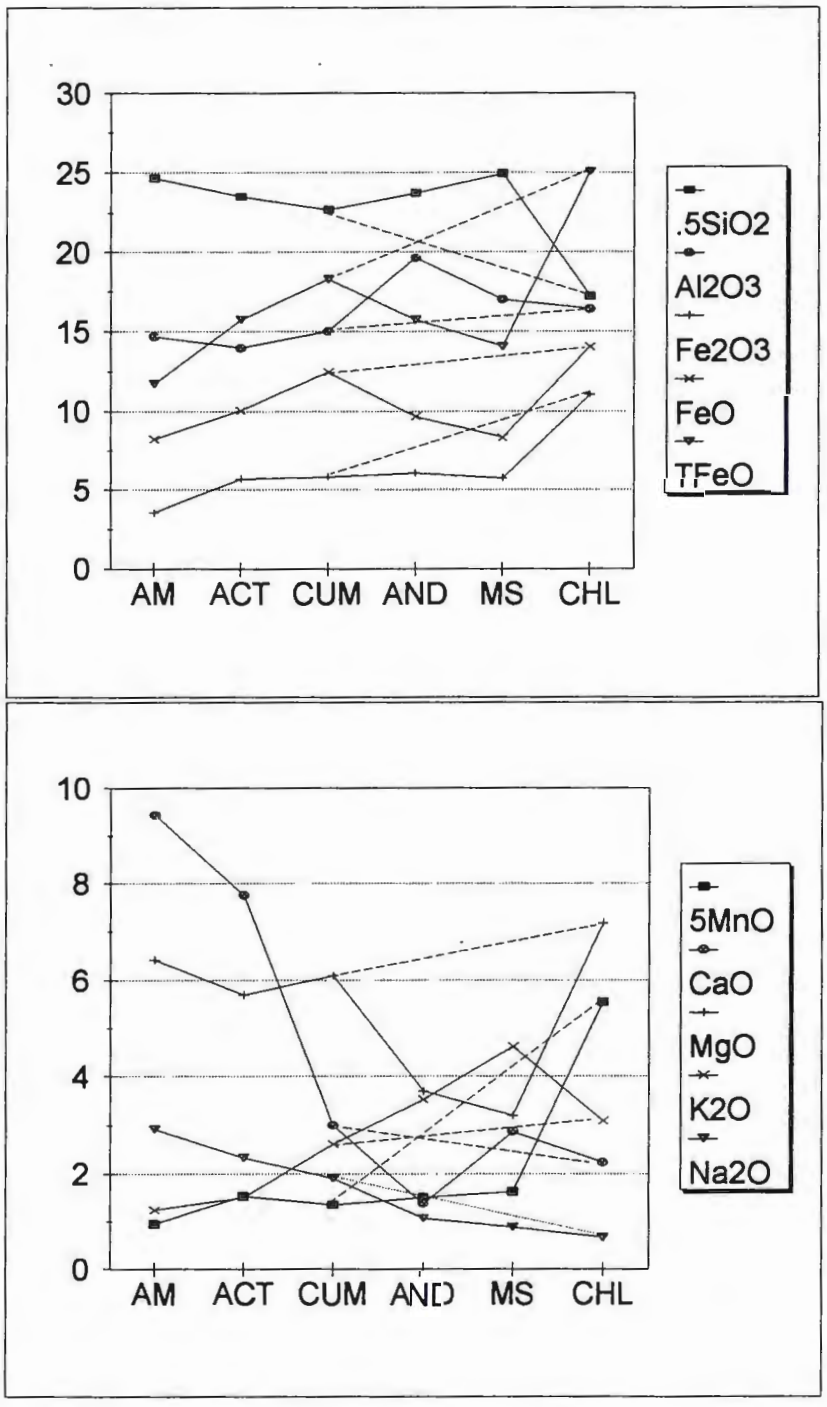

Fig. 13: Chemical Compositions of Metadiabases

Note: There is no andalusite or muscovite schist in the limb of the syncline. See Appendix A for notations.

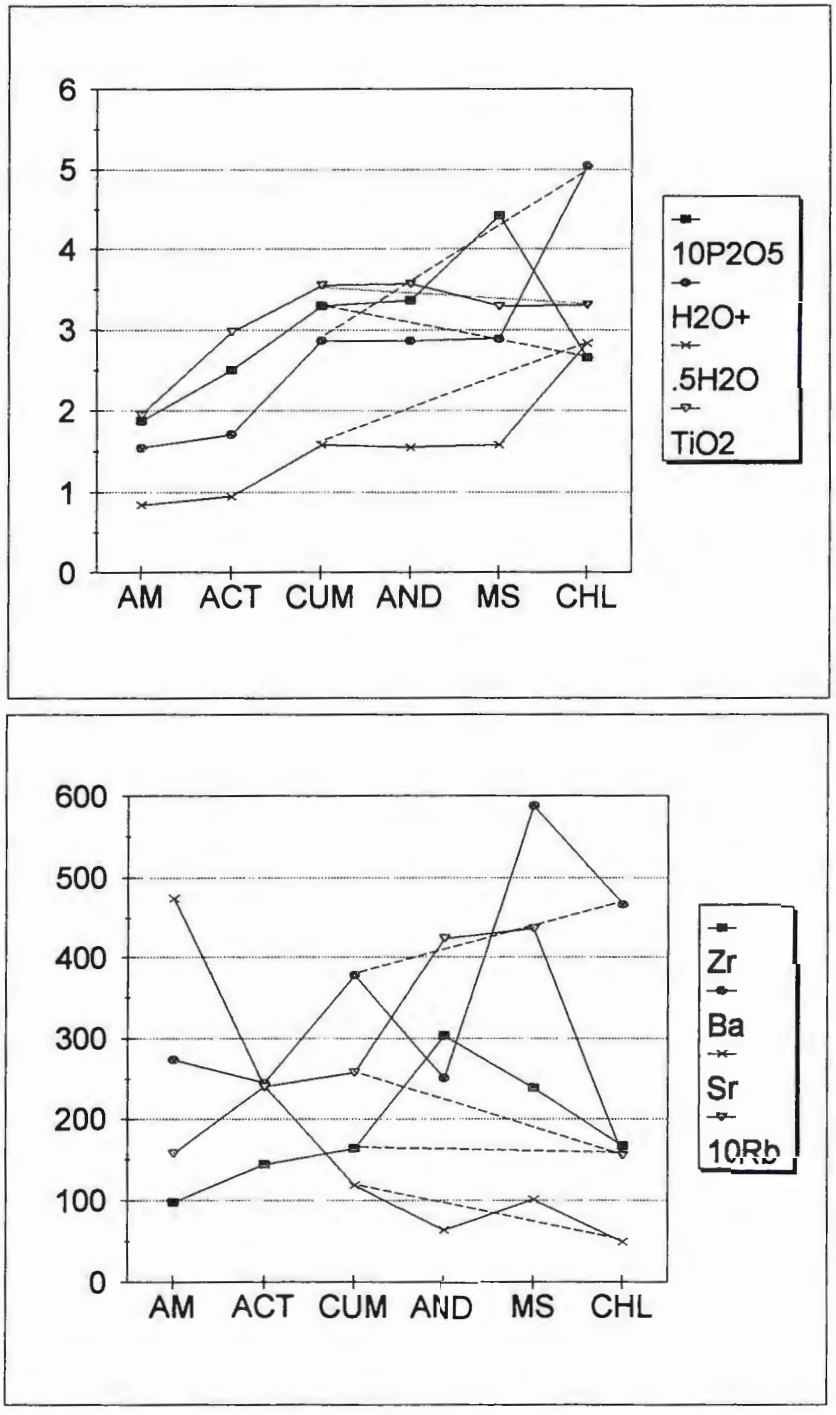

Fig. 13: Chemical Compositions of Metadiabases (continued)
Note: There is no andalusite or muscovite schist in the limb of the syncline. See Appendix A for notations.

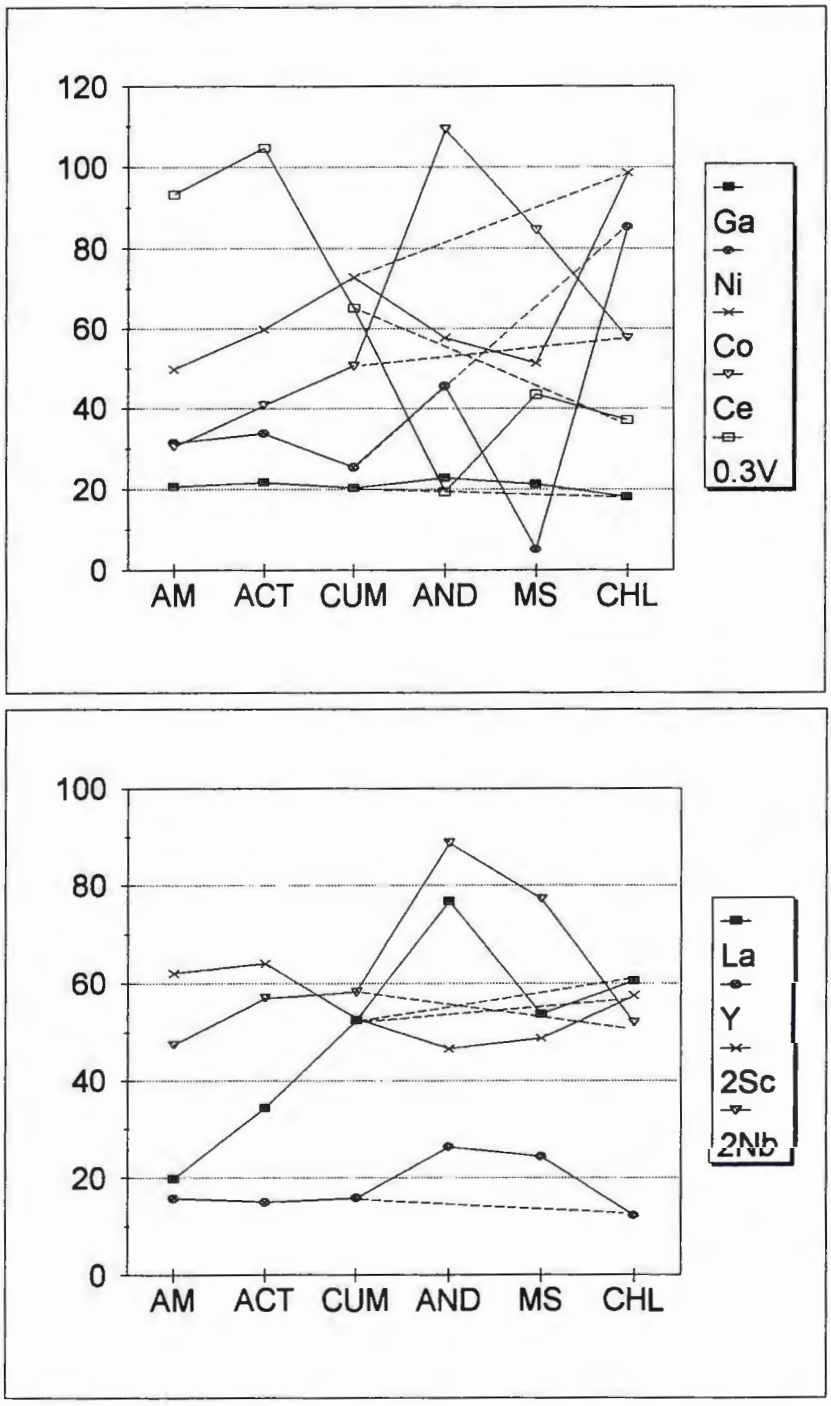

Fig. 13: Chemical Compositions of Metadiabases (continued)
Note: There is no andalusite or muscovite schist in the limb of the syncline. See Appendix A for notations.

Table 3: Selected Element Atomic Ratios

ROCK TYPE	AM	ACT	CUM	AND	MS	CHL
Fe/Mg	2.93	2.22	1.78	2.30	2.68	1.15
AL/SI	0.33	0.33	0.37	0.46	0.38	0.53
K/CA	0.15	0.23	1.01	2.98	1.87	1.61
NA/CA	0.32	0.31	0.66	0.80	0.32	0.31
K/NA	0.48	0.72	1.53	3.70	5.86	5.23
K+NA	3.19	2.98	3.58	3.71	4.48	3.05
FE2/TI	5.48	4.38	4.55	3.51	3.28	5.52
FE2/MG	1.65	2.28	2.63	3.38	3.36	2.52
FE2/FE3	2.59	1.97	2.38	1.78	1.62	1.42
100V/TI	2.67	1.96	1.02	0.45	0.92	0.83
RB/SR	0.03	0.10	0.22	0.67	0.43	0.63
SR/BA	1.73	0.66	0.28	0.17	0.17	0.05
100SR/K	4.62	1.93	0.55	0.22	0.26	0.19
100SR/CA	0.70	0.43	0.55	0.64	0.49	0.31
100RB/K	0.15	0.19	0.12	0.14	0.11	0.12
100RB/CA	0.02	0.04	0.12	0.43	0.21	0.19
CE/Y	1.94	2.71	3.18	4.15	3.46	4.69
LA/Y	1.25	2.29	3.30	2.91	2.20	4.94
100REE/CA	0.10	0.16	0.56	2.16	0.79	0.82
100REE/AL	0.08	0.12	0.15	0.20	0.18	0.15
REE/SC	2.13	2.81	4.50	9.09	6.66	4.53
REE/SR	0.14	0.37	1.01	3.36	1.62	2.63
NB/ZR	0.58	0.70	0.71	1.08	0.94	0.63
GA/ZN	3.28	0.25	0.15	0.22	0.49	0.17
NI/CO	0.63	0.68	0.87	1.19	0.24	1.73
ZN/V	0.02	0.25	0.60	1.05	0.24	0.62
GA/SR	0.04	0.09	0.17	0.36	0.21	0.36
.01TI/ZR	1.20	1.24	1.30	0.71	0.83	1.19

NOTE: All ratios are calculated based on the data in Table 2. See Appendix for notations.

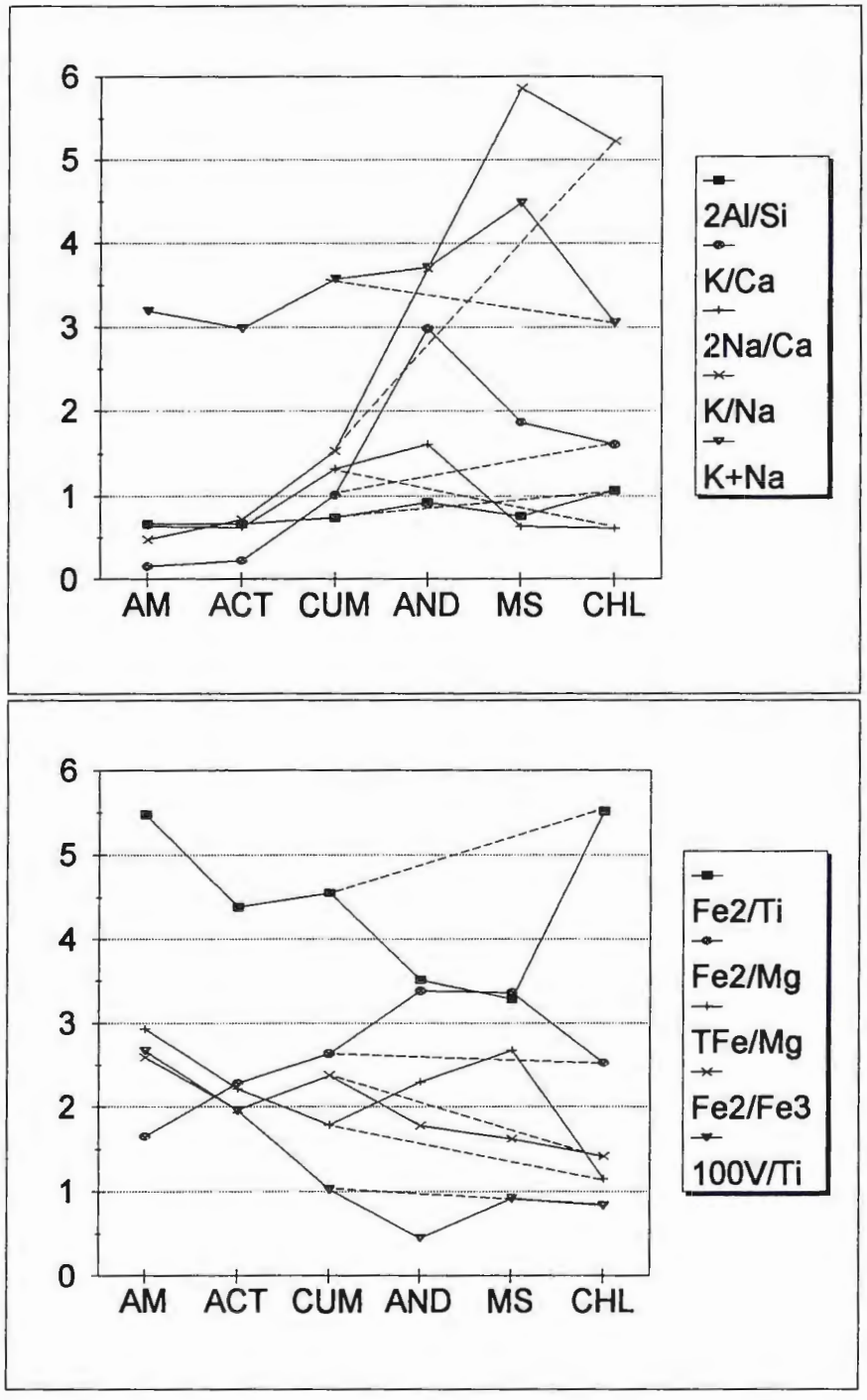

Fig. 14: Selected Element Atomic Ratios

Note: There is no andalusite or muscovite schist in the limb of the syncline.
See Appendix A for notations.

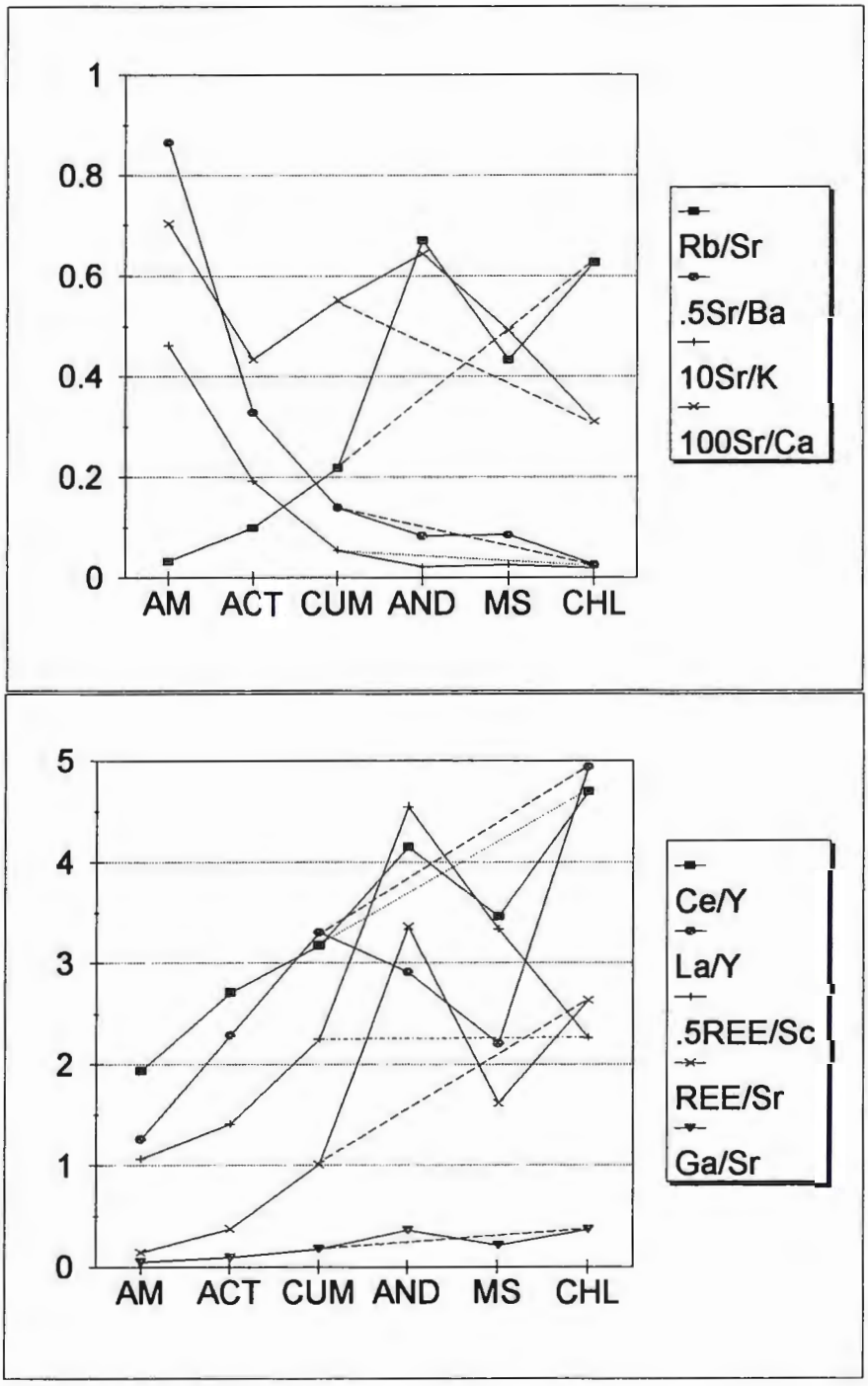

Fig. 14: Selected Element Atomic Ratios (continued)

Note: There is no andalusite or muscovite schist in the limb of the syncline.
See Appendix A for notations.

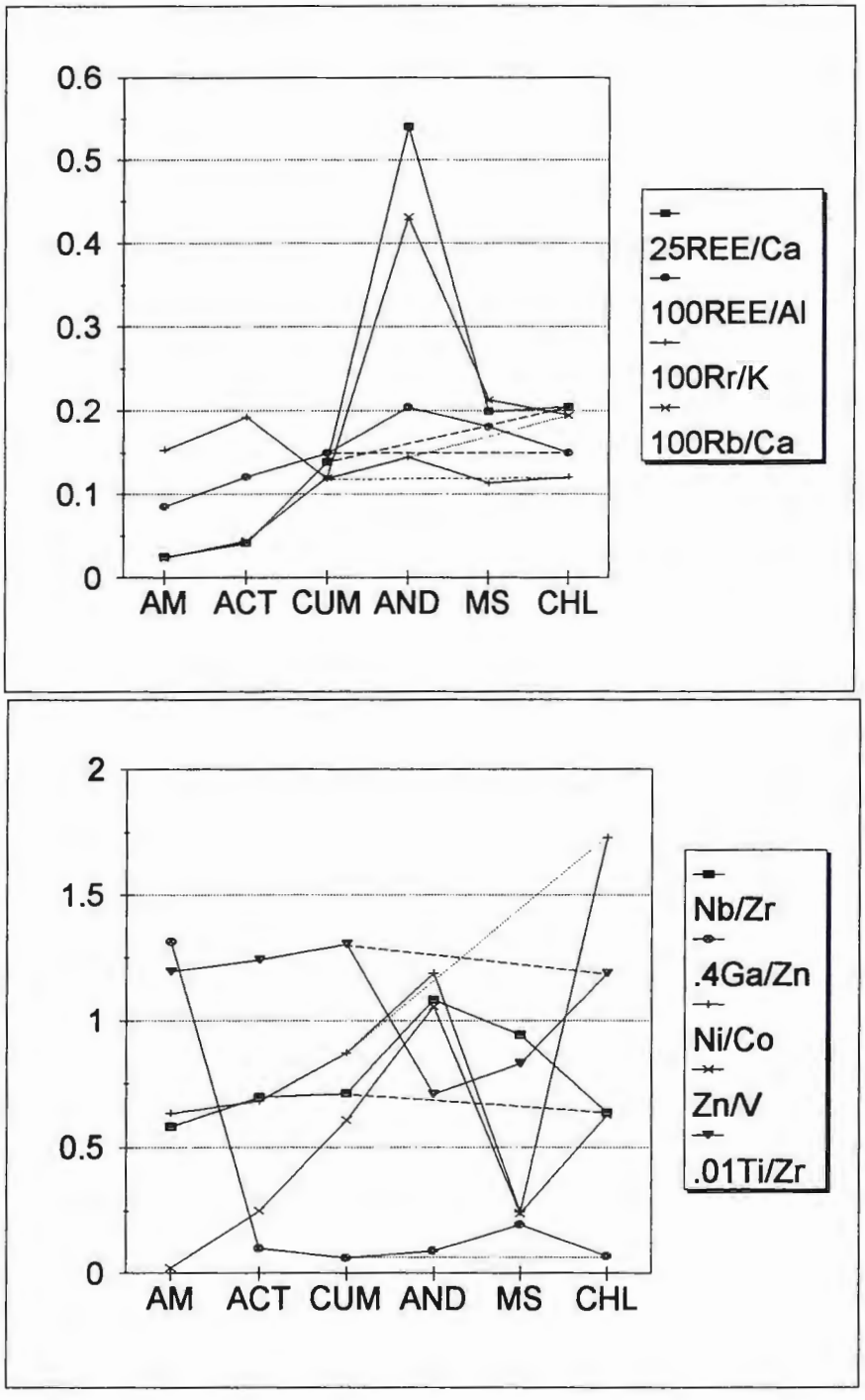

Fig. 14: Selected Element Atomic Ratios (continued)

Note: There is no andalusite or muscovite schist in the limb of the syncline.
See Appendix A for notations.

Table 4: Metadiabase Chemical Compositions for Traverses

TRAVERSE	T1	T2	T3	T4	T5
n	7	6	8	7	7
SIO2	45.89	46.66	40.14	52.09	45.34
TIO2	2.29	3.47	4.14	2.68	3.37
AL2O3	14.71	14.31	18.29	15.02	17.25
FE2O3	4.27	5.52	9.51	6.49	4.43
FEO	10.64	11.09	11.12	7.49	13.06
MGO	7.38	6.36	5.78	3.70	3.66
MNO	0.42	0.19	0.30	0.33	0.62
CAO	7.29	4.55	2.12	3.26	3.94
NA2O	2.51	1.72	1.74	1.01	1.33
K2O	1.21	2.27	2.85	3.89	3.51
P2O5	0.23	0.32	0.22	0.46	0.33
H2O+	2.56	3.00	3.28	2.59	2.37
H2O-	0.32	0.31	0.25	0.30	0.28
TFEO	14.91	16.61	20.64	13.98	17.49
BA	332	555	332	692	347
CE	43	53	75	87	50
CO	66	65	79	46	66
GA	20	21	21	22	22
LA	34	43	70	57	47
NB	23	30	32	44	31
NI	23	77	94	81	24
RB	15	29	19	47	42
SC	30	28	28	23	28
SR	329	153	117	74	134
V	307	283	183	172	190
Y	15	17	17	23	19
ZN	31	120	142	80	66
ZR	128	173	181	284	172

NOTE: Unit: oxide-wt%, element-ppm. Tn=Traverse number. See Fig. 4 for traverses' position.

the other trace elements from the center of metadiabases to the contact between the metadiabases and banded iron formation (Table 2 and Fig. 13). These changes result in increasing Al/Si, K/Na, K/Ca, Na/Ca, Rb/Sr, Rb/Ca, Ce/Y, La/Y, REE/Ca, Ni/Co, Zn/V and Ga/Sr ratios (Table 3, Fig. 14). Similar chemical changes are suggested from the limb to the keel of the syncline in the analysis of data in Table 4. For those metadiabases in the keel of the syncline, there are two distinct inflections along chemical composition and element ratio curves for all the elements. This is consistent with the fact that there are andalusite and muscovite schist in the keel which are not found in the limb (Figures 13 and 14). If all the metadiabases in both the limb and keel of the syncline formed from one protolith, then these chemical changes must reflect differences of the hydrothermal alteration and/or metamorphism between the keel and the limb.

3.3. MINERAL GEOCHEMISTRY

Mineral formulae are calculated by the computer software MINFILE (Afifi and Essene, 1988) based on microprobe data. Data for some minerals are normalized to avoid random analytical error and to compare the chemical changes of them in different rocks. Typical mineral chemical compositions and the calculated formulae are listed in Tables 5-10.

1. AMPHIBOLES

The amphibole species change from hornblende to cummingtonite or grunerite, which corresponds to increase of Si, Fe and Mg and decrease of Ti, Al, K and Na (Table 5). The distinct decrease of calcium and sodium in amphiboles may not result from the breakdown of calcium amphiboles and the formation of iron-magnesium amphiboles (e.g., Veblen and Ribbe, 1982), but reflect the changes in the bulk chemical composition of various metadiabases.

2. FELDSPAR

The An content of the relict plagioclase gradually decreases from 54 to 38, and of the recrystallized plagioclase from 45 to 34 (Table 6). The An content also decreases from the center to the rim of these relict plagioclases in amphibolite, actinolite schist and cummingtonite schist. The increasing sodium and Na/Ca ratio in plagioclase species are consistent with the change in the bulk rock chemical composition of the metadiabases (Table 6 vs. Table 2 and 3). The An content of the plagioclases included in various amphiboles, however, is nearly constant (An=30~32). The appearance of potassium feldspar in the relict peraluminous rocks within chlorite schist in the keel is distinctive and no potassium feldspar has been found in any other metadiabase.

Table 5: Amphibole Chemical Compositions

Rock Type	Amphibolite	Amphibolite	Cum Schist	Cum Schist	Cum Schist
Sample #	MI91039	MI91039	MI91119	MI91119	MI91220
SIO2	45.99	50.98	52.71	52.02	53.70
TIO2	0.57	0.23	0.06	0.06	0.09
AL2O3	11.49	5.14	1.41	1.73	1.07
CR2O3	0.06	0.04	0.05	0.05	0.01
FEO	17.76	15.77	27.87	29.23	24.80
MNO	0.28	0.30	0.36	0.30	0.56
MGO	9.54	13.21	13.92	14.65	18.07
CAO	11.41	12.32	1.84	0.48	0.29
NA2O	1.00	0.51	0.48	0.20	0.10
K2O	0.59	0.19	0.03	0.01	0.00
TOTAL	98.69	98.69	98.73	98.73	98.69
#SI IV	10.15	11.19	11.91	11.78	11.91
T SITE	10.15	11.19	11.91	11.78	11.91
#TI	2.99	1.33	0.38	0.46	0.28
#CR	0.09	0.04	0.01	0.01	0.02
#MG	0.01	0.01	0.01	0.01	0.00
M1,2,3	1.91	3.63	4.60	4.52	4.70
#MG	1.23	0.70	0.09	0.42	1.27
#FE+2	3.28	2.89	5.27	5.53	4.60
#MN	0.05	0.06	0.07	0.06	0.11
M4 SITE	4.56	3.65	5.42	6.01	5.98
#CA	2.70	2.90	0.45	0.12	0.07
#NA	0.43	0.22	0.21	0.09	0.04
#K	0.17	0.05	0.01	0.00	0.00
A SITE	3.29	3.16	0.66	0.21	0.11
#O	22.08	22.09	22.08	22.08	22.08
#OH	1.92	1.92	1.92	1.92	1.92

NOTE: See Appendix A for all notations.

Table 6: Feldspar Chemical Compositions

Rock Type	AM	AM	AM	AM	CUM	CUM	CUM	CUM	CHL
Sample #	MI91039	MI91039	MI91039	MI91039	MI91119	MI91119	MI91119	MI91119	MI91422
Mineral	RPL	RPL	CPL	IPL	RPL	RPL	CPL	IPL	Kfs
Position	C	R	C/R	C/R	C	R	C/R	C/R	C/R
SIO2	55.24	57.03	59.03	66.27	58.55	58.85	59.00	60.03	64.95
TIO2	0.00	0.00	0.00	0.03	0.00	0.06	0.04	0.01	0.04
AL2O3	29.40	28.38	27.71	24.48	26.32	25.07	25.93	25.33	19.01
CR2O3	0.02	0.02	0.02	0.05	0.05	0.00	0.04	0.00	0.00
FEO	0.10	0.15	0.17	0.21	0.33	1.00	0.38	0.16	0.18
MNO	0.02	0.03	0.00	0.00	0.00	0.11	0.06	0.00	0.00
MGO	0.05	0.03	0.07	0.03	0.02	0.44	0.01	0.02	0.01
CAO	10.30	9.14	7.69	3.87	7.72	7.29	7.00	6.72	0.02
NA2O	4.78	5.17	4.83	4.99	6.96	7.16	7.51	7.68	0.40
K2O	0.09	0.07	0.49	0.06	0.04	0.02	0.04	0.05	15.38
TOTAL	100.00	100.02	100.01	99.99	99.99	100.00	100.01	100.00	99.99
#SI+4	2.48	2.54	2.62	2.86	2.62	2.64	2.63	2.67	2.99
#TI+4	0.00	0.00	0.00	0.00	0.00	0.00	0.00	0.00	0.00
#AL+3	1.55	1.49	1.45	1.25	1.39	1.32	1.36	1.33	1.03
#CR+3	0.00	0.00	0.00	0.00	0.00	0.00	0.00	0.00	0.00
#FE+2	0.00	0.01	0.01	0.01	0.01	0.04	0.01	0.01	0.01
#MN+2	0.00	0.00	0.00	0.00	0.00	0.00	0.00	0.00	0.00
#MG+2	0.00	0.00	0.00	0.00	0.00	0.03	0.00	0.00	0.00
#CA+2	0.50	0.44	0.36	0.18	0.37	0.35	0.33	0.32	0.00
#NA+1	0.42	0.45	0.41	0.42	0.60	0.62	0.65	0.66	0.04
#K+1	0.01	0.00	0.03	0.00	0.00	0.00	0.00	0.00	0.90
#TOTAL	4.96	4.93	4.88	4.72	4.99	5.01	5.01	5.00	4.97
#O-2	8.00	8.00	8.00	8.00	8.00	8.00	8.00	8.00	8.00
AN	0.54	0.49	0.45	0.30	0.38	0.36	0.34	0.32	0.00
AB	0.45	0.50	0.51	0.70	0.62	0.64	0.66	0.67	0.04
OR	0.01	0.00	0.03	0.01	0.00	0.00	0.00	0.00	0.96

* R=Rim, C=Center of mineral. RPL, CPL and IPL are Relict, Crystallized and Included Plagioclase, respectively.

3. PHYLLOSILICATES

In general, the annite content and Fe^{+2}/Mg^{+2} ratio of biotite increases from andalusite schist to muscovite schist and chlorite schist, and no big difference of alkali content exists between biotites and between muscovites in various metadiabases (Table 7). There is also little chemical variation within mica mineral grains. However, the chemical difference between the biotite in contact with the rim, the middle zone and center of garnets is distinct. The chemical variation of these biotites corresponding to the chemical differences of garnet with which they are in contact provides important information of physical and chemical conditions during their formation (section 4.2). There is abundant sericite and chlorite included in other mineral grains or along their fractures and/or edges. They, however, can not be confirmed as equilibrium minerals with others and forming at the same time during the regional metamorphism.

4. GARNET AND ITS ZONING

Garnet occurs where all the amphiboles and plagioclases are completely absent in the metadiabases, with increase in the abundances of biotite and quartz. From the limb to the keel of the syncline and from andalusite schist to muscovite and chlorite schist, the diameter of garnet mineral grains and the amount of garnet increase. Garnets in muscovite and andalusite schists are

Table 7: Mica Chemical Compositions

Rock Type	AND	MUS	CHL	CHL	CHL	AND	MS
Sample #	MI91318	MI91420	MI91422	MI91422	MI91422	MI91318	MI91422
Mineral	BIO	BIO	BIO	BIO	BIO	MS	MS
* Position	RIM	RIM	RIM	MIDDLE	CENTER	RIM	RIM
SIO2	33.47	33.22	34.84	30.73	28.84	48.08	46.12
TIO2	1.85	1.78	1.70	1.25	1.27	0.04	0.45
AL2O3	18.32	18.86	20.35	20.40	19.47	37.77	37.41
CR2O3	0.03		0.06	0.00	0.06	0.11	0.06
FEO	24.61	26.94	21.74	28.76	30.38	0.97	1.67
MNO	0.09	0.06	0.03	1.36	1.58	0.03	0.02
MGO	10.40	6.10	8.82	4.98	5.24	0.17	0.42
CAO	0.11	0.04	0.01	0.16	0.21	0.07	0.01
NA2O	0.07	0.04	0.16	0.17	0.18	0.52	
K2O	7.04	9.14	8.25	8.20	8.67	8.02	8.75
TOTAL	95.99	96.18	96.02	96.07	95.89	95.16	95.43
#SI IV	5.15	5.22	5.28	4.91	4.71	6.25	6.07
#AL VI	2.85	2.78	2.72	3.09	3.29	1.75	1.93
T SITE	8.00	8.00	8.00	8.00	8.00	8.00	8.00
#AL VI	0.47	0.71	0.92	0.75	0.47	4.03	3.87
#TI VI	0.21	0.21	0.19	0.15	0.16	0.00	0.04
#CR VI	0.00	0.00	0.01	0.01	0.01	0.01	
#FE+2	3.17	3.54	2.76	3.84	4.15	0.11	0.18
#MN+2	0.01	0.01	0.00	0.18	0.22	0.00	0.00
#MG+2	2.39	1.43	1.99	1.19	1.28	0.03	0.08
O SITE	6.25	5.90	5.88	6.13	6.28	4.18	4.18
#CA+2	0.02	0.01	0.00	0.03	0.04	0.01	0.00
#NA+1	0.02	0.01	0.05	0.05	0.06	0.13	
#K+1	1.38	1.83	1.60	1.67	1.81	1.33	1.47
A SITE	1.42	1.85	1.64	1.75	1.90	1.34	1.60
#MG/FE+2	0.76	0.40	0.73	0.31	0.31	0.31	0.45
xMg	0.38	0.24	0.34	0.19	0.20	0.01	0.02
xFe	0.51	0.60	0.47	0.63	0.66	0.03	0.04
xTi	0.03	0.04	0.03	0.02	0.03	0.00	0.01
xAl	0.08	0.12	0.16	0.12	0.07	0.96	0.93
xK	0.99	0.99	0.97	0.97	0.97	0.91	1.00
xNa	0.01	0.01	0.03	0.03	0.03	0.09	0.00

NOTE: Position=the position of garnets the micas contact with.

Table 8: Garnet Chemical Compositions

Rock Type	And Schist	Ms Schist	Chl Schist	Chl Schist	Chl Schist
Sample #	MI91318	MI91420	MI91422	MI91422	MI91422
Position	Rim	Rim	Rim	Middle	Center
SIO2	36.09	37.27	36.33	36.04	36.05
TIO2	0.05	0.06	0.07	0.08	0.04
AL2O3	21.63	21.23	20.69	20.79	20.66
CR2O3	0.00	0.00	0.03	0.00	0.03
FE2O3	0.26	0.00	1.22	1.07	0.77
FEO	33.51	36.11	34.87	31.04	35.83
MNO	3.58	2.99	3.35	9.94	2.87
MGO	1.98	1.24	1.54	0.90	1.36
CAO	2.87	1.00	2.14	0.79	2.18
TOTAL	99.98	99.89	100.09	100.01	100.09
#SI IV	5.84	5.98	5.90	5.92	5.88
#AL IV	0.16	0.02	0.12	0.12	0.13
T SITE	6.00	6.00	6.00	6.00	6.00
#AL VI	3.96	3.99	3.86	3.94	3.86
#TI VI	0.01	0.01	0.01	0.01	0.00
#CR VI	0.00	0.00	0.00	0.00	0.00
#FE +3	0.03	0.00	0.15	0.13	0.09
O SITE	4.00	4.00	4.01	4.00	4.00
#FE+2	4.53	4.84	4.74	4.26	4.89
#MN+2	0.49	0.41	0.46	1.38	0.40
#MG+2	0.48	0.30	0.37	0.22	0.33
#CA+2	0.50	0.17	0.37	0.14	0.38
A SITE	6.00	5.72	5.94	6.00	6.00
#O	23.92	23.71	23.91	23.96	23.95
#MG/FE+2	0.11	0.06	0.08	0.05	0.06
GR	0.08	0.03	0.06	0.02	0.06
PY	0.08	0.05	0.06	0.04	0.05
ALM	0.76	0.85	0.80	0.71	0.82
SP	0.08	0.07	0.08	0.23	0.07

NOTE:See Appendix A for all notations.

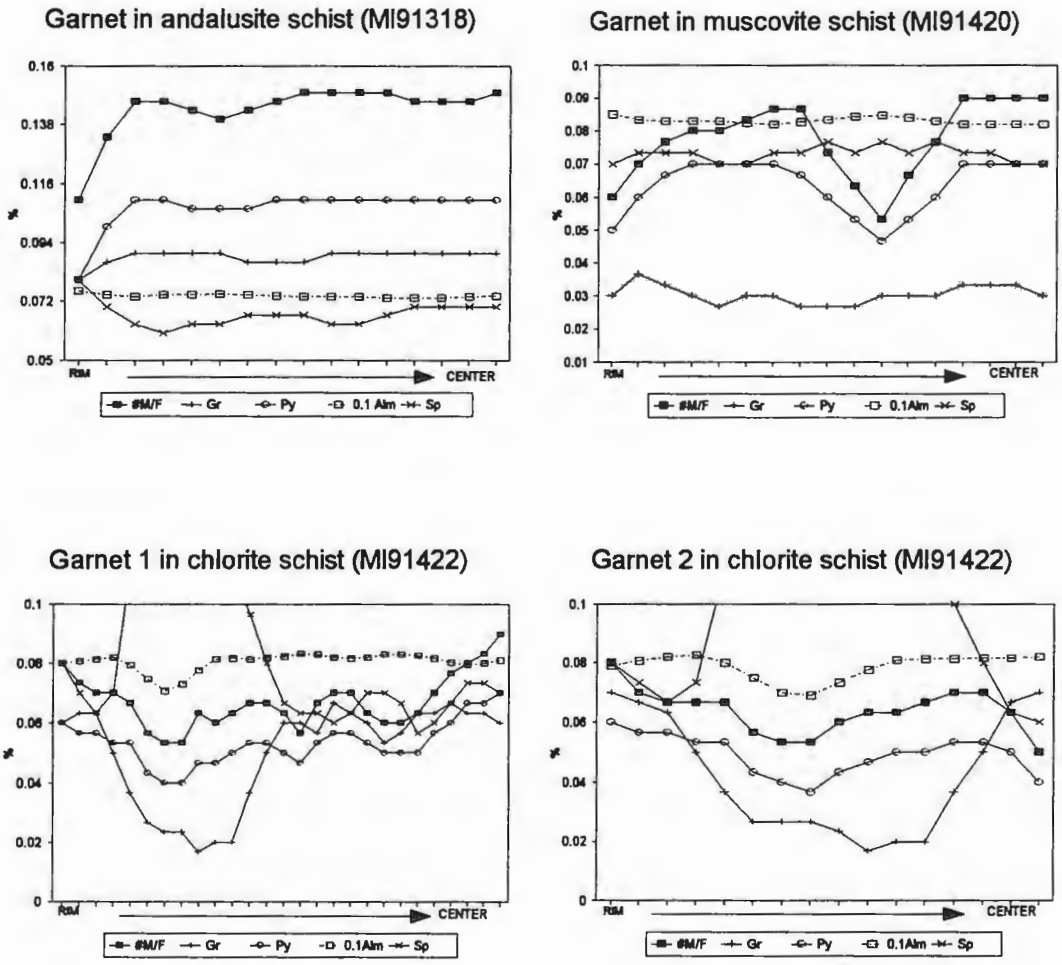

Fig. 15: Garnet Chemical Zoning

Note: #M/F=Mg/Fe atomic ratio. See Table 8 for plotting data and Appendix A for notations.

zoned, with core and rim (Fig. 15). Zoning of garnet in chlorite schist is very distinctive and consists of core, middle zone and rim (Table 8; Fig. 15). These zoned garnets with their coexisting minerals recorded information about P-T-X-t paths as discussed in the next chapter.

5. IRON AND IRON-TITANIUM OXIDES

Ulvospinel-magnetite exsolution textures in a single mineral grain with rounded or other irregular shapes are found in various metadiabases, indicating that these grains of ulvospinel-magnetite have undergone hydrothermal alteration. Ulvospinel, however, may be either the exsolution lamellae from ulvospinel-magnetite solid solution during magmatism or the product of oxidation of the magmatic ilmenite-magnetite solid solution during hydrothermal alteration (Klein and Hurlbut, 1985). The rutile in contact with ulvospinel shows distinctly low titanium and high iron content (Table 10). For metamorphic ilmenite, magnetite mole fraction increases from amphibolite to chlorite schist (Table 9), correlative with increasing titanium content in metamorphic rutile. No distinct difference in ulvospinel mole fraction between the magnetites of various metadiabases has been found so far. The constant and low ulvospinel content of magnetite and high ilmenite mole fraction in ilmenite indicate little variation in redox conditions and possibly low oxygen fugacity in the system (Section 4.3).

Table 9: Ilmenite Chemical Compositions

Rock Type	Amphibolite	Cum Schist	And Schist	Ms Schist	Chl Schist
Sample #	MI91039	MI91220	MI91319	MI91420	MI91422
SIO2	0.09	0.07	0.07	0.00	0.13
TIO2	52.18	50.13	49.59	49.16	47.37
AL2O3	0.05	0.03	0.04	0.02	0.62
CR2O3	0.04	0.05	0.06	0.25	0.35
FEO	44.59	48.42	47.35	45.70	50.49
MNO	1.81	1.25	2.73	4.77	0.98
MGO	0.20	0.03	0.06	0.00	0.04
CAO	0.95	0.02	0.02	0.10	0.02
TOTAL	99.93	99.98	99.92	100.00	99.99
#TI	0.99	0.95	0.94	0.93	0.89
#AL	0.00	0.00	0.00	0.00	0.02
#CR	0.00	0.00	0.00	0.01	0.01
#FE+3	0.02	0.10	0.12	0.14	0.18
#FE+2	0.92	0.92	0.88	0.82	0.87
#MN	0.04	0.03	0.06	0.10	0.02
#MG	0.01	0.00	0.00	0.00	0.00
#CA	0.03	0.00	0.00	0.00	0.00
xIlm	0.99	0.95	0.94	0.93	0.91
xMt	0.01	0.05	0.06	0.07	0.09

* Fomulae calculated using MINFILE (Afifi & Essene, 1988). See Appendix A for all notations.

Table 10: Other Oxide Chemical Compositions

Rock Typ	CUM	AND	MUS	AND	AND	CUM	AND	CHL	CHL
Sample #	MI91220	MI91318	MI91420	MI91318	MI91318	MI91220	MI91318	MI91422	MI91422
Mineral	Rt	Rt	Rt	Rt	Usp	Mt	Mt	Mt	Hm
Genesis	META	META	META	MAG	MAG	META	META	META	META
SIO2	0.08	0.15	0.18	0.12	0.12	0.04	0.14	0.23	0.14
TIO2	98.72	98.42	93.11	87.12	15.55	0.48	0.41	0.34	0.31
AL2O3	0.00	0.21	0.07	0.07	0.07	0.21	0.19	0.16	0.14
CR2O3	0.19	0.11	0.05	0.02	0.00	0.02	0.02	0.01	0.00
FEO*	0.89	0.89	6.31	12.48	84.14	98.40	98.73	99.06	99.19
MNO	0.00	0.08	0.01	0.08	0.07	0.01	0.01	0.00	0.12
MGO	0.03	0.03	0.04	0.00	0.00	0.00	0.04	0.08	0.03
CAO	0.05	0.06	0.17	0.03	0.95	0.03	0.02	0.00	0.00
TOTAL	99.96	99.96	99.94	99.93	99.95	99.22	99.56	99.89	99.93
#SI+4	0.00	0.00	0.00	0.00	0.00	0.00	0.01	0.01	0.00
#TI+4	0.99	0.99	0.96	0.92	0.43	0.01	0.01	0.01	0.01
#AL+3	0.00	0.00	0.00	0.00	0.00	0.01	0.01	0.01	0.00
#CR+3	0.00	0.00	0.00	0.00	0.00	0.00	0.00	0.00	0.00
#FE+3	0.00	0.00	0.00	0.00	1.16	1.96	1.96	1.95	1.98
#FE+2	0.01	0.01	0.07	0.15	1.41	1.01	1.01	1.01	0.00
#MN+2	0.00	0.00	0.00	0.00	0.00	0.00	0.00	0.00	0.00
#MG+2	0.00	0.00	0.00	0.00	0.00	0.00	0.00	0.00	0.00
#CA+2	0.00	0.00	0.00	0.00	0.00	0.00	0.00	0.00	0.00
#TOTAL	1.01	1.01	1.04	1.08	2.99	3.00	3.00	3.00	2.00
xRut	0.99	0.98	0.92	0.86					
xMt					0.86	0.99	0.99	0.99	
xUsp					0.14	0.01	0.01	0.01	0.01
xHm									0.99

NOTE: META=metamorphic, MAG=magmatic; see Appendix A for all notations.

3.4. PROTOLITH OF METADIABASES

Based on the discussion above, the following evidence leads one to conclude that all metadiabases are the metamorphosed and hydrothermally altered products of Early Proterozoic diabase.

(1) Early Proterozoic metadiabase layers are interlayered with the Negaunee banded iron formation in the whole region, and so are the altered metadiabases in the Republic Mine. The unaltered metadiabases outside of the mine grade to altered metadiabases which are similar to the least-altered metadiabase in the mine. Continuous layers of amphibolite are found only in the limb but there are still a few small relict amphibolite bodies in the keel of the syncline. These amphibolite bodies with various other metadiabases are interlayered within the Negaunee banded iron formation, suggesting that they were previously the same unit of the Early Proterozoic diabases in the Republic Mine prior to the hydrothermal alteration and metamorphism.

(2) The unaltered Early Proterozoic metadiabases outside of the mine still retain their typical mineral assemblages plagioclase-

pyroxene and olivine and diabasic fabrics. The altered metadiabases at the center of metadiabases in the limb still keep their mafic chemical characteristics. They gradually change their chemical composition toward the contact between them and the banded iron formation (Fig. 13 and 14, Table 2), suggesting a gradual hydrothermal alteration process to form these metadiabases from a diabasic protolith. These chemical changes are one of main factors controlling the changes in mineral assemblages and the amount of different mineral species.

(3) Typical diabasic texture and mineral assemblages olivine, pyroxene and plagioclase can only be observed in the metadiabases outside of the Republic Mine. In the mine, there are many relict minerals and fabrics inherited from diabases, such as extensive pseudomorphic textures, relict diabasic texture, and especially magmatic magnetite-ulvospinel exsolution texture in all the rock types (Section 3.3.5), suggesting hydrothermal alteration of the Early Proterozoic diabases. These relict minerals and fabrics gradually diminish from the center of the metadiabases to the contact and from the limb to the keel of the syncline.

3.5. ISOCON ANALYSIS

1. INTRODUCTION

Based on Gresens (1967), isocon analysis compares concentrations of species in a protolith and in its altered products to evaluate mass changes for each species and for whole rocks during various geological processes (Grant, 1986). Isocon analysis results combined with geological analysis can be used to unravel the characteristics of different geological processes (e.g., Olsen and Grant, 1991). The isocon method directly uses the measured concentration of species without converting mass to volume units or assuming constant volume of altered rocks compared to their protolith (e.g., Barth, 1952; Gresens, 1967). In a graph of concentrations in an altered rock against these in its protolith, all the points representing the immobile elements should be on a straight line through the origin. This line is the isocon with a slope K_{iso}. $K_{iso}>1$ means mass loss, $K_{iso}<1$ indicates mass gain, and $K_{iso}=1$ indicates that the total mass was constant in the alteration process although there might be mass gain for some elements and mass loss for some others. The slope K_i is the ratio of a mobile element *i* in an altered rock to its protolith with the reference of K_{iso}. $Ki>K_{iso}$ means mass gain while $K_i<K_{iso}$ stands for mass loss of this species. The basic equations, the procedure and various

chemographic approaches of the isocon analysis are briefly described in Appendix E. A small computer program of isocon analysis is available from the author.

2. DISCUSSION

The first important consideration for using the isocon method is to chose the "protolith". Several lines of evidence indicate that the protolith for all the metadiabases in the study area is the Early Proterozoic diabase which is probably associated with rocks of the Clarksburg Volcanics Member of the Michigamme Formation (Section 3.4). There is no chemical analysis of unaltered primary Early Proterozoic diabase outside of the Republic mine in this study. The least-altered metadiabase amphibolite, therefore, may be the best choice of "protolith" in the Republic Mine because it has very similar chemical composition to typical diabases (Section .2). The altered products with different chemical composition may be subject to later metamorphism and/or hydrothermal alteration so that they can serve as the new "protoliths" during succeeding geological processes (Section 5.1). These geological processes may be overlapped with each other, making the observed results very complicated. It is therefore wise to compare the results from using amphibolite as the protolith for all altered metadiabases with those using all the possible "protoliths" for their possible altered products. It is clear that the isocon analysis

will mainly reflect changes in mass and chemical composition during pre-metamorphic hydrothermal alteration (see Section 5.1). The retrograde metamorphism may partially change the chemical compositions of these metadiabases, but it is mostly localized near the contact between the metadiabases and banded iron formation. If the mass and chemical composition as well as the isocon slopes for a series of rocks change continuously and systematically, then it is reasonable to assume that they are altered from the same protolith during a single geological process although the amount of these changes may be different. On the other hand, if there are no such systematics observed, these rocks may form either from different protoliths or under different physical and chemical conditions during different geological processes. It is therefore better to plot a series of rocks in one isocon diagram so that the systematic changes can be observed and irregular changes can be found.

The second consideration is the choice of the "immobile" species to define isocons. Mobility of elements can be evaluated through the comparison of all chemical species between protolith and its altered products. Immobile major rather than trace elements generally serve better for evaluating the mass change of rocks during various geological processes because they dominate the changes in both mass and chemical composition of rocks and because their relative analytical error is far smaller than that of trace elements. For this reason, some major elements with minor amounts, such as phosphorus

and manganese, will be excluded as the reference to evaluate the mass change. The distinct increase of iron, potassium and water and decrease of calcium, sodium and magnesium from amphibolite to chlorite schist suggest their high mobility, which is consistent with the variation of mineral mode and mineral assemblages (Table 1, 2 and 11). Titanium is concentrated in oxides and inosilicates so that the change of the mode of these minerals may affect the concentration of titanium in the system. If titanium is in the form of iron-titanium oxides, it is generally inert during most geological processes if there is no distinct changes in oxygen fugacity, especially during metamorphism (Liu, 1984). On the scale of a thin section, migration of silicon is common (e.g., quartz in the pressure shadow of porphyroblasts or as mm-scale quartz veins). Abundant quartz veins with widths from few mm to tens of cm are widely distributed in all types of metadiabases and silicon gradually decreases from amphibolite to chlorite schist. This suggests that silicon released from preexisting minerals was partially lost, especially from the rocks in the limb. Due to the large amount of silicon comparing to the amount of other chemical components in the system, if the change of silicon is not very large it may still be a good reference to evaluate the mass changes of rock series in some circumstances. A constant-aluminum isocon is chosen because the immobility of aluminum under most geological physical and chemical conditions, as in the research area, is a common observation worldwide (e.g., Korzhinskii, 1970; Carmichael and others, 1970). Aluminum from the decomposition of high calcic plagioclases, pyroxene ard

olivine during hydrothermal alteration can remain in the system, constituting newly formed aluminum silicates. All the calculation of mass balance in Tables 11 and almost all the diagrams are based on constant aluminum. However, aluminum, titanium and/or silicon will be combined together to graphically evaluate more complicated mass and chemical changes.

3. ISOCON ANALYSIS RESULTS

At first, all the data are plotted in one diagram to evaluate the isocons graphically and to compare all the elements of various metadiabases (e.g., Fig 16 and 17). Statistics are used to define the best-fit constant aluminum isocons (Appendix E3). Isocon slopes are used to evaluate the total mass gain or loss for whole rocks. Different types of isocons are calculated and plotted for the comparison between different rock types (Fig. 16~21, Table 11): (1) isocons for all the schists against the least-altered metadiabase: amphibolite (Fig. 16) and against their adjacent metadiabases (Fig. 17); (2) isocons for the main rock series: amphibolite-actinolite-cummingtonite-chlorite schist (Fig. 18); (3) isocons for comparing andalusite and muscovite schist against cummingtonite schist (Fig. 19) and against chlorite schist (Fig. 20); and (4) an isocon for andalusite schist against muscovite schist (Fig. 21).

(1) The isocon for actinolite schist compared to amphibolite is based on constant aluminum. The isocon K_{12} on Figure 16 or 17 has a slope of 0.95, indicating about 5 percent mass gain for actinolite schists during hydrothermal alteration process (Table 11). Compared to amphibolite, manganese, titanium, iron, potassium, phosphorus and water were enriched, silicon kept constant and sodium, calcium and magnesium were lost. Most minor elements were also enriched, except that strontium was lost, corresponding to the loss of calcium because of their similar geochemical behavior.

(2) The isocon for cummingtonite schist compared to amphibolite is based on aluminum. It is K_{13} on Figure 16 or 18, with a slope of 1.02, or about 2 percent mass loss (Table 11). There is major loss of calcium and sodium, some loss of silicon and magnesium and distinct enrichment of potassium, titanium, phosphorus, iron, manganese and water (Table 11). Most trace elements were enriched and there is distinct loss of those elements with similar geochemical behavior to calcium.

Comparing cummingtonite schist to actinolite schist, a constant-aluminum isocon is K_{23} on Figure 17 with a slope of 1.07 and indicates a 7 percent mass loss, with the major gain in potassium and water and the distinct loss of calcium and sodium.

TABLE 11: MASS BALANCE OF METADIABASES

Rp-a	R1-2	R1-3	R1-4	R1-5	R1-6	R2-3	R3-4	R4-5	R5-6	R3-5	R3-6	R6-5	R6-4	R5-4
Kiso	K12	K13	K14	K15	K16	K23	K34	K45	K56	K35	K36	K65	K64	K54
SLOPE	0.95	1.02	1.34	1.16	1.12	1.07	1.31	0.86	0.97	1.13	1.09	1.04	1.20	1.16
ROCK	0.05	-0.02	-0.25	-0.13	-0.10	-0.07	-0.24	0.16	0.04	-0.12	-0.08	-0.03	-0.16	-0.14
SIO2	0.00	-0.10	-0.28	-0.12	-0.37	-0.10	-0.20	0.21	-0.29	-0.03	-0.31	0.40	0.15	-0.18
TIO2	0.61	0.79	0.38	0.47	0.52	0.11	-0.23	0.07	0.04	-0.18	-0.15	-0.04	-0.10	-0.06
AL2O3	0.00	0.00	0.00	0.00	0.00	0.00	0.00	0.00	0.00	0.00	0.00	0.00	0.00	0.00
FE2O3	0.70	0.62	0.29	0.40	1.81	-0.05	-0.21	0.09	1.00	-0.13	0.73	-0.50	-0.54	-0.08
FEO	0.29	0.48	-0.12	-0.12	0.53	0.15	-0.41	-0.00	0.75	-0.41	0.03	-0.43	-0.42	0.00
MNO	0.71	0.41	0.20	0.50	4.29	-0.18	-0.15	0.25	2.54	0.06	2.75	-0.72	-0.77	-0.20
CAO	-0.14	-0.69	-0.89	-0.74	-0.79	-0.64	-0.65	1.41	-0.19	-0.15	-0.32	0.24	-0.48	-0.59
MGO	-0.07	-0.07	-0.57	-0.57	0.00	-0.00	-0.54	0.00	1.33	-0.54	0.08	-0.57	-0.57	-0.00
K2O	0.28	1.06	1.13	2.23	1.23	0.61	0.03	0.51	-0.31	0.56	0.08	0.44	-0.05	-0.34
NA2O	-0.16	-0.36	-0.73	-0.74	-0.80	-0.24	-0.57	-0.04	-0.22	-0.59	-0.68	0.29	0.35	0.05
P2O5	0.40	0.72	0.34	1.04	0.27	0.23	-0.22	0.52	-0.38	0.18	-0.27	0.61	0.06	-0.34
H2O+	0.16	0.82	0.39	0.62	1.93	0.56	-0.24	0.17	0.80	-0.11	0.61	-0.45	-0.53	-0.14
H2O-	0.40	1.17	0.22	0.61	2.86	0.55	-0.44	0.32	1.40	-0.26	0.78	-0.58	-0.68	-0.24
TFE	0.41	0.53	0.00	0.04	0.92	0.08	-0.34	0.03	0.85	-0.32	0.26	-0.46	-0.48	-0.03
NB	0.26	0.20	0.40	0.41	-0.02	-0.05	0.16	0.01	-0.30	0.17	-0.18	0.43	0.42	-0.01
ZR	0.55	0.64	1.33	1.12	0.53	0.06	0.42	-0.09	-0.28	0.29	-0.07	0.38	0.52	0.10
Y	0.00	-0.01	0.25	0.34	-0.30	-0.01	0.27	0.07	-0.48	0.36	-0.30	0.92	0.80	-0.07
SR	-0.47	-0.76	-0.90	-0.82	-0.91	-0.54	-0.59	0.84	-0.49	-0.25	-0.62	0.96	0.07	-0.46
RB	0.60	0.60	1.01	1.40	0.76	0.00	0.25	0.19	-0.26	0.49	0.10	0.36	0.14	-0.16
GA	0.11	-0.03	-0.17	-0.10	-0.21	-0.13	-0.14	0.08	-0.12	-0.07	-0.18	0.14	0.05	-0.08
NI	0.35	0.97	0.62	-0.66	3.85	0.46	-0.18	-0.79	13.12	-0.83	1.46	-0.93	-0.67	3.72
CO	0.26	0.43	-0.13	-0.11	0.77	0.14	-0.40	0.03	0.99	-0.38	0.24	-0.50	-0.51	-0.03
CE	0.40	0.62	1.68	1.40	0.69	0.16	0.65	-0.11	-0.29	0.48	0.04	0.42	0.59	0.12
V	0.18	-0.32	-0.77	-0.50	-0.52	-0.42	-0.66	1.17	-0.06	-0.26	-0.30	0.06	-0.51	-0.54
LA	0.83	1.60	1.91	1.36	1.75	0.42	0.12	-0.19	0.16	-0.09	0.05	-0.14	0.06	0.23
BA	0.41	0.50	0.03	0.86	2.06	0.07	-0.32	0.81	0.64	0.24	1.04	-0.39	-0.66	-0.45
SC	0.08	-0.17	-0.44	-0.32	-0.17	-0.23	-0.32	0.21	0.22	-0.18	-0.00	-0.18	-0.32	-0.17
ZN	13.72	19.56	11.16	5.01	13.77	0.40	-0.41	-0.51	1.46	-0.71	-0.28	-0.59	-0.18	1.02

NOTE: Rp-a=a(ltered) rock against its p(rotolith); see Appendix A for alll other notations.

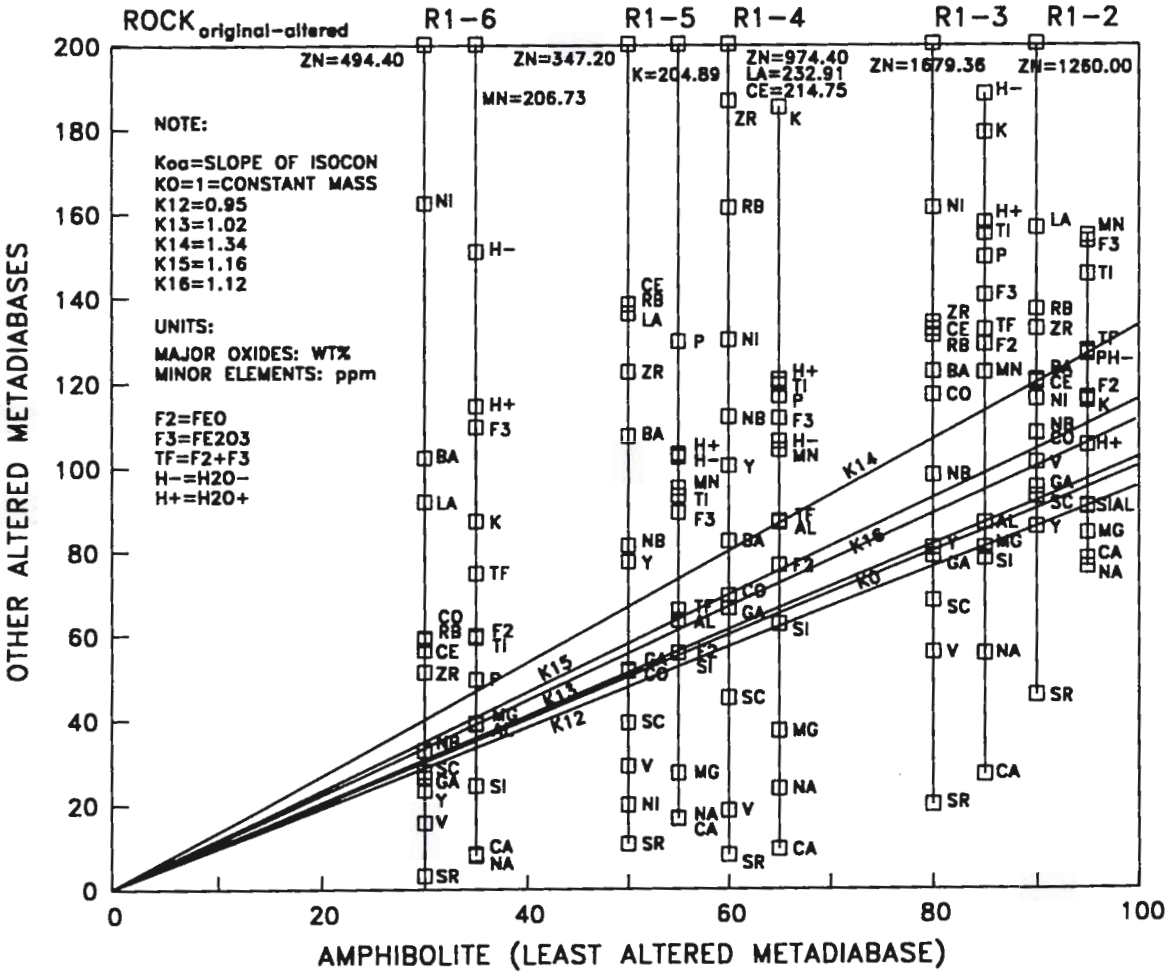

Fig. 16: Isocon Analysis (vs. Amphibolite)

Note: R1-2 means Rock 1 as "protolith" and Rock 2 as altered product, and K12 is its isocon, etc.. See Table 12 for all the calculated results and Appendix A for notations.

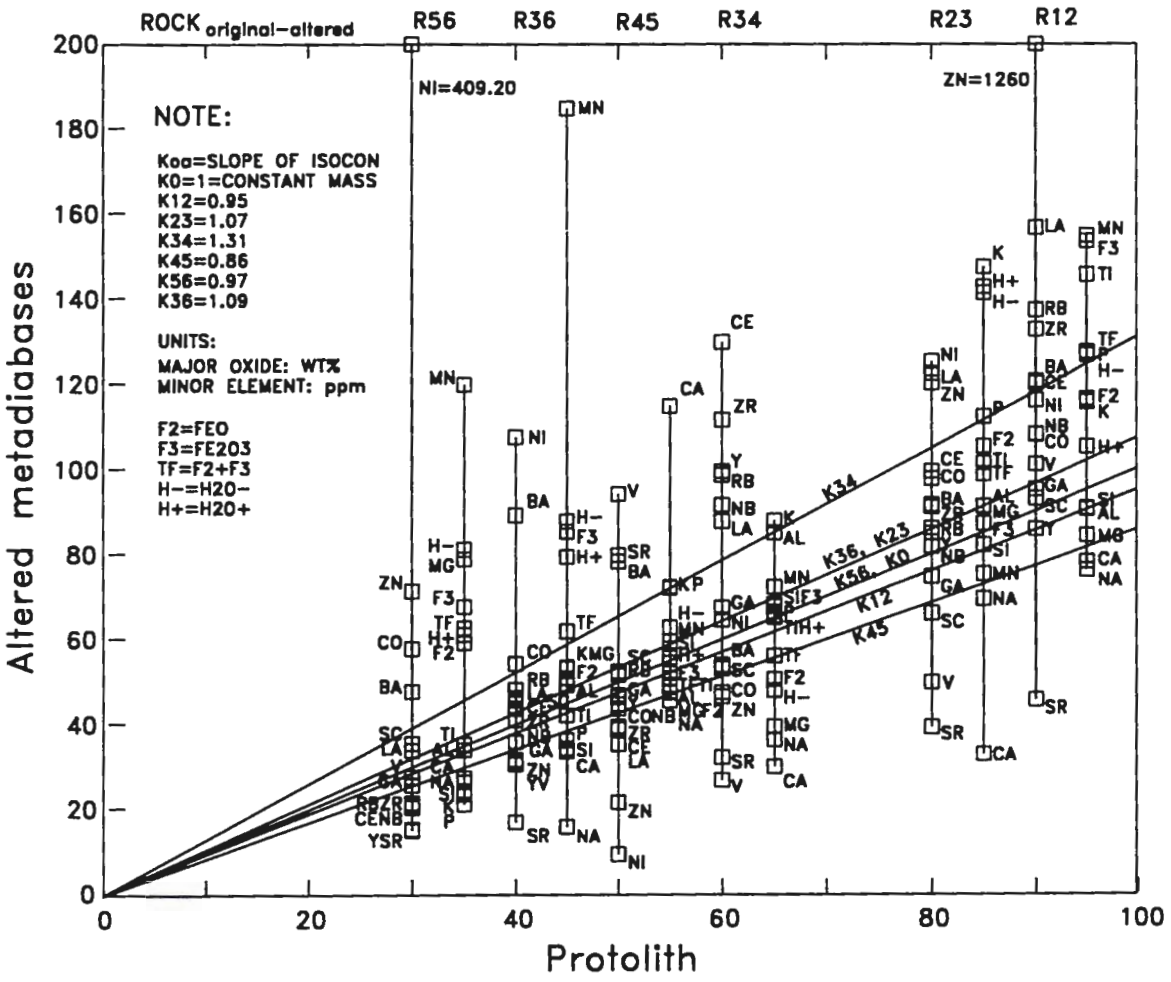

Fig. 17: Isocon Analysis (vs. Adjacent rocks)

Note: R12 means Rock 1 as "protolith" and Rock 2 as altered product, and K12 is its isocon, etc.. See Table 12 for all the calculated results and Appendix A for notations.

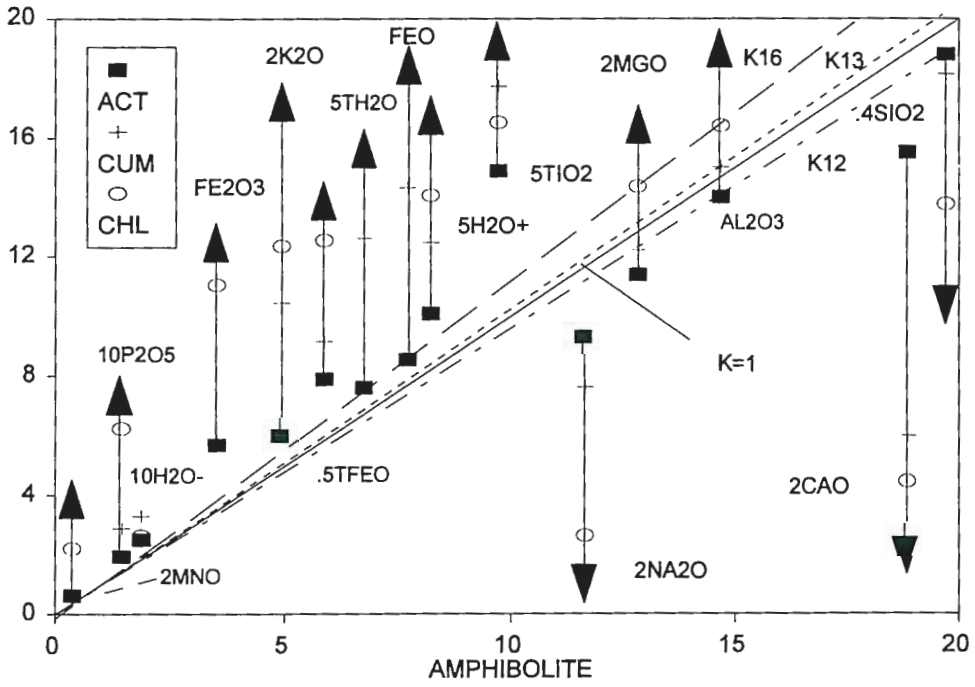

Fig. 18: Isocon Analysis (AM-ACT-CUM-CHL Main Series)

Note: K12, K13 and K16 are the isocons for actinolite, cummingtonite and chlorite schist against amphibolite, respectively. See the text and Table 12 for details. See Appendix A for notations.

(3) The isocon for the comparison of andalusite schist with amphibolite is K_{14} on Figure 16 based on constant aluminum. It has a slope of 1.34, corresponding to the largest (25 percent) mass loss in all the comparisons of various schists with amphibolite. Calcium, sodium, magnesium, silicon and Fe^{+2} were lost and other major elements were gained in andalusite schist. Total iron remained constant, while Fe^{+3} was gained and Fe^{+2} lost, indicating oxidation (Table 11).

Comparing andalusite schist to the adjacent cummingtonite schist, a constant-aluminum isocon (K_{34} on Figure 17 or 19) has a slope of 1.31 which is very closed to K_{14}, indicating about 24 percent mass loss (Table 11). All the major elements except aluminum and potassium were lost. If andalusite schist formed from chlorite schist, the total mass gain would be about 16 percent, with major mass gain of silicon, sodium, phosphorus and most trace elements, and loss of all other major elements (K_{64}, Table 11 and Fig. 20).

(4) The isocon for the comparison of muscovite schist with amphibolite is K_{15} on Figure 16, again based on aluminum. It has a slope of 1.16, indicating 13 percent mass loss, with the loss of silicon, sodium, calcium, magnesium and Fe^{+2} and the gain of potassium, manganese and titanium (Table 11). Total iron remains constant but Fe^{+3} was gained, again indicating oxidation.

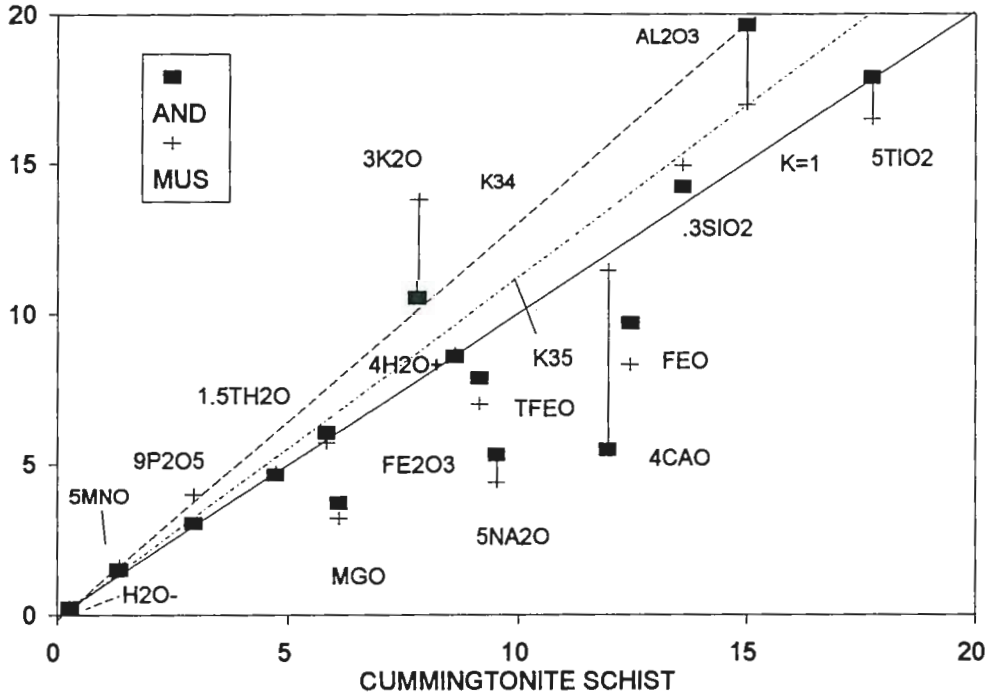

Fig. 19: Isocon Analysis (And & Ms vs. Cum)

Note: K34 and K35 are the isocons for andalusite and muscovite schist against cummingtonite schist, respectively. See the text and Table 12 for details. See Appendix A for notations.

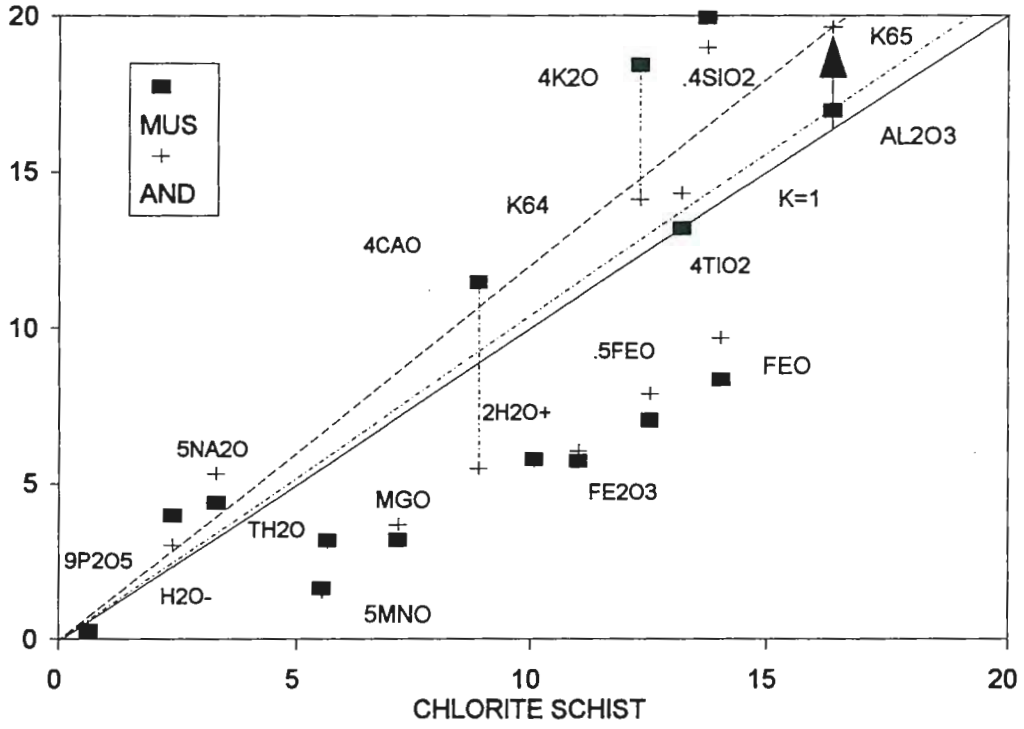

Fig. 20: Isocon Analysis (And & Ms vs. Chl)

Note: K64 and K65 are the isocons for andalusite and muscovite schist agianst chlorite schist, respectively. See the text and Table 12 for details. See Appendix A for notations.

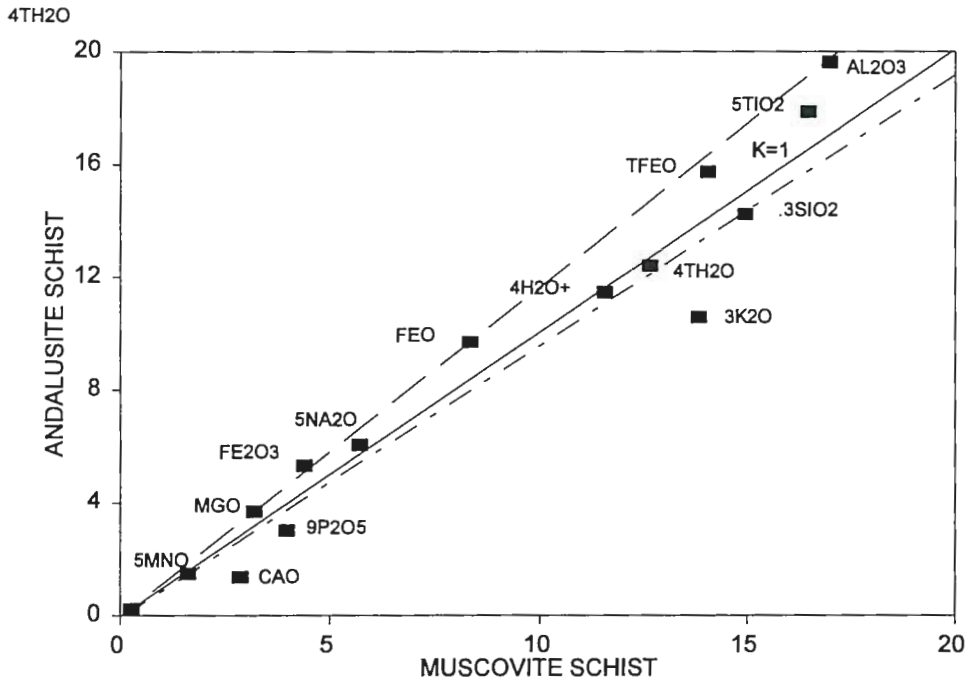

Fig. 21: Isocon Analysis (Andalusite vs. Muscovite Schist)

Note: The upper dashed line is the constant-aluminum isocon. The band between upper dashed line and lower point line is the isocon encompassing aluminum, silicon and titanium. See Appendix A for notations.

If muscovite schist formed from andalusite schist assuming constant aluminum, it would have gained 16 percent mass and been enriched in all the major elements except a little sodium, with the isocon slope K_{45}=0.86 (Fig. 17; Table 11). If muscovite schist formed from cummingtonite schist assuming constant aluminum, it lost about 12 percent mass with isocon slope K_{35}=1.13 and all the major elements, except potassium, manganese and phosphorus, were lost (Table 11 and Fig. 19). If muscovite schist formed from chlorite schist (Fig. 20, Table 11), it lost about 3 percent mass (K_{65}=1.04) with gain of silicon, calcium, sodium and potassium, phosphorus and most trace elements, and loss of other major elements .

(5) The isocon for the comparison of chlorite schist to amphibolite is K_{16} on Figure 16 or 18. It has a slope of 1.12, corresponding to a 10 percent mass loss in chlorite schist. Sodium, calcium and to a lesser extent silicon were lost, manganese, potassium, total iron, titanium and phosphorus were gained (Table 11).

If the chlorite schist formed from the muscovite schist assuming aluminum kept constant (K_{56}=0.97, Fig. 17), the total mass gain would be about 4 percent, with large gains in Fe^{+3}, Fe^{+2}, manganese, magnesium and water, and loss of silicon, potassium, calcium and sodium. If the chlorite schist formed from the cummingtonite schist (K36=1.09, Table 11 and Fig. 18), the total mass loss

would be about 8 percent with distinct gain of manganese, Fe^{+3} and water and loss of sodium, calcium, phosphorus and silicon (Table 11).

4. DISCUSSION AND SUMMARY

It is very clear for those rocks in the limb that there is a gradual increase of isocon slopes and the systematic increase or decrease of almost all the chemical components from the center of the metadiabases to the contact between them and the banded iron formation (Table 11, Fig. 16~18). These good systematics for the main rock series amphibolite-actinolite-cummingtonite-chlorite schist undoubtedly indicates a gradual and continuous mass loss during a single hydrothermal alteration, and further support the conclusion that all the metadiabases were formed from the same protolith: the amphibolite -- the least-altered Early Proterozoic diabases. Isocon slopes for those rocks in the keel of the syncline, on the other hand, change twice (from cummingtonite schist to andalusite schist and from muscovite schist to chlorite schist, see Fig. 16 and 17), corresponding to the changes of chemical composition and element atomic ratio curves (Fig. 13 and 14). The question is thus raised whether the andalusite and muscovite schist were formed from other protolith(s), or were formed during another geological process which may have had little effect on the rocks in the limb of the syncline.

Several lines of evidence have demonstrated that there is only one protolith, the Early Proterozoic diabase, for all altered metadiabases (Section 3.4). It is clear that the metamorphic mineral assemblages of all metadiabases, including andalusite schist and muscovite schist, must be formed during regional metamorphism after pre-metamorphic hydrothermal alteration (Section 5.1). The distinct changes in both mass and chemical composition of andalusite schist and muscovite schist, compared to amphibolite, amphibole schist or chlorite schist, are correlated with the abrupt mineralogical change, and may result from more intense pre-metamorphic hydrothermal alteration or more episodes of hydrothermal alteration on them than those in the center of metadiabase and in the limb prior to the regional metamorphism (see also Sections 5.2 and 5.4). There seem no good systematics for the rocks in the keel if andalusite schist and muscovite schist are left in the series. Given the good systematics for the main amphibolite-actinolite-cummingtonite-chlorite schist series, as in Figure 18, it seems improbable that the compositions of the andalusite and muscovite schists were attained before those of main series, or that they are not the part of that main series. Their composition, therefore, must post-date the main series, or there must be another hydrothermal alteration after the main episode of pre-metamorphic hydrothermal alteration and prior to some stages of the regional metamorphism that formed their mineral assemblages. It is clear that the pre-metamorphic hydrothermal alteration to form the mafic main rock series is distinctly different from the following hydrothermal alteration to form

peraluminous rocks (the protolith of andalusite schist, muscovite schist and relict peraluminous schist in chlorite schist) based on either constant aluminum isocon or any other reasonable isocons. The main pre-metamorphic hydrothermal alteration resulted in the gradual loss of sodium, calcium and silicon and gain of water, iron group elements and almost all other major chemical components with almost constant aluminum and magnesium to form the main series rocks (Table 11, Fig. 16, 17 or 18). On the other hand, the following hydrothermal alteration resulted in the loss of most major chemical components, especially water and iron group elements in forming andalusite schist and muscovite schist (Table 11). There is not enough information to make sure of whether this later hydrothermal event is a later phase of the main hydrothermal alteration, or a discrete later event, or related to fluid-driven regional metamorphism (Ferry, 1992a and 1992b), or simply the pre-metamorphic hydrothermal fluid which is large in amount and long in duration within the fault zones where the more intense hydrothermal alteration resulted in the further alteration of the altered Proterozoic diabases. However, the fact that the later hydrothermal alteration is very different from previous one in the change of most chemical components excludes the last possibility, and the loss of large amount of rock mass and water favor the assumption that the later hydrothermal alteration may be related to fluid-drive regional metamorphism.

The questions then follow whether the muscovite and andalusite schists were formed from cummingtonite schist or chlorite schist, or whether the rock series is cummingtonite-andalusite-muscovite schist or chlorite-muscovite-cummingtonite schist, and which is the most altered product in all the altered diabases. Although the chemical components in both Fig. 19 and 20 show systematic and continuous changes, the gained or lost chemical components are different. Water and iron as well as those elements with similar geochemical character to iron were lost and potassium was gained. However, silicon and sodium were lost for the comparison of andalusite and muscovite schist against cummingtonite schist, but gained against chlorite schist. Calcium was lost for the comparison of muscovite schist against cummingtonite schist, but gained against chlorite schist. In addition, Fig. 20 shows continuous increasing mass loss of whole rocks but Fig. 19 shows continuous decreasing mass loss for whole rocks. Both andalusite and muscovite schists are peraluminous and poor in iron and those elements with similar geochemical behaviors to iron. This indicates that andalusite and muscovite schists must have lost these chemical components. Comparing Figures 19 and 20, the chlorite-muscovite-andalusite schist series may be a better choice because this series shows not only the loss of iron and water, but also the continuous loss of rock mass. Moreover, all the comparisons of andalusite schist with either amphibolite (Fig. 16~17) or cummingtonite schist (Fig. 19), or chlorite schist (Fig. 20), or muscovite schist (Fig. 21) indicate the largest mass loss when andalusite schist formed (Table

11). This implies that the andalusite schist is the most altered product of all metadiabases in the research area no matter whether the aluminum isocon or an aluminum-titanium-silicon isocon is used (e.g., Fig. 21).

In the comparisons with amphibolite, all the altered metadiabases have mass loss. All the altered metadiabases lost sodium, manganese and calcium, and gained potassium, titanium, phosphorus, water and Fe^{+3}. Silicon was lost from all but the actinolite schist. All except the andalusite and muscovite schists gained total iron, and these two show the only substantial losses in magnesium. The isocon analysis of all the metadiabases from amphibolite to chlorite schists shows relatively more increase or less decrease in Fe^{+3} than Fe^{+2}, which may suggest increasing oxygen fugacity in this direction as discussed below.

CHAPTER 4: PHYSICAL AND CHEMICAL ENVIRONMENT

Mineral chemical composition and assemblages as well as fabrics record the evidence of physical and chemical conditions in the rock-fluid system and of the timing of the formation of various minerals during different geological processes. However, it is difficult to define the physical and chemical conditions during pre-metamorphic hydrothermal alterations because the regional metamorphism has overprinted the records of previous physical and chemical conditions. In addition, retrograde metamorphism has also locally affected the records of previous physical and chemical conditions. On the other hand, assuming a closed system during regional metamorphism and minor effects of retrograde metamorphism, the chemistry of minerals and mineral assemblages observed today can yield information about pressure and temperature conditions during regional and retrograde metamorphism. Comparison of rock and mineral chemistry between the least-altered metadiabase and more intensively altered metadiabases also shed light on conditions during pre-metamorphic hydrothermal alterations.

4.1. METAMORPHIC MINERAL ASSEMBLAGES

To estimate the physical and chemical condition during regional metamorphism and evaluate the possible chemical changes during pre-metamorphic hydrothermal alteration and retrograde metamorphism, it is crucial to distinguish equilibrium metamorphic mineral assemblages from those minerals formed by later hydrothermal alteration or retrograde metamorphism. All the altered metadiabases in the Republic Mine were formed from the same protolith -- the Early Proterozoic diabases through pre-metamorphic hydrothermal alteration, regional metamorphism and retrograde metamorphism (Section 3.4 and 5.1). It is clear that the metamorphic mineral assemblages must be formed during regional metamorphism rather than pre-metamorphic hydrothermal alteration or retrograde metamorphism. The large number of minerals, extensive replacement between minerals and large amount of veins in the observed altered metadiabases, however, suggest that retrograde metamorphism during or after regional metamorphism can partially change bulk rock chemical composition, mineral chemistry and mineral assemblages. It is obvious that these minerals formed by later retrograde metamorphism, such as the secondary chlorite, hematite and sericite, and minerals of veins cutting metamorphic minerals and/or rocks should be excluded from equilibrium regional metamorphic mineral assemblages.

Phase diagrams, such as ACF, AKF and AFM diagrams can be used to graphically analyze the equilibrium metamorphic mineral assemblages for various metamorphic facies. They, however, cannot be rigorous phase diagrams because their graphic representations are limited to fewer chemical components than in real rock systems. Nonetheless, these diagrams are well suited for portraying generalized mineral assemblages if the compositional range of the rocks is restricted and if the chemical components causing changes in mineral assemblages can be identified. Many chemical components, therefore, can be excluded from phase diagrams (e.g., Eskola, 1915 and Thompson, 1957), such as those chemical components that occur as pure phases (e.g., silicon in quartz); or in only accessory minerals (e.g., titanium in ilmenite and rutile); or not sufficiently abundant to influence the mineral equilibrium (e.g., trace elements). In addition, some chemical components can be treated as externally controlled (e.g., volatiles); and some phases can be used as projection points through which to project the composition of other phases onto the phase diagrams if they are common to all mineral assemblages (e.g., quartz or muscovite for pelitic rocks).

As discussed above, the altered diabases in the mine can be divided into two chemically different categories of rocks. One, including amphibolite, actinolite schist, cummingtonite schist and chlorite schist, still kept its original mafic chemical composition. Another, including andalusite schist,

muscovite schist and the relict rock bodies with the mineral assemblage of And+Kfs+Bt+Grt+Q (sample MI91422, see Appendix B) within chlorite schist in the keel of the syncline, has been changed to peraluminous. There are no probe data for most minerals in actinolite schist, but their chemical composition may lie between those of amphibolite and cummingtonite schist. There are also no probe data for chlorite, however, most natural chlorite ($A_{10}C_0F_{90}$ ~ $A_{35}C_0F_{65}$) are plotted in ACF diagram for the comparison (Fig. 22). Also note that the garnet occurs only in andalusite schist, muscovite schist and the relict peraluminous bodies in chlorite schist.

The dashed line connecting plagioclase and cummingtonite divides the ACF phase diagram into two sub-diagrams (Fig. 22). One includes actinolite schist and amphibolite schist, and another includes cummingtonite schist and chlorite schist. Fig. 22 shows the possible coexistence of various amphiboles and may be used to explain the gradual transition between these amphibole schists in the field. The differences in amphibole species for these rocks may mainly result from their chemical differences, such as the CaO/(FeO+MgO) ratios (Fig. 16). The equilibrium metamorphic mineral assemblages for those mafic metadiabases are

Am+Pl+Bt+Q±Spn±Carb±Opaque minerals

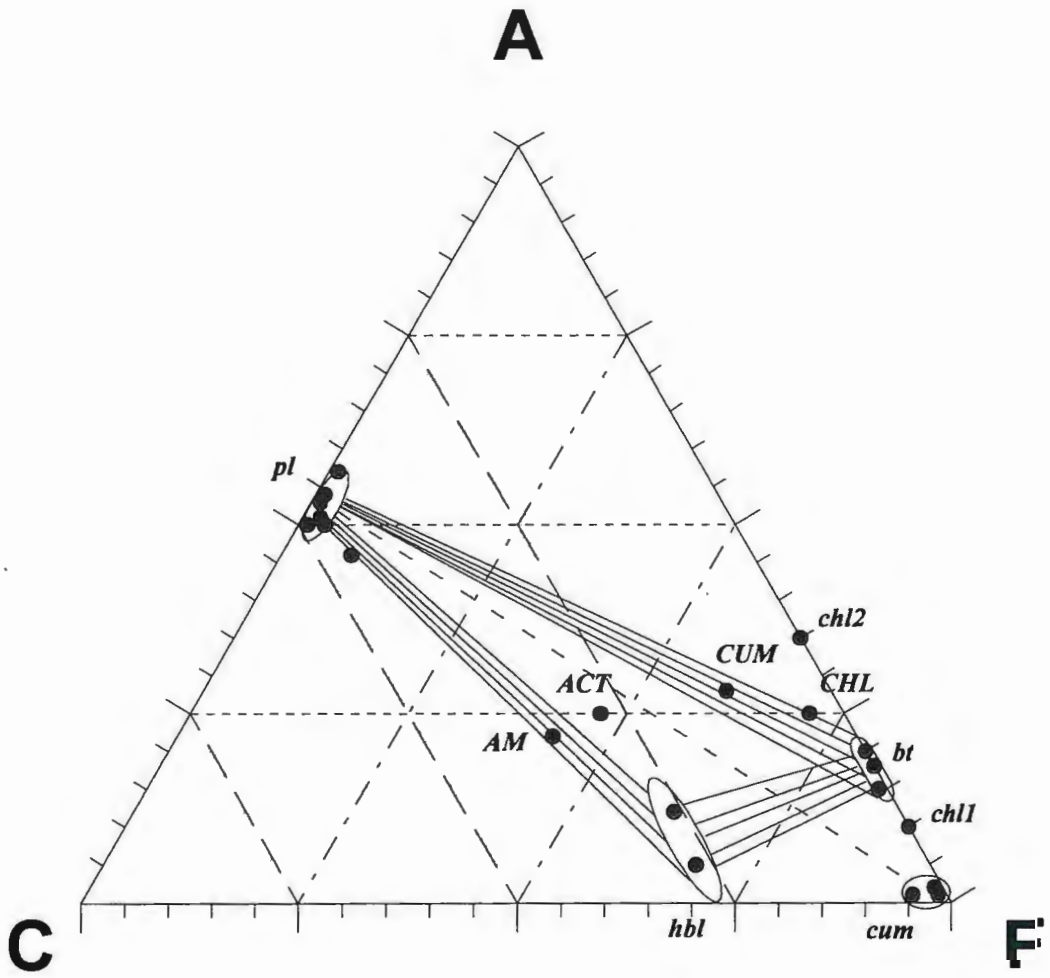

Fig. 22: ACF Phase Diagram

Note: AM, ACT, CUM and CHL are rocks amphibolite, actinolite, cummingtonite and chlorite schist, respectively; and hbl, bt, cum, pl and chl are minerals hornblende, biotite, cummingtonite, plagioclase and chlorite, respectively. There are no probe data for chlorite in this study, chl1 and chl2 are the chemical composition range for most natural chlorite.

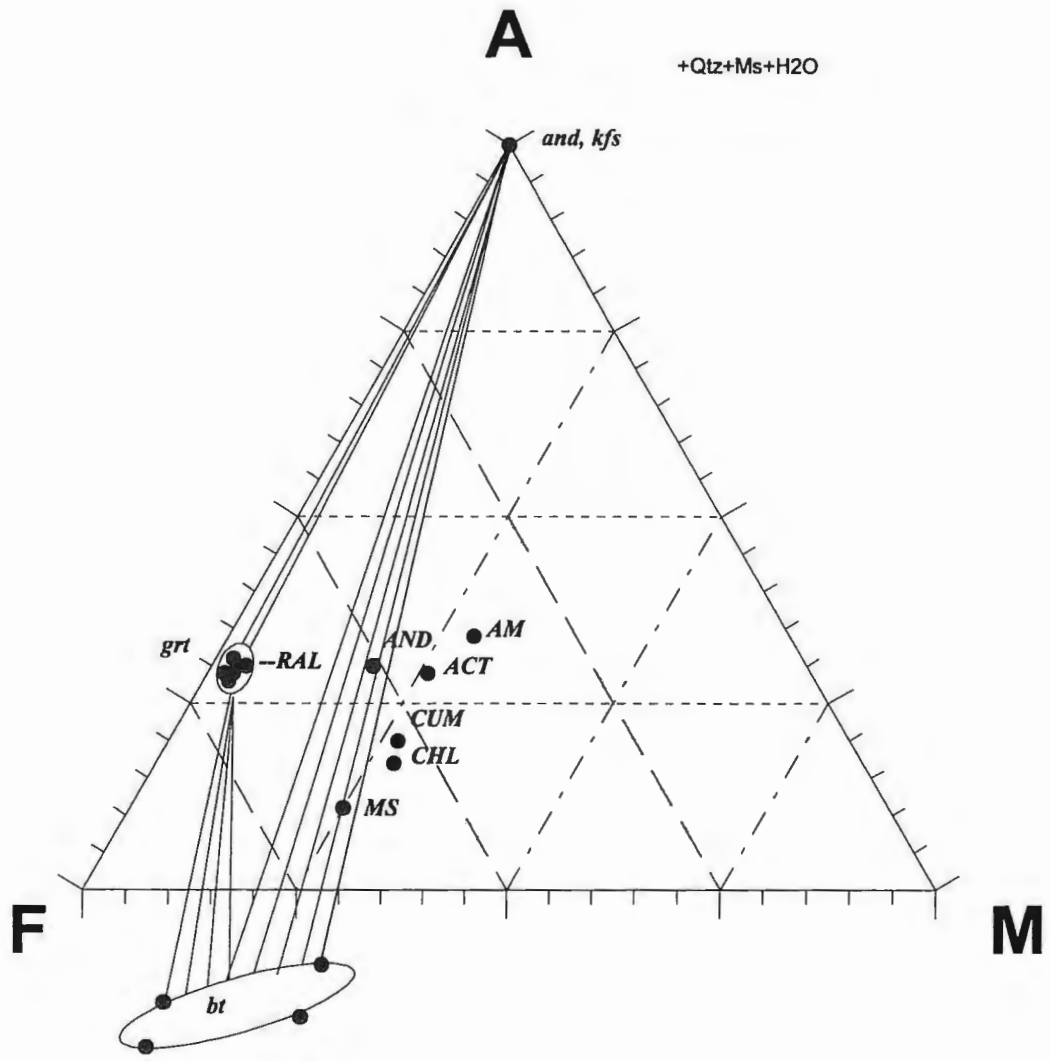

Fig. 23: AFM Phase Diagram

Note: AM, ACT, CUM, AND, MS, CHL and RAL are rocks amphibolite, actionlite, cummingtonite, andalusite, muscovite, chlorite schist and the relict peraluminous rock in chlorite schist (sample MI91422), respectively; and bt, and, grt and kfs are minerals biotite, garnet, andalusite and potassium feldspar, respectively.

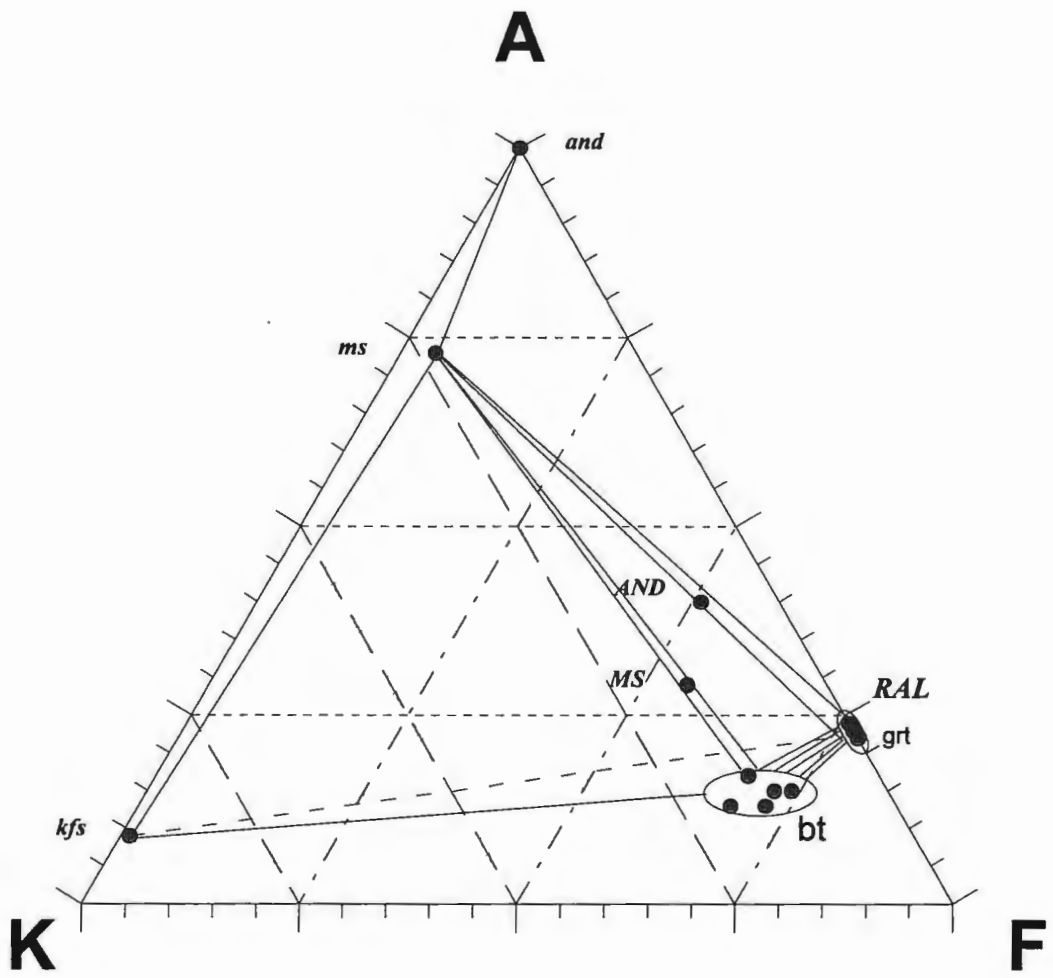

Fig. 24: AKF Phase Diagram

Note: AND, MS and RAL are rocks andalusite, muscovite and the relict peraluminous rock in chlorite schist (sample MI91422), respectively; and bt, and, grt, ms and kfs are minerals biotite, garnet, andalusite, muscovite and potassium feldspar, respectively.

where the amphibole species are hornblende, actinolite, cummingtonite for amphibolite, actinolite schist and cummingtonite schist, respectively. Chlorite schist have either cummingtonite or grunerite. Its high iron content and low pressure metamorphic condition (Section 4.2), suggest that both biotite and chlorite may belong to the equilibrium mineral assemblage (Laird, 1980).

Fig. 23 and 24 show the equilibrium metamorphic mineral assemblage for peraluminous metadiabases

Bt+Ms+Grt+Q±And±Kfs+Opaque minerals

where andalusite may be absent in muscovite schist and potassium feldspar may be absent in andalusite or muscovite schist. The lower aluminum and higher potassium and mafic contents in muscovite schist, comparing andalusite schist, may be the reason why there is no andalusite in muscovite schist under the pressure and temperature conditions of regional metamorphism (Fig. 23 and 24). Nevertheless, the existence of both andalusite and potassium feldspar in the relict peraluminous bodies in chlorite schist suggests possible previous existence of potassium feldspar in muscovite schist and andalusite schist, and of andalusite in muscovite schist. However, the amount of these minerals might be small and they may have been decomposed by retrograde metamorphism.

4.2. PRESSURE AND TEMPERATURE

The Republic Mine is located in the sillimanite zone, the center of a regional metamorphic node (James, 1955; Cannon, 1973; Cannon and Klasner, 1978). Equilibrium metamorphic mineral assemblages Am+Pl+Q±Bt±Spn±Carb for mafic metadiabases and Grt+Ms+Bt+Q±And±Kfs for peraluminous metadiabases are characteristic of low pressure (2~4 kb) and lower amphibolite facies (e.g., Essene, 1982). Recent research on the Negaunee Iron Formation by Haase (1986) suggests metamorphic pressure ranging from 2 to 3 kb and maximum temperature ranging from 550~615 ^{o}C. The GRAIL (almandine-rutile-Al_2SiO_5-ilmenite-quartz) geobarometer applies well to high-pressure regimes but not to the present case (Bohlen and others, 1983). Magnetite-ilmenite geothermometry (Spencer and Lindsley, 1981) is used to define both temperature and oxygen fugacity in this study. Muscovite-quartz-Al_2SiO_5-potassium feldspar-water (Kerrick, 1972; Chatterjee and Froese, 1975), aluminosilicate (Holdway, 1971) and garnet-biotite (Ferry and Spear, 1978) geobarothermometers are most useful here, because these mineral assemblages are widely distributed in various metadiabases and because the zoned garnets with their coexisting biotites may record a possible P-T-X-t path during metamorphism.

Combined with these geobarothermometers and using the chemical composition of garnet core and its coexisting biotite in the chlorite schist (Table 7 and 8), the peak regional metamorphic pressure and temperature were about 2.25 kb and 609 ^{o}C, on the assumption that the activity of water is unity (Fig. 25). Assume that the pressure during regional and retrograde metamorphism was the same, garnet-biotite geothermometry (Ferry and Spear, 1978), using the garnet middle zone and rim with their coexisting biotites in chlorite schist (Table 7 and 8), gives temperatures of 534 and 433 ^{o}C, respectively; and the garnet rims and their coexisting biotites chemical compositions in muscovite schist and andalusite schist yield temperatures of 515 and 505 ^{o}C, respectively, which are very close to the temperature recorded by garnet middle ring with its coexisting biotite in chlorite schist. There is no biotite found in the garnet cores of andalusite and muscovite schists. The garnets in andalusite and muscovite schist, however, show similar chemical zoning patterns to that in chlorite schist (Fig. 15), suggesting they may have a similar P-T-X-t path. The temperatures recorded by the magnetite-ilmenite geothermometers (Spencer and Lindsley, 1981; Table 9 and 10) are 570, 540 and 525 ^{o}C for chlorite schist, andalusite schist and cummingtonite schist, respectively. These temperatures are little different from those recorded by garnet-biotite geothermometers of muscovite and andalusite schist and of the garnet middle ring in chlorite schist.

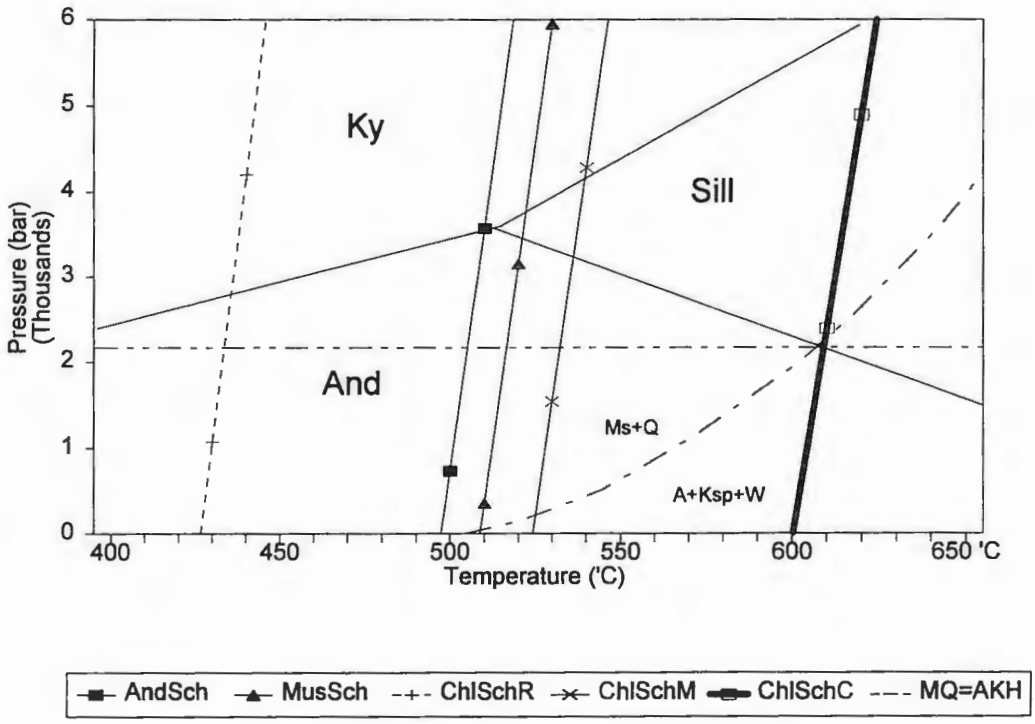

Fig. 25: Metamorphic P-T Conditions

Note: Al2SiO5 phase relations are from Holdway (1971). Reaction curve Ms+Q=And+Kfs+H2O (MQ=AKH) is from Kerrick (1972), assuming activity of water is unity. Other curves are Grt-Bt geothermometry (Ferry and Spear, 1978). Curves AndSch and MusSch are calculated from chemical compositions of garnets and their coexisting biotite in andalusite and muscovite schist, respectively (Table 7 and 8). Curves ChlSchR, M and C are calculated from the chemical compositions of the Rim, Middle and Center of garnets and their adjacent biotites in Chlorite schist, respectively (Table 7 and 8).

See the text for discussion and Appendix A for notations.

Compared to the scale of regional metamorphism in Northern Michigan (over 200 km), there should be no large variation in physical conditions during regional metamorphism over a very short distance of tens of meters from the contact to the center of the metadiabases and of hundreds of meters from the keel to the limb of the syncline (Fig. 1 vs. Fig 2 and Fig. 4). These altered diabases should have been subject to the same sillimanite grade of regional metamorphism, corresponding to the highest pressure and temperature conditions during regional metamorphism in the study area. The temperature gradients, recorded by the core, middle ring and outer rim of garnets with their coexisting biotite in chlorite schist and by magnetite-ilmenite geothermometers from cummingtonite schist to andalusite schist and muscovite schist, therefore, can only be explained as the results of retrograde metamorphism. Retrograde metamorphism must be much more intense and act on the rocks near the contact in the keel for a longer period than those far from the contact and in the limb of the syncline. The lower temperature recorded by garnet rims and their coexisting biotites in chlorite schist therefore may be related to the last stage of retrograde metamorphism which was localized near the contact.

4.2. REDOX ENVIRONMENT

Reducing condition in the system during regional metamorphism is indicated by the Fe^{+2}/Fe^{+3} ratios larger than unity in all the metadiabases, which

agrees with most redox environment for regional metamorphism (Liu, 1984). This conclusion is supported by the existence of pyrite and pyrrhotite consisting of Fe^{+2}, S^{-2} and S^{-1} in the amphibolite, and of fayalite, siderite and ferro-dolomite in the Goodrich Quartzite and the banded iron formation (Cannon, 1973, 1975; Ayers, 1972; Fryer, 1975; Keranck, 1981). Oxygen fugacity during regional metamorphism is quantitatively estimated by magnetite-ilmenite solid solution (Spencer and Lindsley, 1981) as $\log(fO_2)$=-21.2 for cummingtonite schist, -20.0 for andalusite schist and -17.6 for chlorite schist. These calculated results indicate a fairly low oxygen fugacity with a very small variation in the system during regional metamorphism because it is strongly buffered by a larger amount of iron and iron-titanium oxides in a FeO-TiO_2-O_2 system in the metadiabases and in the Goodrich Quartzite and Negaunee Iron Formation (e.g., FMQ buffer in FeO-SiO_2-O_2 system)), Hematite and relatively higher oxygen fugacity occur exclusively in chlorite schist near the contact between metadiabases and banded iron formation in the keel of the syncline, suggesting that they may result from retrograde metamorphism.

Toward the contact between the metadiabases and banded iron formation, increasing Eh value or oxygen fugacity is suggested by the disappearance of pyrite and pyrrhotite in more intensively altered metadiabases and of fayalite, siderite and ferro-dolomite in the banded iron formation near the contact (Cannon, 1973, 1975; Ayers, 1972; Fryer, 1975; Keranck, 1981).

Magnetite occurs in all types of metadiabases but hematite exists only in those rocks close to the contact between the metadiabases and banded iron formation in the keel of the syncline. Isocon analysis results indicate that all the metadiabases gain more Fe^{+3} than Fe^{+2} (Section 4.6) suggesting increasing oxygen fugacity during hydrothermal alteration by which the pre-existing pyrite and pyrrhotite were oxidized and fayalite and iron carbonate minerals were decomposed. This conclusion is supported by decreasing vanadium, chromium, Fe^{+2}, magnesium and manganese and Fe^{+2}/Fe^{+3} ratio, with increasing Fe/Mn and V/Ti ratios, in both mineral and rock chemistry from amphibolite in the center of the metadiabases to chlorite schist at the contact (Table 2 and 3; Laberge, 1964 and Liu, 1984).

4.3. pH VALUES

Based on the principle of acid-base reaction, increasing acidity favors the components with stronger acidity replacing those with weaker acidity (e.g., Henley, 1984). In other words, the replacement relationship between components, minerals and mineral assemblages suggests variation of pH in the system. If a mineral reaction only involves either anions or cations, the changes in acidity can be determined by the comparison of the relative acidity between these ions. Relative acidity of elements increases from left to right and from bottom to top in the periodic table. When both anions and cations are involved

in mineral reactions, the relative changes of acidity can be quantitatively evaluated by the approximate ionization potential y (Zharikov, 1967):

$$y = \frac{\sum N_k I_k + \sum N_a E_a}{\sum N_a + \sum N_k}$$

where E_a is average electronic affinity of anions, I_k is the average ionization potential of cations, and N_k and N_a are the number of cations and anions, respectively. The smaller the *y* value, the weaker the acidity of minerals. Table 12 lists the calculated *y* values of minerals in various metadiabases. The approximate ionization potential of minerals is additive so that the total *y* value of mineral assemblage in the product of a reaction can be compared to that of its protolith to evaluate the change in acidity of the system.

There should be no large variation in pH value during regional metamorphism as observed worldwide (Liu, 1984) and as suggested by the constant low oxygen fugacity because of the negative slope in the *pe* (or fo_2)-pH space for most geologic systems (e.g., Fe-O-H2O system) (Drever, 1988). Increasing acidity during pre-metamorphic hydrothermal alteration is suggested by the disappearance of the igneous minerals, such as high calcic plagioclase, pyroxene and olivine in favor of calcium amphiboles and more sodic plagioclases. Similarly, increasing acidity during retrograde metamorphism is

Table 12: Approximate Ionization Potential Values (y) of Selected Minerals
(After Zharikov, 1967)

MINERAL	CHEMICAL FORMULA IN CALCULATION	Y (kcal/mol)
Forsterite	Mg2SiO4	178.6
Fayalite	Fe2SiO4	188.9
Grossular	Ca3Al2Si3O12	187.6
Almandine	Fe3Al2Si3O12	192.4
Spessartine	Mn3Al2Si3O12	196.3
Pyrope	Mg3Al2Si3O12	197.8
Sphene	CaTiSiO5	193.6
Epidote	Ca2Al1.8Fe1.2Si3O12(OH)	194.8
Augite	CaMg.5Fe.5Al.5Si1.5O6	186.7
Diopside	CaMgSi2O6	190.0
Hedenbergite	CaFeSi2O6	193.6
Hornblende	Na2CaMg2.5Fe2Al2.5Si6O22(OH)2	189.8
Actinolite	Ca2Mg3Fe2Si8O22(OH)2	197.1
Cummingtonite	Mg4Fe3Si8O22(OH)2	199.7
Biotite	KMg1.5Fe1.5AlSi3O10(OH)2	188.7
Chlorite	Mg3Fe2Al2Si3O10(OH)2	193.3
Muscovite	KAl3Si3O10(OH)2	201.6
Anorthite	Ca2Al2Si2O8	197.4
Pl (An=50)	Na.5Ca.5Al1.5Si2.5O8	201.4
Pl (An=30)	Na.7Ca.3Al1.3Si2.7O8	202.5
Albite	NaAlSi3O8	204.7
K-feldspar	KAlSi3O8	203.3
Andalusite	Al2SiO5	204.0
Quartz	SiO2	227.3
Ilmenite	FeTiO3	187.4
Magnetite	Fe3O4	190.9
Hematite	Fe2O3	202.8
Rutile	TiO2	205.7
Calcite	CaCO3	187.0
Dolomite	CaMg(CO3)2	195.0
Ankerite	CaMg.5Fe.5(CO3)2	195.5
Pyrite	FeS2	218.0

suggested by chloritization of amphiboles and garnet, and sericitization of plagioclases, and by disappearance of carbonate minerals and sulfide minerals in more altered metadiabases. The spatial distribution of these minerals in various metadiabases also indicates decreasing acidity from the contact between metadiabases and banded iron formation to the center of metadiabases, which may be correlated to the exotic fluid flow direction.

CHAPTER 5: GEOLOGICAL PROCESSES

5.1. EPISODES AND TIMING OF GEOLOGICAL PROCESSES

Comparing the scale of the metadiabases in the mine with the scale of regional metamorphism, all of the these rocks must have undergone the same sillimanite-grade regional metamorphism (James, 1955) during which the physical conditions in the system should be the same for all the altered diabases in the mine (Section 4.2). The different metamorphic mineral assemblages of this event were therefore due to differences in composition rather than in physical conditions. The assemblages of the mafic metadiabases are attributed to this event. In the peraluminous rocks, the geothermometry and the presence of andalusite rather than sillimanite indicate development of their mineral assemblages during falling temperature, that is, during retrograde metamorphism. This suggests that the chemical compositions of metadiabases in the keel of the syncline were changed from mafic to peraluminous during late hydrothermal alteration after the sillimanite-grade culmination and therefore during the retrograde phase of the regional metamorphism (see also Section 3.5.4).

Element distribution patterns indicate that all the elements of metadiabases in the Republic Mine belong to neither AND nor LND, suggesting

multi-episode geological processes. Three sub-spaces in total sample population imply at least three possible episodes of geological processes to form these altered metadiabases in the area. Porphyroblastic garnets and magnetites, with pressure shadows of quartz and micas, are surrounded by foliation of micas, suggesting their pre-tectonic origin. Alteration of metamorphic minerals, such as extensive chloritization of garnet and amphiboles and sericitization of plagioclases and andalusite, and the existence of large amount of chlorite-quartz veins indicate that these metamorphic minerals have been hydrothermally altered during retrograde metamorphism. The zoned garnets with their coexisting biotite recorded decreasing temperature from the core to the rim of the garnet, suggesting the existence of a retrograde metamorphism in the syncline (see Section 5.2). Rock chemical compositions (Section 3.2) and isocon analysis results (Section 3.5) show a systematic variation of almost all the chemical components and gradual increase of isocon slopes (or loss of total rock mass) for the rock series amphibolite-actinolite-cummingtonite-chlorite schist in the limb but change twice for the rocks in the keel of the syncline, which result from two different types of pre-metamorphic hydrothermal alteration. All the evidence indicates that there were at least three geological processes, in addition to the primary magmatism, to form the Proterozoic diabases, by which these altered metadiabases were formed: pre-metamorphic hydrothermal alterations, regional metamorphism and retrograde metamorphism.

5.2. COMPARISON: MINERALOGY, PETROLOGY AND GEOCHEMISTRY

Mineral chemistry records geochemical behavior of elements and the physical and chemical conditions of the system. The geochemical behavior of an element depends on the element itself (especially its electronic structure), its existing state (e.g., as free ions or in various chemical compounds) and bonding character, its abundance and the physical and chemical conditions in the system. Exotic hydrothermal fluids infiltrating into the system will result in variation in both the physical and chemical character of the rock-fluid system. The interaction between minerals and the fluids directly determines the assemblages of major rock-forming minerals and their major element composition. Trace element distributions, on the other hand, are largely dependent on mineral structures with regard to those major elements for which they can substitute and in some circumstance on the decomposition or formation of accessory minerals constituting them.

The distinct and continuous loss of calcium, magnesium and sodium and gain of titanium, iron, manganese, potassium and phosphorous mainly results from the decomposition of calcic plagioclase, pyroxene and olivine during pre-metamorphic hydrothermal alteration, and may partially result from replacement or leaching of calcium and sodium from calcic amphiboles and plagioclases during retrograde metamorphism (Table 1 vs. 2, 3 and 5, 6). The

loss of sodium may be partially offset by potassium replacement in various minerals as suggested by fairly constant K+Na compared to the distinct variation of K/Na ratios (Table 3) and by possible existence of high concentration of potassium in fluids during pre-metamorphic hydrothermal alteration and/or retrograde metamorphism (Section 4.7).. Potassium is lowest in the amphibolite but it is still higher than normal diabase or other mafic rocks (Turekian and Wedepohl, 1961; Wedepohl and others, 1969-1978). The distinct increase of potassium from amphibolite to the muscovite schist near the contact is correlated with the increasing amount of biotite and muscovite, the increasing degree of sericitization of plagioclases and potassium replacement for sodium in micas (Table 1 vs. 2 and 7). Silicon and aluminum from the decomposition of calcic plagioclase, pyroxene and olivine were dissolved into the intergranular fluids. Silicon was partially lost due to its higher solubility at high pressure, temperature and pH conditions (Section 4.4), while aluminum remained in the system constituting newly formed aluminum silicates, such as plagioclase, amphiboles, garnet, andalusite and micas during following regional metamorphism. The loss of silicon and the constancy of aluminum in the system results in the increase of the Al/Si ratio in the metadiabases from the center of metadiabases toward the contact between metadiabases and banded iron formation. Andalusite and potassium feldspar were formed in these rocks with both the highest aluminum content and the largest Al/Si ratio (comparing Table 1, 2 and 3).

From amphibolite to actinolite schist and cummingtonite schist, magnesium keeps almost constant but iron increases distinctly with increasing Fe^{+2}/Mg^{+2} ratio, because of the exotic infiltrating fluids rich in iron during hydrothermal alteration processes (Table 3, Fig. 13 and 14; see also Section 4.7). With the decomposition of iron-magnesium silicates in diabases, both iron and magnesium were released into intergranular fluids. The low pressure (2.25 kb) and temperature (609 ^{o}C) condition in the system favors to form ferromagnesian silicates with higher Fe^{+2}/Mg^{+2} ratio than in the parent diabases during following regional metamorphism (Liu, 1984). Some iron was concentrated in the system by the formation of iron and titanium oxides into which magnesium can not enter. These two factors together result in the leaching of magnesium from the system with decreasing Mg/Fe ratio from amphibolite to chlorite schist. Titanium and chromium in minerals of metadiabases are most abundant in iron-rich amphiboles. However, the concentration of them may be mainly controlled by the formation of titanium and chromium accessory minerals. The increasing titanium from amphibolite to chlorite schist may be related to increasing amount of ilmenite and rutile, and to the high concentration of titanium in exotic fluids infiltrating into the system during hydrothermal alteration. Chromium, on the other hand, can form metal complexes and move out of the system, especially when the Eh value and acidity increase as in the present case (Liu, 1984).

The geochemical behavior of trace elements mainly depends on those major elements for which they can substitute so that the character of these major elements themselves and their existing states control the dispersion or enrichment of trace elements. For example, Sr^{+2} can substitute for Ca^{+2} but not for K^{+1} in micas. However, Rb^{+1} favors substitution for K^{+1} because of their similar ionic radii and charge. The geochemical behavior of strontium, barium and rubidium is therefore mainly controlled by both the concentration of calcium and potassium, and the amount of minerals containing calcium and potassium (comparing Table 1, 2 and 3). The leaching of calcium from the system resulted in the loss of strontium, while increasing potassium and the formation of various micas lead to enrichment of barium and rubidium. Consequently, the calcium content, the Sr/K and Sr/Ba ratios decrease with increasing potassium content and Rb/Sr ratio from the center of metadiabases to the contact and from the limb to the keel of the syncline (Table 1~3, and Fig. 14). On the other hand, some trace elements (e.g., Zr and P) are concentrated in accessory minerals rather than major rock-forming minerals, which they cannot enter. The decomposition or formation of these accessory minerals therefore control the dispersion or enrichment of these trace elements. For example, the increasing REE content from the center of the metadiabases to the contact may be attributed to the change in the amount of apatite which concentrates these rare earth elements (e.g., Henderson, 1984).

5.3. FLUID SOURCES AND COMPOSITION

The intensive hydrothermal alteration in the area can only be explained as the result of exotic fluid infiltrating into the system along various channels, especially fractures and faults (e.g., Fletcher and Hofmann, 1974; Walter and Orville, 1982; Bickle and McKenzie, 1987; Sibson, 1990, Ferry, 1992a). A large amount of fluid is not expected to be released from the Early Proterozoic diabase because of its anhydrous mineral assemblages and small volume compared to the Early Proterozoic sedimentary sequences. Exotic meteoric fluids could be introduced into the system through convecting fluid system around these Early Proterozoic diabases during their intrusion at shallow crust levels (e.g., Fleck and Criss, 1986). They, however, can not be major part of the fluid resulting in pre-metamorphic hydrothermal alteration because the small volume of the Early Proterozoic diabases. Pore fluids in the Early Proterozoic sediments could be released during sedimentary accumulation and burial, and dehydration reaction during prograde regional metamorphism of these sedimentary rocks could release large amount of fluids (e.g., Walther and Orville, 1982; Etheridge and others, 1983; Etheridge and others, 1984; Walther and Wood, 1984). These fluids therefore may be responsible for pre-metamorphic hydrothermal alteration. Quantitative calculation of fluid chemical composition in this research is beyond the scope of this study but a qualitative estimate of fluid chemical composition can be made from the comparison of the

bulk rock chemical composition and mineral chemistry between the least-altered metadiabases and more altered metadiabases. The distinct enrichment of iron, phosphorus, potassium and titanium suggests that the exotic fluids are rich in these components which may be leached from the nearby Negaunee Iron Formation and the pelitic components of the Goodrich Quartzite.

5.4. STRUCTURAL CONTROLS ON FLUID FLOW

During folding and faulting of Penokean Orogeny, many fractures and faults were developed due to brittle deformation at a shallow crustal level which is suggested by the pressure and temperature recorded by metamorphic mineral assemblages. In the Republic Mine, many of these fractures and faults are parallel to the fold axis, cutting rock layers in the keel and along the previously existing weak surfaces, especially the contact between the metadiabases and banded iron formation and the unconformity between Archean and Early Proterozoic rocks.

The intensity of deformation and structural distribution patterns in the Republic syncline are consistent with the increasing intensity of hydrothermal alteration from the limb to the keel of the syncline and from the center of the metadiabases to the contact between the metadiabases and the Negaunee Iron Formation. The more intense the deformation of rocks near the

contact and in the keel of the syncline, the more fractures and faults were developed, the more channels for fluid flow and the higher permeability of rocks, the larger amount of fluids and more heat carried by fluids into the system, the more intensive hydrothermal alteration and so the higher changes in rock and mineral chemical composition. It is obvious that the folding and faulting must happen before pre-metamorphic hydrothermal alteration and that the deformation in the keel must be very intense and the difference of the deformation intensity between the limb and the keel of the syncline must be very large.

The F1 phase structures of the Penokean Orogeny have not been found in the research area (Chapter 1 and the references therein). Field geology and structural analysis indicate that the F2 phase folding and faulting during the Penokean Orogeny may be responsible for deforming the diabases in the syncline and resulting in the intense strain difference between the limb and the keel due to their different structural position (Cannon and Klasner, 1972). These F2 fractures and faults along the contact between the metadiabases and banded iron formation and crossing rock layers in the keel increased the permeability of rocks within or near these structures and served as fluid flow channels. They therefore defined fluid flow patterns, controlled the amount of fluids and hence the heat carried by the fluids into the diabases. This further determines the fluid chemical and temperature gradients along fluid flowing

paths so as to control the intensity of hydrothermal alteration and possibly the retrograde metamorphism, and to change chemical composition of metadiabases.

5.5. DISCUSSION AND CONCLUSIONS

The discussion above indicates that all the altered metadiabases in the research area came from the same protolith: the Early Proterozoic diabase which has undergone pre-metamorphic hydrothermal alterations, regional metamorphism and retrograde metamorphism. It is clear that the metamorphic mineral assemblages of metadiabases in the Republic Mine were mainly formed by regional metamorphism rather than contact metamorphism or autometamorphism during the intrusion of the Early Proterozoic diabases and that there should be no significant variation in physical conditions during regional metamorphism over a very short distance in the research area. On the other hand, the distinct change in chemical composition and the mass of the metadiabases near the contact and in the keel of the syncline must result from very intense and extensive pre-metamorphic hydrothermal alterations. More fluids and possible more heat carried by the exotic fluids therefore should be involved near the contact and in the keel than away from the contact and in the limb of the syncline. The conclusion of a possible geological history to form

these altered metadiabases from the Early Proterozoic diabase can be summarized as follows:

Large amounts of hydrothermal fluids were formed by heating pore water released from Early Proterozoic sediments during their accumulation and burial at the beginning of the Penokean Orogeny, and by dehydration reaction of these rocks during regional prograde metamorphism which culminated after F2 deformation of Penokean Orogeny. Some meteoric fluids could also be involved. These fluids flowed along the F2 fracture-fault system into the Republic syncline shortly after F2 deformation, and leached potassium and iron from the nearby Negaunee banded iron formation and Goodrich quartzite. It is these fluids that resulted in the first episode of pre-metamorphic hydrothermal alteration to form the altered diabases with different mafic chemical compositions. Pre-metamorphic hydrothermal alteration is characterized by the distinct loss of silicon, calcium and sodium; and gain of water and other major elements, especially iron and potassium, and most trace elements, with possibly increasing acidity and oxygen fugacity. The regional metamorphism is characterized by low pressure amphibolite facies with the peak pressure 2.25 kb and temperature at least 609 °C and with constant reducing conditions, during which the cores of zoned garnets were formed. The mineral assemblages of the mafic series of metadiabases were formed near the culmination of the regional metamorphism. Chemical compositions of some diabases near the contact

between the metadiabases and banded iron formation in the keel of the syncline were then altered from mafic to peraluminous during later hydrothermal alteration which is characterized by distinct loss of total rock mass, water and iron group elements. Metamorphism of these peraluminous rocks resulted in the formation of muscovite and andalusite schists, and related enclaves in the chlorite schist. This retrograde metamorphism, characterized by decreasing temperature and increasing oxygen fugacity and concentrated again in the contact between the metadiabases and banded iron formation and in the keel of the syncline, resulted in the overgrowth and hydrothermal alteration of these metamorphic minerals, such as the overgrowth of the outer rims and/or middle ring of garnets. All the garnet zones in chlorite schist are cut by chlorite-biotite-quartz veins, which may result from either the latest stage of retrograde metamorphism or later hydrothermal activity which was similarly concentrated near the contact between the metadiabases and banded iron formation and in the keel of the syncline.

REFERENCES

Afifi, A.M., and Essene, E.J., 1988, MINFILE computer program, University of Michigan, Ann Arbor, Michigan.

Aldrich, L.T., Davis, G.L., and James, H.L., 1965, Ages of minerals from metamorphic and igneous rocks near Iron Mountain, Michigan: J. Petrology, V. 6, p. 445-472.

Anderson, G.J., 1968, The Marquette district, Michigan, in Ridge, J.D. ed., Ore deposits of the United States, 1933-1967 (Craton-Scales Volume), V. 1: New York American Inst. Mining, Metall., and Petroleum Engineers, p. 505-517.

Ayers, D.E., 1972, Genesis of iron-bearing minerals in banded iron formation mesobands in the Dales George Member, Hamersley Group, Western Australia: Econ. Geol., v. 67, p. 1214-1233.

Barth, T.F.W., 1952, Theoretical petrology, Wiley, New York

Bohlen, S.R., Wall, V.J., and Boettcher, A.L., 1983, Experimental investigation and geological application of equilibria in the system FeO-TiO_2-Al_2O_3-SiO_2-H_2O: Am. Mineral. 68, p. 1049-1058.

Bickle, M. and McKenzie, D., 1987, The transport of heat and matter by fluids during metamorphism, Contrib. Min. Petrol., 95, p. 384-392.

Boyum, B.H., 1964, The Marquette mineral district, Michigan: 10th Ann. Inst. on Lake Superior Geology, Ishpeming, MI, May 1964.

Boyum, B.H., 1975, The Marquette mineral district of Michigan: 21st Ann. Inst. Lake Superior Geology, Marquette, Michigan 1975, Field Guidebook, p. 189-261.

Brady, J.B., 1983, Intergranular diffusion in metamorphic rocks, Am. J. Sci., v. 283A, p. 181-200.

Cannon, W.F., 1971, Geologic map of the Republic 2.5 minute quadrangle, Michigan, USGS, open-file map, Scale 1:12000

Cannon, W.F., 1973, The Penokean Orogeny in northern Michigan, in Young, C.M., ed., Huronian stratigraphy and sedimentation: Geol. Assoc. Canada Spec. Paper 12, p. 251-271.

Cannon, W.F., 1975, Bedrock geologic map of the Republic Quadrangle, Marquette County, Michigan (with the Detailed Geologic Map of the Republic Mine area, Scale 1:6000): USGS, open-file map, Scale 1:24000

Cannon, W.F., and Gair, J.E., 1970, A revision of stratigraphic nomenclature for Middle Precambrian rocks in northern Michigan: GSA Bull., V. 81, no. 9, p. 2843-2846.

Cannon, W.F. and Klasner, J.S., 1972, Guide to Penokean deformational style and regional metamorphism of the western Marquette range, Michigan, in Field Trip Guidebook, 18th Ann. Inst. on Lake Superior Geology, Houghton, Michigan, p. B1-B38.

Carmichael, I.S.E., Nicholls, J.C. and Smith, A.L., 1970, Silica activity in igneous rocks, Am. Min., v. 55, p. 246-263.

Chatterjee, N.D. and Froese, E., 1975, A thermodynamic study of pseudobinary join muscovite-paragonite in the system $KAlSi_3O_8$-$NaAlSi_3O_8$-Al_2O_3-SiO_2-H_2O, Am. Mineral., 60, p. 985-983.

Cleveland Cliff Iron Company, 1981, Republic Mine open pit map, Scale 1:1200.

Drever, J.I., 1988, The geochemistry of natural waters, 2nd ed., Prentice Hall, New Jersey, pp. 437.

Eskola, P., 1915, On the relation between the chemical and mineralogical composition in the metamorphic rocks of the Orijavi region, Bull. Comm. Geol. Finland, no. 44 (English summary, p. 109-145).

Essene, E.J., 1982, Geologic thermometry and barometry, In: Ferry, J.M., ed., Characterization of metamorphism through mineral equilibria, Rev. Mineral. 10, p. 153-206.

Essene, E.J., 1989, The current status of thermobarometry in metamorphic rocks, In: Evolution of metamorphic belts, Daly, J.S., Cliff, R.A., and Yardley, B.W.D., eds., Spec. publ. 43, Geol. Soc. Lond., p.1-44.

Etheridge, M.A. Wall, V.J., and Vernon, R.H., 1983, The role of the fluid phase during regional metamorphism and deformation, J. Met. Geology, 1, p. 205-226.

Etheridge, M.A., Cox, S.F., and Vernon, R.H., 1984, High fluid pressures during regional metamorphism and deformation: implication for mass transport and deformation mechanisms. J. Geophys. Res., 89, B6, 4344-4358.

Ferry, J.M., 1992a, Dehydration and decarbonation reactions as a record of fluid infiltration, In Contact metamorphism, Kerrick, D.M. ed., Rev. Mineral. 26, p. 45-94.

Ferry, J.M., 1992b, Regional metamorphism of the Waits River Formation, eastern Vermont: Delineation of a new type of giant metamorphic hydrothermal system, J. Petrol., 33, p.45-94

Ferry, J.M. and Spear, F.S., 1978, Experimental calibration of the partitioning of Fe and Mg between biotite and garnet, Contrib. Min. Petrol., 66, p. 113-117.

Fleck, R.J. and Criss, R.E., 1985, Strontium and oxygen isotopic variations in Mesozoic and Tertiary plutons of central Idaho., Contrib. Min. Petrol., 90, p. 291-308.

Fletcher, R.C. and Hofmann, A.W., 1974, Simple models of diffusion and combined diffusion-infiltration metasomatism, In: Geochemical transport and kinetics, Hofmann, A.W., Giletti, B.J., Yoder, H.S. Jr., and Yund, R.A., eds., Carnegie Institution of Washington, D.C., p. 243-259.

Freer, R., 1981, Diffusion in silicate minerals and glasses: a data digest and guide to the literature: Contrib. Mineral. Petrol., v. 76, p. 440-454.

Fryer, J.E., 1975, Rare-earth evidence in iron-formations for changing Precambrian oxidation states, Geochim. et Cosmo. Acta, 41, p. 361-367.

Goldich, S.S., Nier, A.O., Baadsgaard, Hog, Hoffman, J.H., and Krueger, H.W., 1961, The Precambrian geology and geochronology of Minnesota: Minnesota Geol. Survey Bull. 41, pp. 194.

Goldich, S.S., 1973, Ages of Precambrian banded iron-formation: Econ. Geol., v. 68, p. 1126-1134.

Grant, J.A., 1986, The isocon diagram-A simple solution to Gresen's equation for metasomatic alteration, Econ. Geol., 81, p.1976-1982.

Gresens, R.L., 1967, Composition-volume relationship of metasomatism: Chem. Geol., 2, p. 47-55.

Haase, C.S., 1986, Metamorphic petrology of the Negaunee Iron Formation, Marquette distract, northern Michigan: Mineralogy, metamorphic reactions and phase equilibria, Econ. Geol., 77, 60-81.

Henderson, P., 1984, General geochemical properties and abundances of the rare earth elements, in Henderson, P. ed. Rare earth element geochemistry, Elsevier Sci. Pub. B.V., Amsterdam, p.1-29.

Henley, R.W., 1984, pH calculation for hydrothermal fluid, in Robertson J.M., ed. Fluid-mineral equilibria in hydrothermal system, Reviews in Economic Geology, V. 1, p. 83-98.

Hofmann, A., 1972, Chromatographic theory of infiltration metasomatism and its application to feldspars, Am. J. Sci., 272, p. 69-90.

Holdway, M.J., 1971, Stability of andalusite and the aluminum silicate phase diagram: Am. J. Sci., 271, p. 97-131.

Huang, X., 1979, Geochemical exploration method (in Chinese), Geologic Press, Beijing, pp. 329.

James, H.L., 1955, Zones of regional metamorphism in the Precambrian of northern Michigan: , GSA Bull., 66, no. 12, p. 1465-1488.

Keranck, S.H., 1981, Study of phase equilibria in a metamorphic iron-formation: J. Petrology, v. 2, p. 1457-1470.

Kerrick, D.M., 1972, Experimental determination of the muscovite+quartz stability with $P_{H_2O}<P_{Total}$: Am. J. Sci., 272, p. 946-958.

Klasner, J.S., 1978, Penokean deformation and associated metamorphism in the western Marquette Range, Northern Michigan, GSA Bull. 89, p. 711-722.

Klasner, J.S., and Cannon, W.F., 1974, Geologic interpretation of gravity profiles in the western Marquette district, Northern Michigan, GSA Bull., 85, p. 213-218.

Klein, C. and Hurlbut, Jr., C.S., 1985, Manual of mineralogy, John Wiley & Sons, New York, p. 303-311.

Korzhinskii, D.S., 1970, Theory of metasomatic zoning, Clarendon Press, Oxford, pp. 162.

Laberge, G.L., 1964, Development of magnetite in iron-formations of the Lake Superior region: Econ. Geol., v. 59, p. 1313-1342.

Laird, J., 1980, Phase equilibria in mafic schist from Vermont, J. Petrology, 21, p.1-37.

Liu, Y., 1984, Element geochemistry (in Chinese), Science Press, Beijing, pp. 548.

Olsen, S.N. and Grant, J.A., 1991, Isocon analysis of migmatization in the Front Range, Colorado, USA: J. Met. Geol., 9, p. 151-164.

Sibson, R.H., 1990, Faulting and fluid flow, In: Nesbitt, B.E., ed., Short course on fluids in tectonically active regimes of the continental crust, Min. Assoc. Can. Short Course Handbook, 6, p. 93-132.

Spencer, K.J. and Lindsely, D.H., 1981, A solution model for coexisting iron-titanium oxides: Am. Mineral., 66, p. 1189-1201.

Spry, A., 1976, Metamorphic textures, Pergamon Press, Oxford, pp. 350.

Thompson, J.B., 1957, The graphical analysis of mineral assemblages in pelitic schist, Am. Mineral., 42, p. 842-858.

Turekian, K.K., and Wedepohl, K.H., 1961, Distribution of the elements in some major units of the earth's crust, Geol. Soc. Am. Bull. 72.

Van Schmus, W.R. and Hinze, W.J., 1985, The midcontinent rift system, Ann. Rev. Ear. Plan. Sci., 13, p. 345-383.

Van Schmus, W.R. and Woolsey, L.L., 1975, Rb-Sr geochronology of the Republic area, Marquette County, Michigan: Canadian J., Earth Sci., 12, p. 1723-1733.

Veblen, D.R, and Ribbe, P.H. ed. 1982, Amphiboles: Petrology and Experimental phase relations, Reviews in Mineralogy, v. 9B, Min. Soc. Amer., pp. 121.

Walther, J.V. and Orville, P.M., 1982, Volatile production and transport in prograde metamorphism, Contrib. Min. Petrol., 79, 252-257.

Walther, J.V. and Wood, B.J., 1984, Rate and mechanism in prograde metamorphism, Contrib. Min. Petrol., 88, p. 246-259.

Wedepohl, K.H., et al, 1969-1978, Handbook of geochemistry, V. I-II, Springer-Verlag, Berlin

Woolsey, L.L., 1971, A Rb-Sr geochronological study of the Republic metamorphic node, Republic, Michigan: Lawrence Kans. Kans. Univ. M.S. thesis.

Yardley, B.W.D., 1990, Atlas of metamorphic rocks and their textures, Longman, John Wiley & Sons, New York, pp. 120.

Yin, X., and Grant, J.A., 1992, Geochemistry of the metadiabases in the Republic Mine area, Northern Michigan, 38th Ann. Inst. on Lake Superior Geology, Hurley, Wisconsin, p. 95-97.

Zharikov, V.A., 1967, The acidic-basic characteristics of minerals (in Russian), Geol. Rud. Mestorozhd., v. 9, no. 5, p. 75-89.

APPENDIX A: NOTATIONS

A, a	Altered rock
Ab	Albite
Act	Actinolite/Actinolite schist
Alm	Almandine
Am	Amphibole/Amphibolite
Am*	Iron-magnesium amphiboles
An	Anorthite
And	Andalusite/Andalusite schist
Ap	Apatite
APL	Altered Plagioclase (in Volume)
Avg	Average
Bt	Biotite
C	Concentration
Carb	Carbonate mineral
Chl	Chlorite/Chlorite schist
CPL	ReCrystallized plagioclase
Cum	Cummingtonite/Cummingtonite schist
Ep	Epidote
F	Felsic component
FSP	Feldspar
Grt	Garnet
Gr	Grossular
Gru	Grunerite
Hb, Hbl	Hornblende
Hm	Hematite
i, j	Component i, j
Ilm	Ilmenite
IPL	Plagioclase as inclusion in other minerals
i	Species i
K_{iso}	isocon slope
Kfs	Potassium feldspar
M	Mass/Mafic component
Max	Maximum
Min	Minimum
Mt	Magnetite
Ms, Mus	Muscovite/Muscovite schist
n	Number of samples
O, o	Original rock
Pl	Plagioclase
Q	Quartz
ρ	Specific density
R	Rock
R1~6	Amphibolite, Act, Cumm, And, Ms and Chl schist
RPL	Relict plagioclase
Rut	Rutile
σ, Std	Standard deviation
Ser	Sericite
Sn	Section/Traverse number
Sp	Spessartine
Spn	Sphene
V	Volume
x	Mole fraction
Y	Approximate ionization potential

APPENDIX B1: Chemical Analysis of Major Oxides (Unit: wt%)

OXIDE	R	SIO2	TIO2	AL2O3	FE2O3	FEO	MNO	CAO	MGO	K2O	NA2O	P2O5	H2O+	H2O2-	LOSS	TOTAL
MI91021	6	36.21	2.44	13.42	6.80	12.69	1.19	5.55	11.66	0.59	0.53	0.26	6.65	0.99	0.93	99.91
MI91024	3	39.46	3.34	16.88	4.30	19.26	0.71	1.82	7.56	0.59	2.07	0.38	3.22	0.48	0.28	100.35
MI91028	2	48.47	2.49	13.89	4.70	9.68	0.26	5.91	6.77	2.31	3.31	0.24	1.87	0.18	0.35	100.43
MI91031	1	49.69	2.04	14.42	3.49	9.03	0.20	9.32	6.35	0.71	3.09	0.19	1.41	0.05	0.18	100.17
MI91037	1	49.99	1.94	14.55	3.29	8.01	0.18	8.90	6.39	1.73	2.93	0.17	1.71	0.19	0.31	100.29
MI91038	1	47.39	1.86	15.33	4.22	7.71	0.18	10.61	6.70	0.79	2.72	0.19	1.48	0.07	0.12	99.37
MI91039	1	50.04	1.94	14.49	3.10	8.12	0.19	8.91	6.22	1.72	2.92	0.20	1.57	0.27	0.17	99.86
MI91114	5	52.54	2.86	13.82	6.80	7.68	0.24	4.94	4.23	1.51	2.17	0.48	2.27	0.29	—	99.83
MI91116	5	49.57	2.80	13.88	5.69	9.05	0.18	6.31	5.54	2.93	0.71	0.26	3.03	0.24	—	100.19
MI91117	3	49.85	3.25	13.94	4.08	8.73	0.09	1.86	8.52	2.51	1.07	0.38	4.79	0.63	—	99.70
MI91119	2	46.34	4.63	13.49	4.39	14.64	0.22	3.24	6.07	2.12	2.33	0.30	2.04	0.18	0.34	100.33
MI91120	2	38.39	3.49	17.30	6.41	14.36	0.19	2.27	6.58	3.71	1.65	0.38	4.10	0.13	0.77	99.73
MI91122	2	43.26	3.76	13.40	5.76	12.07	0.23	8.65	7.22	0.81	2.39	0.14	1.74	0.36	0.27	100.06
MI91206	6	34.94	3.69	16.71	12.37	9.80	0.68	0.61	9.30	4.31	0.25	0.09	6.55	0.74	0.64	100.68
MI91207	4	38.74	5.11	25.63	7.94	10.82	0.28	0.17	4.27	3.49	0.34	0.03	2.94	0.34	0.56	100.66
MI91208	4	38.34	5.21	25.52	8.08	10.72	0.27	0.18	4.18	3.55	0.34	0.02	3.13	0.03	0.39	99.96
MI91209	4	34.81	3.83	19.20	10.56	12.81	0.27	1.00	6.10	3.76	1.73	0.41	5.22	0.30	—	100.00
MI91211	3	43.90	4.37	14.18	9.95	10.89	0.24	2.86	5.30	2.79	2.37	0.26	2.47	0.09	0.43	100.10
MI91215	3	39.32	3.90	15.96	9.39	14.11	0.17	2.48	7.15	1.93	2.76	0.32	2.44	0.15	0.25	100.33
MI91220	3	42.94	3.48	14.82	8.88	11.08	0.23	3.17	6.53	1.72	3.23	0.35	2.35	0.22	0.62	99.62
MI91223	2	48.09	3.49	14.31	8.94	8.75	0.27	6.47	3.40	1.25	2.87	0.26	1.15	0.15	0.32	99.72
MI91306	6	36.31	3.18	16.86	20.34	5.90	0.30	1.11	3.13	6.85	1.32	0.40	2.80	0.34	0.64	99.48
MI91309	5	57.26	2.78	16.77	3.79	5.08	0.35	1.77	2.24	4.53	0.46	0.78	3.48	0.06	0.89	100.24
MI91313	4	58.44	2.03	14.13	3.64	7.62	0.48	2.61	3.10	3.78	0.76	0.63	2.47	0.32	0.29	100.30
MI91315	4	63.12	1.74	14.76	2.84	4.88	0.10	2.88	1.82	2.72	2.51	0.50	1.33	0.20	0.51	99.91
MI91318	4	51.12	2.52	14.92	3.56	10.13	0.22	2.97	4.73	4.43	0.40	0.26	3.56	0.51	0.30	99.63
MI91321	3	54.05	3.07	14.40	3.38	7.98	0.27	4.14	4.35	3.76	0.34	0.28	2.49	0.50	0.77	99.78
MI91325	2	44.33	3.43	13.30	7.91	10.82	0.59	7.33	6.54	1.14	1.27	0.36	2.01	0.20	0.18	99.41
MI91409	2	49.03	2.24	14.60	3.11	9.47	0.22	9.40	5.30	1.84	1.88	0.23	1.70	0.14	0.44	99.60
MI91411	2	48.86	2.45	14.40	3.71	9.59	0.26	8.77	4.88	1.68	2.28	0.27	1.77	0.13	0.44	99.49
MI91413	3	48.23	3.44	14.17	3.93	13.40	0.36	5.09	4.16	2.52	2.82	0.39	1.17	—	0.67	100.35
MI91415	4	51.26	3.53	18.53	3.28	11.25	0.40	1.40	2.68	3.84	0.71	0.43	2.09	0.23	0.44	100.07
MI91417	5	42.92	4.09	21.88	8.74	6.02	0.09	0.47	1.42	9.79	0.59	0.34	2.67	0.39	0.29	99.70
MI91420	5	46.92	3.94	18.53	3.58	13.85	0.76	0.83	2.54	4.29	0.47	0.35	3.01	0.37	0.36	99.80
MI91422	6	30.14	3.91	18.61	4.63	27.84	2.26	1.64	4.64	0.59	0.54	0.31	4.17	0.43	0.23	99.94
MIN.		30.14	1.74	13.30	2.84	4.88	0.09	0.17	1.42	0.59	0.25	0.02	1.15	0.00	0.00	99.37
MAX.		63.12	5.21	25.63	20.34	27.84	2.26	10.61	11.66	9.79	3.31	0.78	6.65	0.99	0.93	100.68
AVG		45.84	3.21	16.03	6.16	10.68	0.38	4.16	5.36	2.76	1.66	0.31	2.77	0.28	0.38	99.97
STD.		7.22	0.90	3.06	3.52	4.18	0.39	3.13	2.16	1.87	1.03	0.15	1.36	0.21	0.24	0.34
STD/AVG%		15.75	27.98	19.11	57.13	39.18	104.30	75.21	40.26	67.72	62.09	48.06	49.06	73.36	63.63	0.34

NOTE: See Appendix A for all notations.

APPENDIX B2: CHEMICAL ANALYSIS (TRACE ELEMENTS) (Unit: ppm)

ELEMENT	R	NB	ZR	Y	SR	RB	TH	GA	NI	CO	CR	CE	V	LA	BA	SC	ZN
MI91021	6	27	245	16	116	—	—	16	—	84	18	83	336	66	—	26	121
MI91024	3	18	140	13	60	4	—	19	7	114	—	54	299	60	119	28	72
MI91028	2	24	120	15	228	25	—	21	4	66	20	39	271	34	777	31	—
MI91031	1	23	101	12	419	9	—	21	4	49	36	17	356	10	202	35	25
MI91037	1	27	108	16	492	28	3	20	2	46	38	41	281	26	319	33	—
MI91038	1	30	92	16	486	4	—	18	91	59	49	28	327	33	227	29	—
MI91039	1	15	89	19	500	22	1	23	29	45	40	36	280	10	347	27	—
MI91114	5	42	262	21	216	22	—	21	16	54	—	80	323	50	299	19	55
MI91116	5	27	135	18	148	48	1	21	—	54	—	49	256	31	746	26	113
MI91117	3	28	268	23	67	28	—	23	—	52	—	56	319	39	376	21	86
MI91119	2	30	147	13	130	30	—	19	79	79	—	41	203	44	—	28	175
MI91120	2	33	162	17	160	35	—	19	—	85	—	69	94	63	1237	29	177
MI91122	2	20	65	10	197	11	—	21	136	68	—	22	502	28	115	43	113
MI91206	6	29	164	11	49	19	—	19	134	89	—	90	14	82	572	38	145
MI91207	4	40	270	25	29	28	—	23	—	66	—	115	—	85	—	29	132
MI91208	4	38	260	22	26	31	—	23	127	72	—	94	—	87	18	23	136
MI91209	4	27	170	23	59	22	—	20	8	93	—	45	31	61	—	32	145
MI91211	3	41	157	16	131	22	—	21	—	78	—	71	124	79	206	28	160
MI91215	3	33	127	11	140	7	—	18	—	93	—	48	211	49	573	24	178
MI91220	3	25	168	14	143	13	—	20	106	80	—	75	292	62	343	24	134
MI91223	2	22	128	17	355	11	—	20	—	64	—	62	423	54	282	27	106
MI91306	6	23	125	14	24	43	—	22	207	93	—	43	—	47	1295	19	90
MI91309	5	70	448	34	27	38	—	22	9	21	—	146	110	75	1061	21	49
MI91313	4	52	391	26	58	85	4	20	90	37	—	124	112	68	579	22	79
MI91315	4	71	488	35	136	37	—	24	—	21	—	168	132	87	778	11	38
MI91318	4	19	126	12	71	69	—	20	62	45	14	14	158	17	210	26	122
MI91321	3	31	155	23	104	33	—	20	—	38	—	51	238	55	231	34	65
MI91325	2	39	253	17	95	26	1	23	38	70	—	66	282	52	—	28	119
MI91409	2	31	144	17	251	18	—	23	2	42	27	6	298	23	293	30	80
MI91411	2	35	152	14	319	53	3	22	23	48	—	49	318	15	—	33	107
MI91413	3	33	183	17	175	17	—	23	—	64	—	26	233	57	482	22	143
MI91415	4	38	241	27	71	51	2	26	48	56	—	109	110	72	129	23	79
MI91417	5	27	183	28	60	73	—	21	—	51	—	86	—	63	442	26	—
MI91420	5	27	166	21	52	37	—	21	—	76	—	61	35	50	391	30	—
MI91422	6	25	133	8	9	—	—	15	—	128	—	14	145	47	—	32	56
MIN.		15	65	8	9	4	1	15	2	21	14	6	14	10	18	11	0
MAX.		71	488	35	500	85	4	26	207	128	49	168	502	87	1295	43	178
AVG		33	193	19	165	30	2	21	58	65	30	63	228	51	448	27	86
STD		13	100	6	139	19	1	2	57	23	12	37	114	22	321	6	57
STD/AVG%		38	52	34	85	63	56	10	98	36	38	58	50	42	72	24	66

NOTE: See Appendix A for all notations.

APPENDIX C1: THEORY OF ELEMENT DISTRIBUTION TESTING

According to Koch and Link (1971), Huang (1979) and Davis (1986), the theoretical equation of normal distribution is:

$$P(X) = \frac{1}{\sigma\sqrt{2\pi}} e^{\frac{-1}{2}(\frac{x-\mu}{\sigma})^2}$$

where *P(x)* is the normal distribution density, σ is the standard deviation and μ is the expected mean. The maximum frequency corresponds to the median of the cumulative frequency curve while the other frequencies decrease nonlinearly away from the median. Statistics parameters used to examine the deviation of the tested distribution curve from theoretical normal distribution pattern are:

$$C_3 = \frac{\mu_3}{\sigma_3}$$

$$C_4 = \frac{\mu_4}{\sigma_4} - 3$$

$$\mu_3 = \frac{\sum (x_i - \bar{x})^3}{n}$$

$$\mu_4 = \frac{\sum (x_i - \bar{x})^4}{n}$$

where Cs is the skewness, Ct is the kurtosis, μ3 and μ4 are third and fourth moment, respectively. Based on the statistical theory, Cs and Ct should be zero and both of them should belong to the normal distribution, or

$$C_s^0 = N(0, \sqrt{\frac{6}{n}})$$

$$C_t^0 = N(0, \sqrt{\frac{24}{n}})$$

at the 95% confidence interval. If the tested sample space is belonged to the normal distribution, then

$$C_s \le C_s^0$$
$$C_t \le C_t^0.$$

APPENDIX C2: ARITHMETIC NORMAL DISTRIBUTION TESTING

ELEMENT	AVG	STD	U3	U4	CS	CS0	CT	CT0	AND/NOT
AL	8.45E+00	1.61E+00	5.96E-01	4.17E+00	1.43E-01	8.40E-01	-2.98E+00	1.68E+00	NOT
BA	4.48E+02	3.21E+02	4.03E+07	4.00E+10	1.22E+00	9.10E-01	1.86E+08	1.82E+00	NOT
CA	2.96E+00	2.21E+00	6.28E+00	4.83E+01	5.84E-01	8.16E-01	-2.78E+00	1.63E+00	NOT
CE	6.31E+01	3.69E+01	4.23E+04	6.43E+06	8.45E-01	8.16E-01	2.99E+04	1.63E+00	NOT
CO	6.46E+01	2.33E+01	6.23E+03	9.52E+05	4.91E-01	8.16E-01	4.42E+03	1.63E+00	NOT
FE2	8.16E+00	3.32E+00	7.44E-02	1.22E+02	2.03E-03	8.28E-01	-2.43E+00	1.66E+00	NOT
FE3	4.26E+00	2.44E+00	2.13E+00	2.25E+01	1.46E-01	8.28E-01	-2.90E+00	1.66E+00	NOT
GA	2.08E+01	2.15E+00	-3.84E+00	7.93E+01	-3.85E-01	8.16E-01	-2.63E+00	1.63E+00	NOT
HO+	1.51E-01	7.58E-02	5.83E-04	1.46E-04	1.34E+00	8.16E-01	-3.00E+00	1.63E+00	NOT
HO-	1.62E-02	1.12E-02	3.68E-07	2.18E-08	2.61E-01	8.40E-01	-3.00E+00	1.68E+00	NOT
K	2.26E+00	1.54E+00	4.51E-01	6.18E+00	1.23E-01	8.28E-01	-2.97E+00	1.66E+00	NOT
LA	5.08E+01	2.15E+01	-1.69E+03	4.79E+05	-1.69E-01	8.16E-01	2.22E+03	1.63E+00	NOT
MG	3.18E+00	1.32E+00	1.10E+00	1.03E+01	4.80E-01	8.16E-01	-2.95E+00	1.63E+00	NOT
MN	2.85E-01	3.00E-01	7.31E-03	5.51E-03	2.70E-01	8.28E-01	-3.00E+00	1.66E+00	NOT
NA	1.30E+00	8.46E-01	2.29E-01	1.23E+00	3.77E-01	8.16E-01	-2.99E+00	1.63E+00	NOT
NB	3.26E+01	1.25E+01	1.54E+03	7.46E+04	7.82E-01	8.28E-01	3.44E+02	1.66E+00	NOT
NI	5.82E+01	5.67E+01	1.67E+05	3.10E+07	9.14E-01	1.07E+00	1.44E+05	2.14E+00	NOT
P	1.34E-01	6.45E-02	-4.01E-05	3.15E-05	-1.49E-01	8.28E-01	-3.00E+00	1.66E+00	NOT
RB	3.02E+01	1.89E+01	7.23E+03	5.03E+05	1.07E+00	8.40E-01	2.34E+03	1.68E+00	NOT
SC	2.69E+01	6.34E+00	-5.25E+01	6.09E+03	-2.06E-01	8.16E-01	2.53E+01	1.63E+00	NOT
SI	2.19E+01	3.60E+00	4.54E+00	4.51E+02	9.75E-02	8.16E-01	-9.03E-01	1.63E+00	AND
SR	1.65E+02	1.39E+02	3.13E+06	1.24E+09	1.15E+00	8.16E-01	5.78E+06	1.63E+00	NOT
TI	1.89E+00	5.57E-01	3.25E-02	2.35E-01	1.88E-01	8.16E-01	-3.00E+00	1.63E+00	NOT
V	2.28E+02	1.14E+02	4.58E+04	4.39E+08	3.07E-02	8.66E-01	2.04E+06	1.73E+00	NOT
Y	1.85E+01	6.38E+00	1.98E+02	5.13E+03	7.64E-01	8.16E-01	2.09E+01	1.63E+00	NOT
ZN	1.07E+02	4.18E+01	-4.78E+03	6.42E+06	-6.57E-02	9.10E-01	2.99E+04	1.82E+00	NOT
ZR	1.93E+02	9.99E+01	1.43E+06	4.38E+08	1.43E+00	8.16E-01	2.04E+06	1.63E+00	NOT
*TFE	1.24E+01	4.01E+00	-9.65E+00	3.12E+02	-1.49E-01	8.28E-01	-1.55E+00	1.66E+00	AND
*THO	1.67E-01	8.43E-02	4.03E-04	1.28E-04	6.72E-01	8.28E-01	-3.00E+00	1.66E+00	NOT

NOTE: See Appendix A for all notations.

APPENDIX C3: LOGARITHMIC NORMAL DISTRIBUTION TESTING

ELEME	AVG	STD	U3	U4	CT	CT0	CS	CS0	LND/NOT
AL	0.91	0.05	0.00	0.00	-3.00	1.68	1.13	0.84	NOT
BA	2.53	0.37	-0.06	0.11	-3.00	1.82	-1.18	0.91	NOT
CA	0.30	0.46	-0.09	0.15	-3.00	1.63	-0.95	0.82	NOT
CE	1.71	0.31	-0.03	0.03	-3.00	1.63	-0.91	0.82	NOT
CO	1.78	0.17	-0.00	0.00	-3.00	1.63	-0.70	0.82	NOT
FE2	0.87	0.15	-0.00	0.00	-3.00	1.66	-0.54	0.83	NOT
FE3	0.56	0.18	0.00	0.00	-3.00	1.66	0.43	0.83	NOT
GA	1.32	0.05	-0.00	0.00	-3.00	1.63	-0.80	0.82	NOT
HO+	-0.87	0.20	0.00	0.00	-3.00	1.63	0.33	0.82	NOT
HO-	-1.92	0.31	-0.02	0.03	-3.00	1.68	-0.76	0.84	NOT
K	0.24	0.29	-0.01	0.02	-3.00	1.66	-0.48	0.83	NOT
LA	1.65	0.24	-0.02	0.01	-3.00	1.63	-1.20	0.82	NOT
MG	0.46	0.20	-0.01	0.01	-3.00	1.63	-0.67	0.82	NOT
MN	-0.69	0.25	0.01	0.01	-3.00	1.66	0.52	0.83	NOT
NA	-0.01	0.36	-0.02	0.03	-3.00	1.63	-0.45	0.82	NOT
NB	1.48	0.14	0.00	0.00	-3.00	1.66	0.40	0.83	NOT
NI	1.43	0.63	-0.11	0.29	-3.00	2.14	-0.42	1.07	NOT
P	-0.96	0.30	-0.06	0.07	-3.00	1.66	-2.19	0.83	NOT
RB	1.38	0.31	-0.02	0.03	-3.00	1.68	-0.75	0.84	NOT
SC	1.42	0.12	-0.00	0.00	-3.00	1.63	-1.31	0.82	NOT
SI	1.34	0.07	-0.00	0.00	-3.00	1.63	-0.31	0.82	NOT
SR	2.05	0.41	-0.03	0.08	-3.00	1.63	-0.40	0.82	NOT
TI	0.26	0.14	-0.00	0.00	-3.00	1.63	-0.40	0.82	NOT
V	2.27	0.34	-0.06	0.07	-3.00	1.73	-1.63	0.87	NOT
Y	1.24	0.15	0.00	0.00	-3.00	1.63	0.01	0.82	NOT
ZN	1.99	0.21	-0.01	0.01	-3.00	1.82	-0.97	0.91	NOT
ZR	2.24	0.20	0.00	0.00	-3.00	1.63	0.45	0.82	NOT
*TFE	1.06	0.13	-0.00	0.00	-3.00	1.66	-0.49	0.83	NOT
*THO	-0.84	0.19	0.00	0.00	-3.00	1.66	0.24	0.83	NOT

NOTE: See Appendix A for all notations.

APPENDIX D: MULTI-POPULATION ANALYSIS

By changing nonuniformly the vertical scale on the graph of the cumulative-normal-distribution curve, it is possible to have the cumulative-normal-distribution curve take on the shape of a straight line for a subpopulation (Koch and Link, 1971; Huang, 1979 and Davis 1986). Although the cumulative probability method is used in this paper, the same results can be obtained from histogram as showed in Figure 11. If the cumulative normal distribution curve for an element plotted on normal probability paper is a straight line, the total sample space of this element contains only one subspecies or sub-population. If the cumulative normal distribution curve for an element is not a straight line, there must be more than one subspaces in the total sample space. The procedure of analysis for different sub-spaces is as follows:

1). If the distribution pattern of an element belongs to AND, the arithmetic value of element concentration is used. Otherwise, the logarithmic value is used.

2). Inflection points in the cumulative curve are determined as the limits to divide the total population into different sub-populations.

3). The data ranging from the left beginning point to the first inflection point belong to subspecies A. In this range, the new cumulative probability for the single population A is changed to 100% by the proportion of the cumulative probability of subspecies A in the total sample space. Connect these new cumulative points in the paper to have a straight line, which is the cumulative-normal-distribution curve for subspace A.

4). All the data from the first inflection point to the last point are assumed belonging to subspecies B. Similarly the new cumulative probability for the single population B is changed to 100%. Note that the probability at the left first inflection point for subspecies B is zero.

5). If the cumulative curve of B is not a straight line, the same procedures are repeated to get the subspace B1, B2 and so on until each subspace is separated.

Figure 12 shows that almost all the major and minor elements have three sample subspaces in the cumulative probability diagrams (or multi-peak curves of distribution patterns in the histograms). For example, Al has major inflection points near 67.75 and 85.29 percent in the cumulative probability diagram. The left subspace occupies 67.75 percent of total sample space, middle and right subspace occupy about 17.54 and 14.71 percent of total sample space, respectively. The left sample subspace of Si occupies only 27.78 percent of total sample space and the middle and right sample subspaces occupy about 61.11 and 11.11 percent of total sample space, respectively.

APPENDIX E1: ISOCON ANALYSIS METHOD THEORY

Detailed discussion of the isocon method can be found in Grant (1986), and the notations are listed in Appendix A. Following are the basic equations used in isocon method. Change in the mass of a rock before and after alteration can be expressed as

$$dM = M^A - M^O \tag{1}$$

The mass and the concentration of a component *i* before and after alteration are connected by the equations:

$$dM_i = M_i^A - M_i^O = M^A C_i^A - M^O C_i^O \tag{2}$$

$$C_i^O = \frac{M_i^O}{M^O} \tag{3}$$

$$C_i^A = \frac{M_i^A}{M^A} = \frac{M_i^O + dM_i}{M^A} \tag{4}$$

Multiply equation (4) by $\frac{M_i^O}{M^O}$ and rearrange it to get

$$C_i^A = \frac{M_i^O}{M^A} \bullet (C_i^O + dC_i) \tag{5}$$

The relative changes in mass and concentration of a component *i* can be expressed as

$$\frac{dM_i}{M_i^O} = \frac{M_i^A}{M^O} \bullet C_i^A - C_i^O \tag{6}$$

$$\frac{dC_i}{C_i^O} = \frac{M_i^A}{M^O} \bullet \frac{C_i^A}{C_i^O} - 1 \tag{7}$$

For an immobile element *i* (noted as iso) which keeps constant before and after the alteration, dMi=0, or

$$M_i^A = M_i^O \tag{8}$$

$$C_{iso}^A = \frac{M_i^O}{M^A} \bullet C_{iso}^O \tag{9}$$

Define the isocon slope as

$$K_{iso} = \frac{M^O}{M^A} = \frac{C_{iso}^A}{C_{iso}^O} \tag{10}$$

If total mass of a rock keeps constant before and after the alteration, or dM=0 and $M^A=M^O$

$$C_{iso}^A = C_{iso}^O \tag{11}$$

If total volume of a rock keeps constant before and after the alteration, or dV=0, $V^A=V^O$ and $M=\rho V$,

$$C_{iso}^A = C_{iso}^A \bullet \frac{\rho^O}{\rho^A} \tag{12}$$

If Kiso>1, mass is lost; if Kiso<1, mass is gained; if Kiso=1, the mass keeps constant through the alteration. To calculate the mass changes of rocks before and after alteration, we have

$$dM = M^A - M^O = M^O(\frac{1}{K_{iso}} - 1) \tag{13}$$

$$\frac{dM}{M^O} = \frac{1}{K_{iso}} - 1 \tag{14}$$

To calculate the mass change of each mobile element during an alteration,

$$dM_i = \frac{C_i^A}{K_{iso}^O} - M_i^O C_i^O \tag{15}$$

$$dC_i = K_{iso} C_i^A - C_i^O \tag{16}$$

$$\frac{dM_i}{M_i^O} = \frac{C_i^A}{K_{iso} C_i^O} - \tag{17}$$

$$\frac{dC_i}{C_i^O} = \frac{C_i^A}{C_i^O} \bullet K_{iso} - 1 \tag{18}$$

APPENDIX E2: ISOCON ANALYSIS PROCEDURE

Two different kinds of chemographic expression are used in this thesis. One is discussed in detail by Grant (1986). The procedure for another chemography is as follows (Fig. 16 and 17):

1). All the elements are divided into major elements and minor elements groups based on their different concentration ranges. The unit for all the major oxides is weight percent and for all the minor elements is ppm.

2). All the concentrations from each of the two groups in each altered rock are scaled to a convenient fixed value for their protolith. In Fig. 17, for example, the concentration of each major oxide in actinolite schist is multiplied by 9 and then divided by concentration of the same oxide in the least altered metadiabase, so that the relative gain or loss of elements for each altered metadiabase can be easily evaluated. Those elements above the isocon are enriched while the elements below the isocon are lost.

3). Different fixed values are used for different altered metadiabase so that the changes of concentration for all components in each altered metadiabase can be observed and compared in one diagram. A isocon with larger (or smaller) slope than one indicates the total mass loss (or gain) for an altered metadiabase compared to its protolith, while the increase (or decrease) of isocon slope compared to the previous isocon in a series means the mass loss (or gain) for one alteration zone compared to the previous one.

APPENDIX E3: Selected Linear Regression Results

METADIABASES	(All constants = 0)	SIO2	AL2O3
All Rocks (N=35)	Std Err of Y Est	9.86	14.90
	R Squared	0.75	0.25
	X Coefficient(s)	0.95	1.06
	Std Err of Coef.	0.02	0.03
ROCK 1-3 (N=20)	Std Err of Y Est	7.19	5.89
	R Squared	0.66	0.56
	X Coefficient(s)	0.95	0.99
	Std Err of Coef.	0.02	0.02
ROCK 1-4	Std Err of Y Est	9.79	16.00
	R Squared	0.55	-0.40
	X Coefficient(s)	0.95	1.05
	Std Err of Coef.	0.02	0.04
ROCK 3-4	Std Err of Y Est	11.97	18.79
	R Squared	0.05	-0.38
	X Coefficient(s)	0.93	1.12
	Std Err of Coef.	0.04	0.06
ROCK 3-5	Std Err of Y Est	10.99	17.44
	R Squared	0.16	-0.07
	X Coefficient(s)	0.95	1.13
	Std Err of Coef.	0.03	0.05
ROCK 3-6	Std Err of Y Est	11.19	16.13
	R Squared	0.55	0.23
	X Coefficient(s)	0.93	1.12
	Std Err of Coef.	0.03	0.05
ROCK 4-5	Std Err of Y Est	12.70	19.98
	R Squared	0.06	0.24
	X Coefficient(s)	0.98	1.27
	Std Err of Coef.	0.06	0.09
ROCK 4-6	Std Err of Y Est	12.82	17.61
	R Squared	0.46	0.42
	X Coefficient(s)	0.93	1.24
	Std Err of Coef.	0.05	0.07

NOTE: See Appendix A for all notations.